

In-depth Characterization of Human iPSC-Cardiomyocytes Models of Long QT-3 and Brugada Syndromes during in vitro Maturation

Inaugural Dissertation

zur

Erlangung des Doktorgrades
philosophiae doctor (PhD) in Health Sciences
der Medizinischen Fakultät
der Universität zu Köln

vorgelegt von

Michelle Vanessa Kamga Kapchoup

aus Duala, Kamerun

(Hundt Druck, Köln)

2022

Betreuer: PD Dr. Filomain Nguemo

Gutachter: Prof. Dr. Stefan Herzig
Prof. Dr. Dirk Isbrandt

Datum der Mündlichen Prüfung: 31.10.2022

Summary

Cardiovascular diseases can be congenital or acquired and represent the main cause of mortality worldwide. Long QT Syndrome 3 (LQTS3) and Brugada Syndrome (BrS) are congenital channelopathies mostly caused by *SCN5A* mutation. Both diseases have been associated with gain-of-function and loss-of-function of the channel respectively. However, some mutations display an overlapping phenotype between the two diseases, rendering the diagnostic as well as the therapy of the diseases challenging. Although several studies have been done to date, the disease-related mechanisms are still elusive and require more investigation at the molecular as well as the functional levels. The use of disease-specific pluripotent stem cells to develop disease models has enabled the research of pathogenic pathways related to diseases and the search for new treatments. Human-induced pluripotent stem cell-derived cardiomyocytes (hiPSC-CMs) represent a platform that has allowed advancement in personalized therapy circumventing the problem of genotype-phenotype differences existing between individuals. Despite the immaturity of the cardiomyocytes engineered in-vitro, these cells represent a good tool for disease investigation.

This study aimed to characterize both disease phenotypes at a cellular, molecular, and functional level. For this purpose, we used different stages of cardiomyocytes maturation to perform our experiments. The transcriptomic analysis, RT-PCR, immunohistochemistry, FACs, MEA, patch-clamp and calcium imaging experiments were done to (i) access the gene expression profiles between the cardiomyocytes of healthy control and the patients; (ii) evaluate the structural and functional characterization of cardiomyocytes and also look at the impact of cell maturation on experimental disease modelling; (iii) check the hypothesis of loss-of-function and gain-of-function attributed to BrS and LQTS3, respectively, through patch-clamp analysis.

In the present study, we used hiPSC-CMs from a healthy subject and LQTS3 as well BrS patients and observed that genes involved in the mechanism of excitation-contraction coupling as well as cell repolarization (*RyR2*, *CaV1.2*, *CASQ2*, *TNNT2*, *TNNI3*, *KCNH2*, *Cavβ* subunits), are dysregulated in patients. Moreover, although, the *SCN5A* gene was upregulated in BrS cardiomyocytes, the sodium current (I_{Na}) was reduced in those -cells, and we also observed a positive shift of activation characteristic of loss-of-function of the channel. These data suggest that Na_v channel impairment might occur at the protein level. In LQTS3-derived cardiac cells, on the contrary, we also observed a loss-of-function of the channel and a reduced *SCN5A* gene

compared to the control. However, we were able to identify the existence of the long QTc phenotype, and therefore, hypothesized that the V240M mutation could be associated with a mixed phenotype between LQTS3 and BrS. Nevertheless, performing the patch-clamp assay with more mature cells is advisable to make a proper statement regarding this mutation. The calcium transient was prolonged in both disease models characterized by the emergence of trigger activity in BrS-derived CMs at D40 of differentiation. The latter observation shows the importance of using a late time point of cardiac cell differentiation during experimental studies. Moreover, the bradycardia phenotype associated with BrS as well as the long QTc phenotype were identified only at this late stage of differentiation. Using single cells and cell sheets during our study, additionally show that the use of distinct cell types during functional analysis can significantly impact the interpretation of the FP rate.

Our studies provide more insight into LQTS3 and BrS on a molecular as well as functional level. It also delivers a probability of a mixed phenotype associated with the V240M mutation. However, additional studies using more mature CMs are necessary, and the use of CRISPR-Cas9 will be of great interest to avoid the problem related to the genotype background and, therefore, provide a more precise outcome of each mutation.

Zusammenfassung

Herz-Kreislauf-Erkrankungen können angeboren oder erworben sein und stellen weltweit die Hauptursache für Todesfälle dar. Das lange QT-Syndrom 3 (LQTS3) und das Brugada-Syndrom (BrS) sind angeborene Kanalopathien, die meist durch eine *SCN5A*-Mutation verursacht werden. Beide Krankheiten werden mit einem Funktionsgewinn bzw. Funktionsverlust des Kanals in Verbindung gebracht. Einige Mutationen weisen jedoch einen überlappenden Phänotyp zwischen den beiden Krankheiten, was sowohl die Diagnose als auch die Therapie der Krankheit erschwert. Obwohl bereits mehrere Studien durchgeführt wurden, sind die mit der Krankheit zusammenhängenden Mechanismen immer noch schwer fassbar und müssen sowohl auf molekularer als auch auf funktioneller Ebene weiter untersucht werden. Die Verwendung krankheitsspezifischer pluripotenter Stammzellen zur Entwicklung von Krankheitsmodellen hat die Erforschung krankheitsbezogener Pathogenitätswege und die Suche nach neuen Behandlungsmöglichkeiten ermöglicht. Aus humanen induzierten pluripotenten Stammzellen abgeleitete Kardiomyozyten (hiPSC-CMs) stellen eine Plattform dar, die Fortschritte in der personalisierten Therapie ermöglicht hat, indem sie das Problem der Genotyp-Phänotyp-Unterschiede zwischen Individuen umgeht. Trotz der Unreife der in vitro gezüchteten Kardiomyozyten sind diese Zellen ein gutes Instrument für die Untersuchung von Krankheiten.

Das Ziel dieser Studie war es, beide Krankheitsphänotypen auf zellulärer, molekularer und funktioneller Ebene zu charakterisieren. Zu diesem Zweck haben wir verschiedene Stadien der Kardiomyozytenreifung für unsere Experimente verwendet. Die Transkriptomanalyse, RT-PCR, Immunhistochemie, FACs, MEA, Patch-Clamp und Calcium-Imaging-Experimente wurden durchgeführt, um (i) Zugang zu den Genexpressionsprofilen zwischen den Kardiomyozyten der gesunden Kontrolle und der Patienten zu erhalten; (ii) die strukturelle und funktionelle Charakterisierung der Kardiomyozyten zu bewerten und auch die Auswirkungen der Zellreifung auf die experimentelle Krankheitsmodellierung zu untersuchen; (iii) die Hypothese des Funktionsverlusts und Funktionsgewinns, die BrS bzw. LQTS3 zugeschrieben werden, durch Patch-Clamp-Analyse zu überprüfen.

In der vorliegenden Studie verwendeten wir hiPSC-CMs von einem gesunden Probanden und von LQTS3- sowie BrS-Patienten und beobachteten, dass Gene, die am Mechanismus der Erregungs-Kontraktions-Kopplung, der Zellkontraktion sowie der Zellrepolarisation beteiligt sind (*RyR2*, *CaV1.2*, *CASQ2*, *TNNT2*, *TNNI3*, *KCNH2*, *Cavβ*-Untereinheiten), bei Patienten

dysreguliert sind. Obwohl das *SCN5A*-Gen in BrS-Kardiomyozyten hochreguliert war, war der Natriumstrom (I_{Na}) in diesen Zellen reduziert, und wir konnten auch eine positive Verschiebung der Aktivierung beobachten, die für einen Funktionsverlust des Kanals charakteristisch ist. Diese Daten deuten darauf hin, dass die Beeinträchtigung des Nav-Kanals möglicherweise auf Proteinebene stattfindet. In den von LQTS3 abgeleiteten Herzzellen hingegen konnten wir ebenfalls eine Funktionsstörung des Kanals und eine Verringerung des *SCN5A*-Gens im Vergleich zu den Kontrollzellen feststellen. Wir konnten jedoch das Vorhandensein des langen QTc-Phänotyps feststellen und stellten daher die Hypothese auf, dass die V240M-Mutation mit einem gemischten Phänotyp zwischen LQTS3 und BrS verbunden sein könnte. Dennoch ist es ratsam, den Patch-Clamp-Versuch mit reiferen Zellen durchzuführen, um eine genaue Aussage über diese Mutation zu treffen. Der Kalziumtransient wurde in beiden Krankheitsmodellen verlängert, was durch das Auftreten von Triggeraktivität in BrS-abgeleiteten CMs bei D40 der Differenzierung gekennzeichnet ist. Die letztgenannte Beobachtung zeigt, wie wichtig es ist, bei experimentellen Untersuchungen einen späten Zeitpunkt der Herzzelldifferenzierung zu verwenden. Außerdem wurden der mit dem BrS assoziierte Bradykardie-Phänotyp sowie der lange QTc-Phänotyp erst in diesem späten Stadium der Differenzierung identifiziert. Die Verwendung von Einzelzellen und Zellblättern in unserer Studie zeigt außerdem, dass die Verwendung unterschiedlicher Zelltypen bei der Funktionsanalyse die Interpretation der Feldpotentialrate erheblich beeinflussen kann.

Unsere Studien geben weitere Einblicke in LQTS3 und BrS, sowohl auf molekularer als auch auf funktioneller Ebene. Sie gibt auch die Wahrscheinlichkeit eines gemischten Phänotyps in Verbindung mit der V240M-Mutation an. Es sind jedoch weitere Studien mit reiferen CM erforderlich, und die Verwendung von CRISPR-Cas9 wird von großem Interesse sein, um das Problem des Genotyp-Hintergrunds zu vermeiden und somit ein präziseres Ergebnis für jede Mutation zu erhalten.

Acknowledgments

First of all, I would like to express my gratitude to my supervisor PD Dr. Filomain Nguemo, who supported and guided me and helped me with my work and the writing of my thesis. I cannot thank my supervisor without also expressing my gratitude to Prof. Dr. Jürgen Hescheler for allowing me to carry out my research at the Institute for Neurophysiology.

My appreciation goes to my tutors Prof Dr. Dirk Isbrandt and Prof Dr. Stefan Herzig who did not fail to advise me regarding my experiences and thus enabled me to be much more objective in my work.

I am grateful to have the support of PD Dr. Jan Matthes from the Pharmacological Institute and Ms. Nour Katnahji my lovely collaborator who agreed to work with us and made sacrifices to perform the patch-clamp experiment.

I would like to thank Prof Dr. Simeon Papadopoulos and Prof Dr. Agapios Sachinidis for their kindness, help, and input. My gratitude also goes to Dr. Dr. Tomo Saric for providing me with the cells without which this work would not be possible.

My thanks also go to Dr. Robin Bayer who designed the software that helped me to analyze my electrophysiological data.

I also want to acknowledge Frau Annette Köster and Frau Susanne Rohani for their support, their advice, and the wonderful atmosphere they always established.

Finally, I am grateful to have had wonderful team members as well as colleagues who helped me a lot during my journey and encouraged me when I was down. I would also like to give thanks to the Lord who has made the way for me to do this Ph.D. and strengthened me throughout the process.

My sincere thanks to all

Table of Contents

1	Introduction	1
1.1	Introduction to cardiac muscle.....	1
1.2	Structure and function of cardiac muscle.....	1
1.3	Cardiac muscle cells function and associated pathologies	3
1.4	Cardiac action potential and ion channels.	5
1.5	Cardiac cells: gene expression and related pathologies	8
1.6	<i>SCN5A</i> gene and disease-related mutations	9
1.7	Pharmacodynamics of antiarrhythmic drugs on Nav1.5 channel: Case of Lidocaine	10
1.8	In-vitro studies of cardiac diseases	12
1.8.1	Generation of human-induced pluripotent stem cells (hiPSCs).....	13
1.8.2	Differentiation of hiPSCs into cardiomyocytes and functional properties	14
1.9	Channelopathies associated with cardiac dysfunctionality: the case of LQTS3 and BrS	17
1.9.1	Long QT Syndrome type 3 (LQTS3).....	17
1.9.2	Brugada Syndrome (BrS).....	18
1.9.3	Overlapping phenotype between LQTS3 and BrS.....	20
1.10	Aim of study	21
2	Materials and Methods	22
2.1	Materials	22
2.2	Laboratory equipment.....	22
2.3	Reagents.....	23
2.4	Media and Buffers.....	25
2.5	hiPSCs culture.....	26
2.6	Differentiation of hiPSCs to hiPSC-CMs	27
2.7	HiPSC-CMs dissociation	28

2.8	Immunostaining	29
2.9	FACs analysis of hiPSC-CMs.....	30
2.10	gDNA extraction.....	30
2.11	PCR sequencing.....	30
2.12	RNA isolation for gene expression profiling	31
2.13	Protocol for cDNA synthesis	32
2.14	RT-PCR protocol with Platinum SYBR Green qPCR SuperMix-UDG.....	32
2.15	Multi-electrode Array (MEA) Experiment	33
2.16	Calcium Imaging.....	35
3	Results	36
3.1	Culture of hiPSCs in a xeno-free and feeder-free system.....	36
3.2	High effectiveness of cardiomyocytes differentiation with RPMI supplemented with ascorbic acid.....	37
3.3	Characterization of the sarcomeric and connexin 43 organization at a late stage of differentiation between the control and the disease models	38
3.4	Validation of the disease mutations.	39
3.5	Gene expression profiles between healthy control and disease models	41
3.6	Genes expression regulation in LQTS3 and BrS compared to the control	42
3.7	Gene ontology analysis of healthy and defective cardiomyocytes	44
3.8	Field potential recording of healthy control and LQTS3 patient cardiomyocytes and QTc analysis.....	46
3.9	Lidocaine effect on LQTS3-derived cardiomyocytes.....	47
3.10	Field potential comparison between healthy control and disease models in different maturation time points	49
3.11	Calcium transient measurement for field potential rate evaluation on cell sheets.....	51
3.12	Calcium transient measurement for field potential rate evaluation on single cells CMs.	52

3.13	Comparison of the field potential rate between early and late stages CMs in single cells and cell sheets	53
3.14	Cardiomyocyte calcium transient in healthy control and disease models	54
3.15	Time to 50% relaxation in healthy and unhealthy cardiomyocytes	55
4	Discussion.....	58
4.1	Culture of hiPSCs in a xeno-free and feeder-free system.....	58
4.2	High effectiveness of cardiomyocytes differentiation with RPMI supplemented with ascorbic acid.....	58
4.3	Late-stage characterization of the sarcomeric and connexin 43 organization between the control and the disease models.....	59
4.4	Validation of the disease mutations.	60
4.5	Gene expression profile between healthy control and disease models	61
4.6	Genes expression regulation in LQTS3 and BrS compared to the control	61
4.7	Gene ontology analysis of healthy control and defective cardiomyocytes (BrS & LQTS3)	64
4.8	Field potential recording of healthy control and LQTS3 patient cardiomyocytes and QTc analysis.....	65
4.9	Lidocaine effect on LQTS3-derived cardiomyocytes.....	66
4.10	Field potential comparison between healthy control and disease models in different maturation time points	66
4.11	Calcium transient evaluation in healthy control and disease models	69
4.12	Conclusion	73
5	Appendix	74
6	References	75
7	Publications	93
8	Curriculum Vitae	94

Abbreviations

AADs	Antiarrhythmic drugs
AC	Adenylate Cyclase
AF	Atrial Fibrillation
AP	Action Potential
APD	Action Potential Duration
Arg	Arginine
AV	Atrioventricular
BMPs	Bone Morphogenic Proteins
BrS	Brugada Syndrome
β-AR	Beta-Adrenergic receptors
CaMKII	Calcium-calmodulin-dependent protein kinase
CAD	coronary artery disease
cAMP	cyclic AMP, adenosine 3', 5'-cyclic monophosphate
CAP	Cardiac action potential
CICR	calcium-induced-calcium release
c-MYC	c-Myelocytomatosis
CO ₂	Carbon Dioxide
CPVT	Catecholaminergic Ventricular Tachycardia
CV	Conduction Velocity
DNA	Deoxyribonucleic acid
EAD	Early Afterdepolarization
ECG	Electrocardiogram
ESCs	Embryonic Stem Cells

FGFs	Fibroblast Growth Factors
HCN4	Hyperpolarization activated cyclic Nucleotide gated Potassium channel 4
HERG	Human Ether-à-go-go-related gene
hiPSCs	human induced pluripotent stem cells
hiPSC-CMs	human induced pluripotent stem cell-derived cardiomyocytes
I_{Ca}	Calcium current
I_k	outward rectifier potassium channel
I_{Na}	Fast Sodium Inward current
I_{NaL}	Late Sodium Inward current
I_{to}	outward current transient
K^+	Potassium current
KCNH2	Potassium voltage-gated channel subfamily H member 2
Kif4	Kinesin Family member 4
LC	Link Cells
LTCCs	L-type calcium channels
LQTS	Long QT Syndrome
Lys	Lysine
MF	Myofilament
mRNA	messenger Ribonucleic Acid
MYBPC3:	Cardiac myosin binding protein C encoding gene
MYH7	Myosin Heavy chain beta isoform
MYL2	myosin regulatory Light chain 2
Na^+	Sodium ions

Nav1.5	Sodium voltage-gated channel alpha subunit 5
NCX	Sodium-Calcium exchangers
$^+\text{H}_3\text{N}$	Ammonia
Oct $\frac{3}{4}$	Octamer-binding transcription factor 3/4
Phe	Phenylalanine
PLN	Cardiac phospholamban
RVOT	right ventricular outflow tract
RyR	Ryanodine Receptor
S1	α -helical transmembrane segment 1
S2	α -helical transmembrane segment 2
S3	α -helical transmembrane segment 3
S4	α -helical transmembrane segment 4
S5	α -helical transmembrane segment 5
S6	α -helical transmembrane segment 6
SC	Single Cells
<i>SCN5A</i>	Cardiac sodium channel
SOX2	Sex determining region Y- box2
SID	sudden infant death syndrome
SLC8A1	Sodium/Calcium exchanger 1 precursor
SR	Sarcoplasmic Reticulum
SSS	Sick Sinus Syndrome
TDR	Terminal Density Reversal
TNNC1	Troponin C encoding gene
TNNI3	cardiac Troponin I encoding gene

TNNT2	Cardiac troponin T encoding gene
Trp	Tryptophan
TTN	Titin gene
Tyr	Tyrosine
VPA	Valproic Acid
WNTs	Wingless/INT Proteins

Lists of figures

1. Introduction

Figure 1-1. Sarcomeric structure-function relation.....	2
Figure 1-2. T-tubule structure and key proteins involved in excitation-contraction (EC) coupling in the cardiomyocytes.	4
Figure 1-3. Cardiac Action Potential (CAP).....	6
Figure 1-4. Ca-dependent signaling to cardiac myocyte ion channels	7
Figure 1-5. Voltage-gated sodium channel.....	10
Figure 1-6. Picture of sodium current after a repetitive block by lidocaine.	12
Figure 1-7. Advantages of induced pluripotent stem cells (iPSCs) over mutant embryonic stem cells (ESCs) and genetically modified mouse models.....	14
Figure 1-8. Deciphering role of Wnt signalling in cardiac mesoderm and cardiomyocyte differentiation from Human iPSCs: four-dimensional control of Wnt pathway for hiPSC-CMs differentiation.....	15
Figure 1-9. Maturation of hiPSC-CMs clearly revealed differences in several ion channel regulators and cardiac-derived cells' electrophysiology properties	16
Figure 1-10. Cardiac tissue engineering and its applications.	17
Figure 1-11. Molecular and electrophysiological mechanisms underlying arrhythmogenesis in Brugada syndrome.	20
Figure 2-1. Schematic illustration of human cardiac muscle cells differentiation and characterization	28
Figure 2-2 Part of the Set up for field potential (FP) recording.....	34
Figure 2-3 Example of beating human cluster attached on a MEA plate.	34
Figure 3-1. hiPSCs culture in E8 media.....	36
Figure 3-2. hiPSC-CMs differentiation and characterization.	38
Figure 3-3. Characterization of cardiomyocytes and distribution of Cx43 within the cells. ...	39
Figure 3-4. Validation of LQTS3 Mutation.....	40
Figure 3-5. Validation of BrS mutation	41
Figure 3-6. PCA and hierarchical clustering.....	42
Figure 3-7. Gene-level expression and qPCR validation.....	43
Figure 3-8. Gene ontology analysis.	45
Figure 3-9. QTc evaluation between healthy control and LQTS3 CMs and between early and late stages cardiomyocytes.....	47

Figure 3-10. Effect of lidocaine on LQTS3-derived cardiomyocytes.	48
Figure 3-11. Amplitude and field potential rate of control cell line and disease models	50
Figure 3-12. Calcium transient in control and patient-derived cardiomyocytes.....	51
Figure 3-13. Evaluation of field potential rate using single cells	53
Figure 3-14. Field potential rate comparison between single cells and cell sheets	54
Figure 3-15. Calcium transient in healthy control and disease models	55
Figure 3-16. T50% of calcium extrusion in healthy control and disease models	57

List of Tables

Table 2.2.1 List of equipment	22
Table 2.3.1 List of reagents	23
Table 2.4.1 RPMI media for Differentiation (100 ml)	25
Table 2.4.2 RPMI media for purification (50 ml)	25
Table 2.4.3 Tyrode's solution for Ca ²⁺ Imaging	25
Table 2.4.4 Agarose gel' preparation.....	25
Table 2.4.5 TAE buffer (50x)	26
Table 2.4.6 Tris-wash buffer (10x)	26
Table 2.4.7 4% Paraformaldehyde.....	26
Table 2.11.1 PCR primers and sequencing primers designed for Mutation detection.....	31
Table 2.14.1 Designed primers for qPCR	33

1 Introduction

1.1 Introduction to cardiac muscle

Heart muscle is made of three layers: the epicardium, the myocardium, and the endocardium [1, 2]. Among these three layers, the myocardium represents in a functional aspect the major component of the heart [2]. The myocardium is made by sheets of unicellular cardiac muscle cells, also known as myocytes, which are interconnected through intercalated discs that allow the cardiac muscle to beat in a coordinated way [3]. Cardiomyocytes mostly possess one centrally located nucleus, but they can also contain more than one nucleus which can be eccentric [4]. The myocardium contract involuntarily through the so-called pacemaker cells, assuring the distribution of nutrients and oxygen throughout the body by heart pumping [5]. Compared to skeletal muscle, cardiac muscle cells harbour a longer action potential [6, 7].

1.2 Structure and function of cardiac muscle

The heart is the first organ to form during embryogenesis. The myocardium is made of four chambers: two atria and two ventricles which are subdivided into two pumps: the right and the left heart ensuring the purification of blood and the distribution of nutrients and oxygenated blood throughout the body, respectively [8]. Chambers of the heart are separated by atrioventricular (AV) valves known as the tricuspid valve in the right heart and the mitral valve in the left heart [9]. Atria have a relatively thin wall compared to the ventricles due to the difference in pressure to which both are subjected. Moreover, the wall of the left ventricle is two to three-times thicker than the right ventricle due to the resistance force to which both are subjected during the systole phase (blood ejection) [10].

The heart muscle is a striated muscle with contractile units known as the sarcomere, formed by actin (thin filaments) and myosin filaments (thick filaments). The centre of the sarcomere is made up of the A band, which is composed of overlapping thicker myofilaments known as myosin interconnected in the middle through the M-band. The thinner myofilaments actin is attached to the Z-disk, the elastic filament titin stretched from the Z-disk to the M-band [11] (**Figure 1.1**), and the I band contains only the actin protein [12]. During mechanical stimulation, those filaments are involved either in the generation of active or passive forces in cardiomyocytes as illustrated in the figure. *Crocini and Gotthardt* also speculate that there is a direct proportionality between sarcomeres and muscle length, determining the force of contraction of the ventricle during the systolic phase that might be the prerequisite of the Frank-Starling law [11]. Indeed, the cardiac output, which is the amount of blood pumped into the

systemic circulation per minute, has been proposed as one of the suitable ways to describe cardiac functionality [5]. The heart rate and the stroke volume, which is the volume of blood ejected during each systolic phase, determine the cardiac output. Three factors influenced this later. The preload, which is associated with the end-diastolic volume, and the afterload, which is analogous to systemic blood pressure. Finally, we have the force of contraction given by the so-called Frank-Starling law of the heart. This law affirms that the greater the amount of blood filled up in the ventricle during the preload phase, the greater the contraction and therefore the greater the amount of blood pumped into all parts of the body during systole [9, 13].

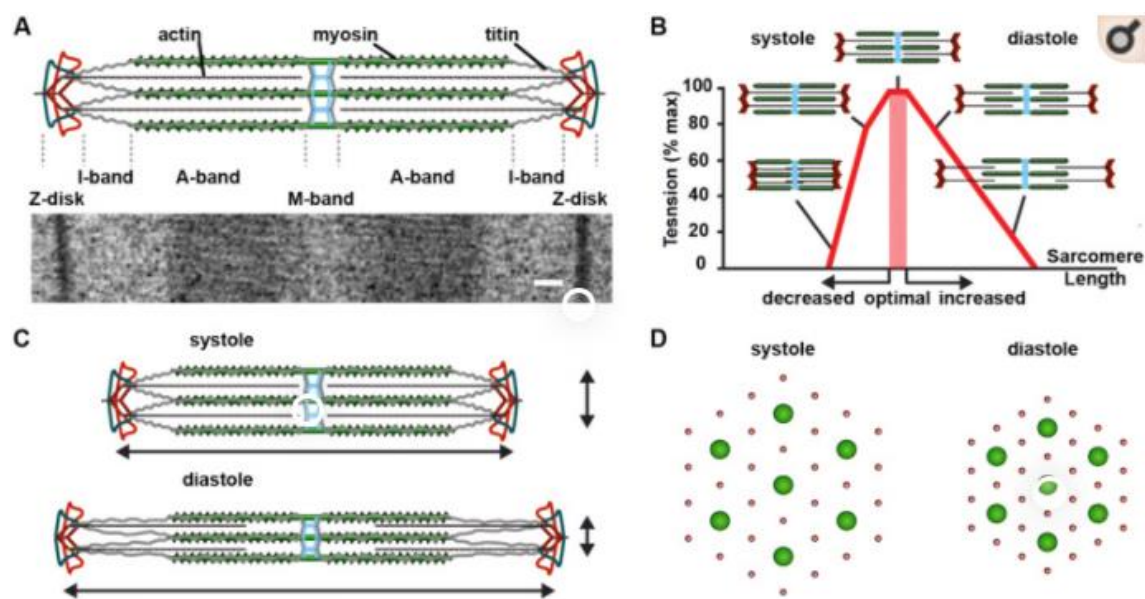


Figure 1-1. Sarcomeric structure-function relation

A, Schematic structure of the sarcomere (above) and sarcomere ultrastructure observed by electron microscopy (below). The sarcomere is an elastic scaffold that consists of structural proteins lined out from Z-disk to M-band, including actin (black), myosin (green), and titin (grey) that extends through the half-sarcomere. The scale is 100nm. **B**, Length-tension relation, a contributor to the Frank-Starling Law of the heart. **C**, Sarcomere length changes during systole and diastole. **D**, Myofilament compressions during diastolic filling, myosin in green, and actin in red. (Crocini, C. & Gotthardt, M. 2021) [11].

Cardiac automaticity is based on special formations called pacemakers of which the sinus node is the major element. Due to changes in the membrane voltage of the myocytes, the sinus node localized in the right atria will generate an electrical impulse that will induce atria contraction. The impulse is conveyed through the atrioventricular node into the ventricles with a delay via the bundles of His, which are divided into small branches known as Purkinje-fibres that will allow the electrical signal to propagate throughout the ventricles allowing, therefore, a synchronized contraction of these chambers [14]. However, some features such as ion channel

mutations, heart malformations, and even age can affect the above-described mechanisms and lead to heart failure.

1.3 Cardiac muscle cells function and associated pathologies

Cardiac muscle cells, also known as cardiomyocytes, are striated muscle cells that constitute the myocardium (heart muscle). They are interconnected through intercalated discs in an end-to-end or an end-to-side interdigitation [4], and in heart failure, these interconnections can be impaired [15]. Cardiomyocytes are externally surrounded by a plasma membrane called the sarcolemma, which is formed by a bilayer lipid acting as a barrier during diffusion. The invagination of the sarcolemma in the cytoplasm forms the T-tubules and intercalated discs [16, 17]. Indeed, these invaginations of the sarcolemma bring LTCCs appoximal to the calcium discharge system of the sarcoplasmic reticulum (SR) [18] (**Figure 1-2**), which contributes to the strong regulation of the phenomenon of calcium-induced calcium release occurring during the action potential (AP) [19]. T-tubules are formed of several proteins involved in the mechanism of excitation-contraction couplings, such as L-type calcium channels (LTCCs), sodium-potassium ATPase, and sodium-calcium exchanger (NCX) [20, 21]. Therefore, the t-tubular system is very important for the proper contractility of the heart, and impairment in T-tubule protein might result in cardiac arrhythmia and dysfunctional cardiomyocyte contractility [22, 23], impairing the required cardiac output. It has also been shown that in heart failure, cardiomyocytes die through apoptosis and cannot be regenerated [24] limiting the ability of the heart to restore its function with the urgency in developing a suitable therapy for patients suffering from heart dysfunctionality.

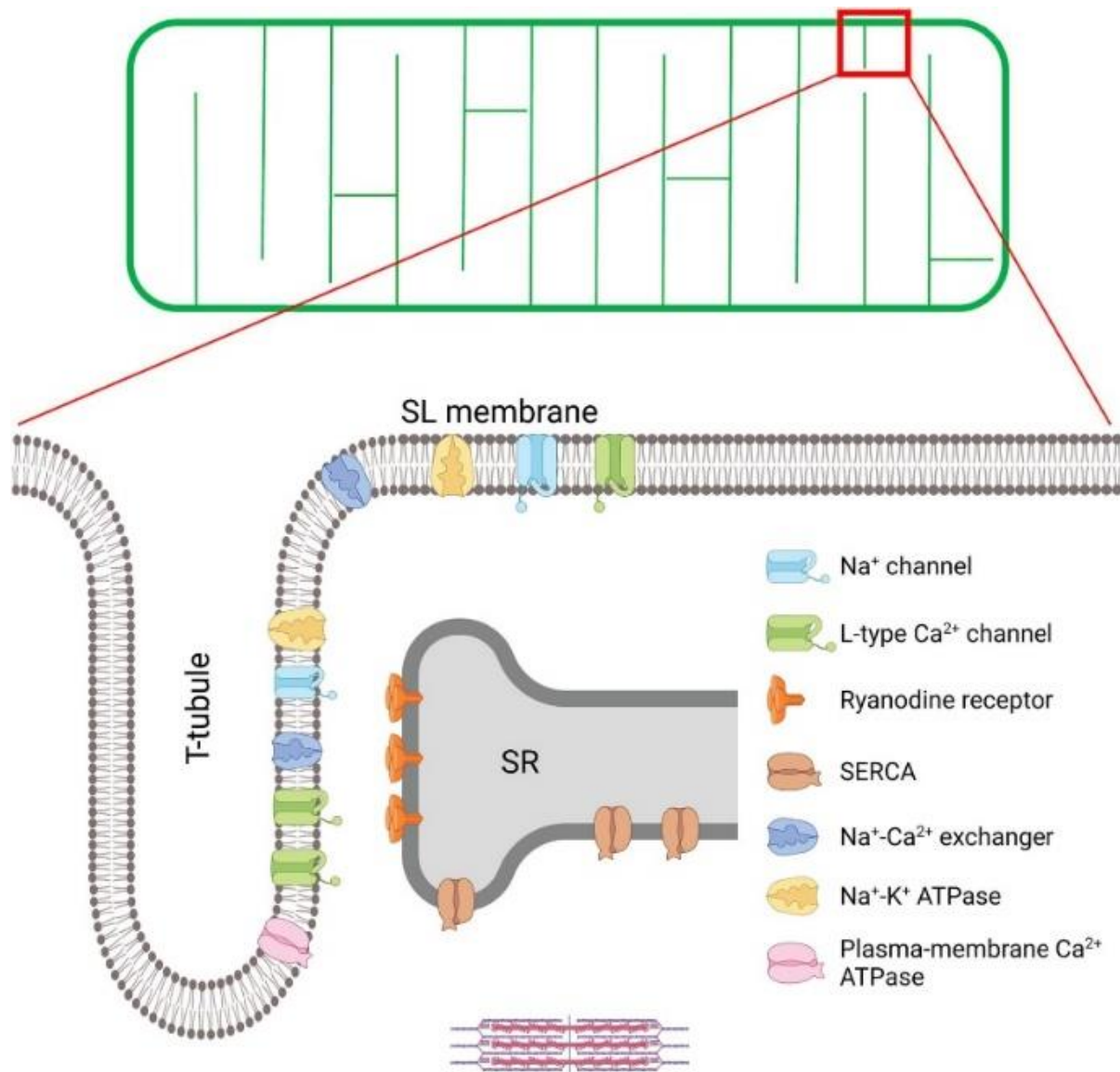


Figure 1-2. T-tubule structure and key proteins involved in excitation-contraction (EC) coupling in the cardiomyocytes.

A schematic overview of the t-tubule network is provided in the upper panel, while enlargement of the indicated region is provided below to illustrate the positioning of EC coupling proteins. EC coupling is initiated as Na^+ channels are opened, and the cell membrane depolarizes during the action potential. This depolarization triggers the opening of voltage-gated L-type Ca^{2+} channels (LTTCs) in the t-tubules and subsequent Ca^{2+} -induced Ca^{2+} release from the SR through the opening of Ryanodine Receptors (RyRs). This process occurs at specialized junctions called dyads, where LTTCs and RyRs are in close proximity. After released Ca^{2+} binds to the myofilaments to trigger contraction, Ca^{2+} is recycled into the SR by the sarcoendoplasmic reticulum ATPase (SERCA) and removed from the cell by the Na^+ - Ca^{2+} exchanger (NCX), and the plasma membrane Ca^{2+} ATPase. NCX activity is critically regulated by Na^+ levels, set by the Na^+ channel and the Na^+ - K^+ ATPase within t-tubules (Hong *et al.* 2017) [18].

1.4 Cardiac action potential and ion channels.

Cardiac action potential (CAP) results from a change in the membrane potential voltage across the cell membrane of cardiomyocytes. The AP is initiated by the so-called pacemakers with the sinus atrial (SA) node acting as the main precursor of the electrical activity of the heart [25]. The AP is subdivided into five phases: phase 0 (rapid AP upstroke), phase 1 (partial repolarization), phase 2 (plateau phase), phase 3 (final repolarization) and phase 4 (resting membrane potential) [26, 27]. Numerous ion channels contribute to these phases. At a certain threshold, the rapid sodium (Na^+) channel will open, allowing the influx of these ions into the cardiac cells, making the inner part of the cells more positive. The rapid upstroke of the AP is followed by a closure of the sodium channel and by an activation of potassium channels which begins at approximately -30 mV and which carries the transient outward current I_{to1} , resulting in a partial repolarization of the cells [28]. The depolarization caused by the rapid sodium channels also leads to the activation of voltage-gated calcium channels. Calcium will flow into the cells through these L-type calcium channels and will trigger the release of calcium from the sarcoplasmic reticulum (SR) via ryanodine receptors (RyRs), known as the calcium-induced-calcium release (CICR) phenomenon, which consequently empowers the contraction of the myocyte. Indeed, during phase 2, the released Ca^{2+} binds to troponin which enables sarcomere contraction. Permeability to calcium will slowly drop down and a plateau will be maintained through an inflow of Na^+ ions via the NCX pump. As phase 2 is ending, outward rectifier K channels (I_K) will be activated and K^+ will flow into the cells enabling the cells to repolarize and reach the resting potential which is maintained via the Na^+ - K^+ pump which enables an outflow and an inflow of the Na^+ and K^+ ions, respectively, in a ratio of 2 K^+ to 3 Na^+ [29] (**Figure 1-3**).

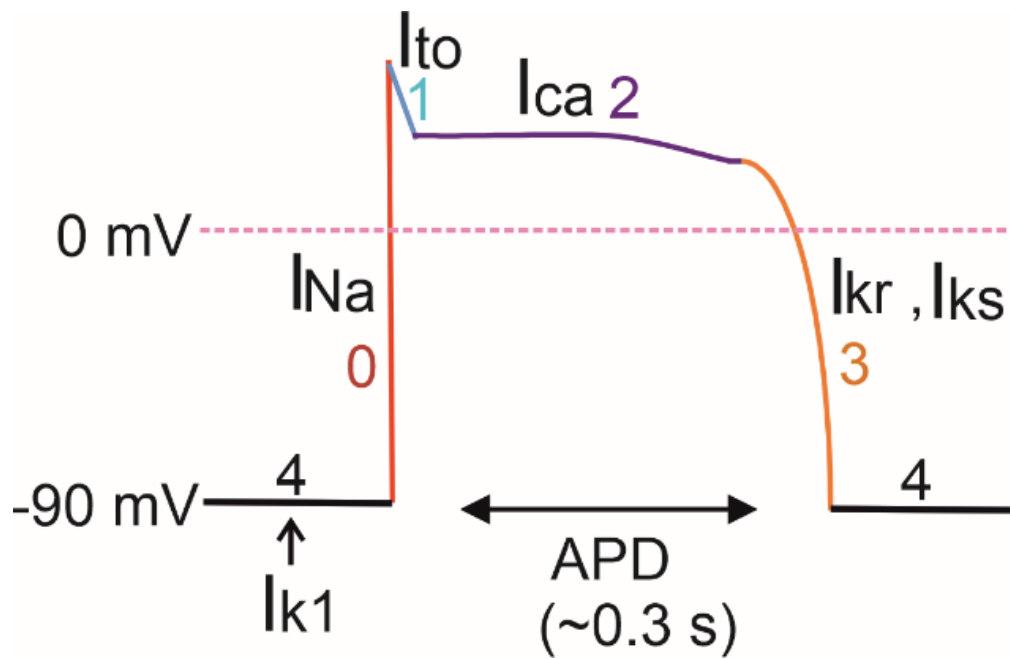


Figure 1-3. Cardiac Action Potential (CAP)

The cardiac action potential is subdivided into four phases: phase 0, phase 1, phase 2, phase 3 and phase 4. Phase 0 corresponds to the rapid AP upstroke driven by the Na^+ influx through the rapid sodium channel rendering the inner part of the cells more positive. At a certain threshold, the transient-outward potassium channels open and enable an outward potassium current (I_{to}) contributing to a partial repolarization of the cells. This will create a modest decrease in the membrane's electrochemical potential that trigger the initiation of phase two, therefore allowing the contraction of the cell muscle through a process named calcium-induced-calcium release (CICR) which corresponds to the plateau phase. The plateau phase or phase 2 is maintained mainly by the antagonism between delayed rectifier potassium channels (I_{Ks}) and L-type calcium channels. The permeability to calcium will slowly drop down due to the closure of the calcium channel and the extrusion of the calcium out of the cytosol. K^+ currents will eventually prevail, leading to repolarization of the cell (phase 3) which reaches the resting potential (phase 4).

Adapted from (*Renganathan et al., 2017*) [30]

In a failing heart, AP might be impaired and cells might fail to depolarize or repolarize properly and present signs of trigger arrhythmia, such as early afterdepolarizations (EADs) or delay after depolarizations (DADs) [31]. The latter author has proposed a mechanism behind these arrhythmogenic features which is illustrated in **Figure 1-4**. Indeed, in his review, *Bers* postulated that in cardiac myocytes an enhanced Ca^{2+} release from the SR might activate the inward NCX current leading to DADs and the phosphorylation of calcium and sodium channel by calcium-calmodulin-dependent protein kinase (CaMKII) could alter the I_{Ca} and I_{Na} responsible for EADs observed during arrhythmia [31].

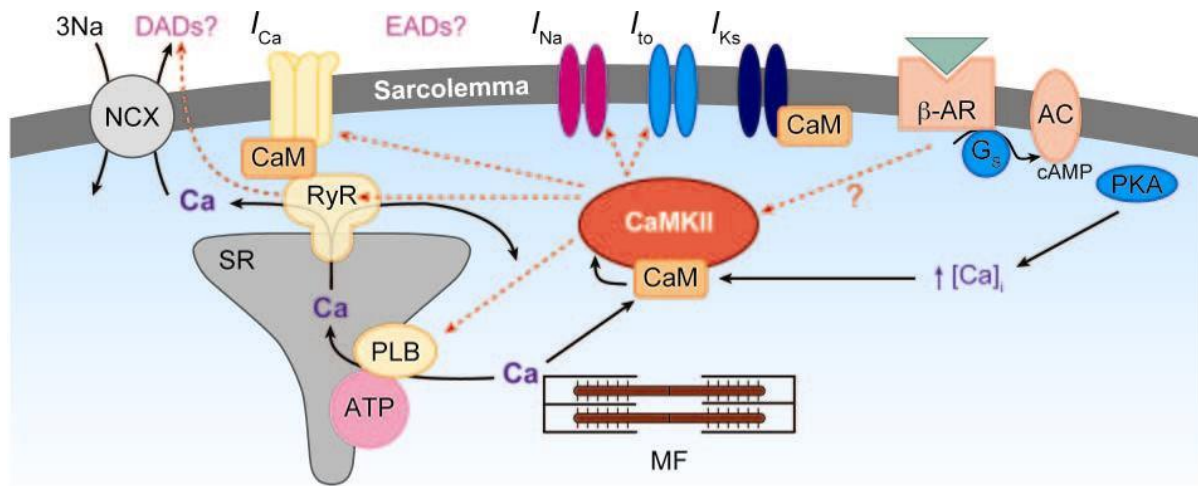


Figure 1-4. Ca-dependent signaling to cardiac myocyte ion channels

Ca entry via I_{Ca} activates sarcoplasmic reticulum (SR) Ca release via the ryanodine receptor (RyR), resulting in the activation of contraction. SR Ca uptake via the SR Ca-ATPase (ATP) and extrusion via Na/Ca exchange (NCX) allow relaxation. Calcium-calmodulin-dependent protein kinase (CaMKII) can phosphorylate phospholamban (PLB), causing enhanced SR Ca uptake, and also activates inward NCX current and arrhythmogenic delayed afterdepolarization (DADs). CaMKII can also phosphorylate Ca and Na channel subunits, thereby altering I_{Ca} and I_{Na} gating and prolonging APD, and increasing the propensity for early afterdepolarizations (EADs). CaMKII can also modulate I_{to} , whereas calmodulin (CaM) itself can modulate RyR, I_{Ca} , and I_{Ks} gating. Activation of β -adrenergic receptors (β -AR) activates adenylyl cyclase (AC) to produce cyclic AMP (cAMP) and activate PKA. PKA phosphorylates PLB and regulates SR Ca uptake, I_{Ca} , I_{Ks} , and RyR, with a net increase in Ca transient amplitude. This is accepted to contribute to CaM and CaMKII activation, but there may also be a more direct, Ca-independent pathway by which β -AR can activate CaMKII. MF, myofilaments. (Bers, DM. 2008) [31].

Ion permeation and gating are the two basic characteristics of ion channels [27]. Gating channels are subdivided into three subclasses: voltage-dependent which rests on membrane voltage changes, ligand-dependent which is determined by the binding of a ligand to a receptor, or mechano-sensitive which relies on mechanically induced changes in channel conductivity [32]. All these three types of gating channels are found in the cardiac muscle machinery, whereby voltage-gated ion channels are the main channels involved in the mechanism of contraction of cardiac cells. During AP, ion channels are found in three states: open, closed inactive (refractory state), and closed resting state (resting membrane potential) [33]. These properties of ion channels to open and close are a response to chemical or mechanical signals or changes in the membrane voltage of the cells. Voltage-dependent ion channels are pore-forming proteins allowing a selective flow of ions. They are tetrameric proteins made out of α and β subunits, and six α -helical transmembrane segments (S1-S6), with the S4 segment acting

as the voltage sensor of the channel and S5-S6 as the selective filter [34] (Figure 1-4). Compared to the Nav1.5 channel, voltage-gated K⁺ channels are highly selective and also present a large conductivity, which is crucial to bringing back excitable cells in their resting state after depolarization [35]. Mutation on these segments might influence the permeability of ions through the channel [36, 37] which might result in an improper ion transient during AP responsible for impaired cardiac function.

1.5 Cardiac cells: gene expression and related pathologies

Cardiomyogenesis is defined as the process of cardiomyocyte formation. During cardiomyogenesis, the phenomenon of gastrulation takes place in which ectoderm, mesoderm and endoderm layers are formed. The early stages of cardiogenesis are controlled by three main proteins: bone morphogenic proteins (BMPs), the Wingless/INT proteins (WNTs) and the fibroblast growth factors (FGFs) [38]. During *in-vitro* studies, small molecules modulating Wnt activation and inactivation have been used to stimulate and inhibit the Wnt signaling pathway [39], enabling, therefore, the process of cardiogenesis. During cardiomyocyte formation, different genes crucial for the proper functionality of the myocardium are expressed. We have for example *TTN*, *MYBPC3*, *TNNT2*, *MYH7*, *MYL2* encoding sarcomeric proteins and *RyR2*, *PLN*, or *SLC8A1* encoding proteins involved in the mechanisms of excitation-contraction coupling [40]. The proper transcription and translation of those genes are required to ensure adequate functionality of the heart. A study has shown that during cardiac diseases, cis-regulatory elements (cCREs) being in control of these genes can be affected leading, therefore, to a dysregulated gene expression as is the case for *KCNH2/HERG* involved in the repolarisation phase during AP [41]. Moreover, during their study on healthy and failing hearts of cadavers, *Luo et al.* revealed that in a failing heart, some genes such as *MYH7*, *FHL2*, *TNNC1*, *TNNI3* and *HCN4* are dysregulated and the latter might be responsible for distinct pathology: dilated cardiomyopathy, Long QT Syndrome (LQTS), coronary artery disease (CAD) and other cardiac diseases [42]. It has also been postulated that during cardiac diseases, L-type and T-type calcium channels might be dysregulated [43, 44]. Indeed, T-type Ca²⁺ channels are predominantly expressed during heart development [45], but in the adult heart they are mostly localized in the pacemaker and are re-expressed in cardiac muscle cells during heart defect [44]. These studies unveil that pathophysiological mechanisms occurring in failing hearts could be the consequence of dysregulated gene expression, which requires additional investigation.

1.6 *SCN5A* gene and disease-related mutations

The sodium channels are responsible for the generation and propagation of AP [46, 47]. They were first discovered in jellyfish, and are described as integral membrane proteins consisting of various α and β subunits with the α subunit mainly involved in the functionality of the cells [48]. The sodium channel is located on chromosome 3p21 and is made up of 28 exons [49]. Ten α subunits have been identified, among which only nine have been described to be functional [50]. The sodium channel (Nav) is distinctly distributed in the organism. For example, $\text{Nav}1.8$ and $\text{Nav}1.9$ are found principally in the peripheral neurons, $\text{Nav}1.4$ is expressed in skeletal muscle and $\text{Nav}1.5$ is mainly expressed in cardiac muscle cells [51]. A study using a mouse heart revealed that this channel with some of its subunits, such as $\beta1$ and/or $\beta4$, are localized in the intercalated discs [52] and, just like the conventional voltage-gated channel, the α -subunit of $\text{Nav}1.5$ consists of four repeats (I, II, III, IV) each of them containing six membrane-spanning segments (S1-S6), representing the main functional subunit of the channel. Furthermore, β -subunits are very important for a fast kinetic and fast inactivation of the channel [53, 54]. S4 carries charged residues, and therefore acts as a sensor for voltage changes, and S5-S6 forms the pore conducting sodium channel [48] and the selective filter [34]. Each end of the S6 segments of each domain carries one amino acid residue forming the activation gate (**Figure 1-5**). The selectivity filter is composed of distinct amino acids in the four domains namely: aspartate, glutamate, lysine, and alanine in DI-DIV, respectively, whose mutation might lead to the dysfunctionality of the filter [55].

Mutations on $\text{Nav}1.5$ channel subtypes cause diseases called channelopathies, which can be inherited or acquired. As the sodium channel is crucial for the initiation and propagation of the AP, a defect in this gene might consequently affect the functional states of the channel (open, close inactive, and close) or the conduction velocity, which in turn will affect the normal functionality of the heart. Several diseases have been associated with the mutation of the $\text{Nav}1.5$ channel among which are: Brugada syndrome (BrS), long QT syndrome type 3 (LQTS3), atrial fibrillation (AF), sudden infant death syndrome (SIDS), sick sinus syndrome (SSS) [56] and many more. Although channelopathies have been mainly described as electrical diseases without structural anomalies of the myocardium, recent affirmation reveals that some patients harboring *SCN5A* present abnormalities in the structure of their cardiac muscle [57], but with vague fundamental mechanisms [58]. Recent studies postulated that during heart failure, sodium channel downregulation is the consequence of the increase of intracellular calcium [59]. However, another study postulated that high intercellular calcium is beneficial

for patients presenting a gain-of-function of the channel such as LQTS3 by regulating the I_{NaL} and enabling a proper repolarization [60]. However, this hypothesis does not apply to all patients, as demonstrated by the study of *Abdelsayed et al.* after performing the functional analysis with cells of patients carrying mixed syndromes, which shows that in some cases increasing the cytosolic calcium may promote gain-of-function [61]. Additionally, studies demonstrated that in *SCN5A* associated with loss-of-function mutation, disease phenotype severity might be affected by multiple variants within or between patients [62, 63] presenting a considerable challenge for the therapy approach.

Outside cell

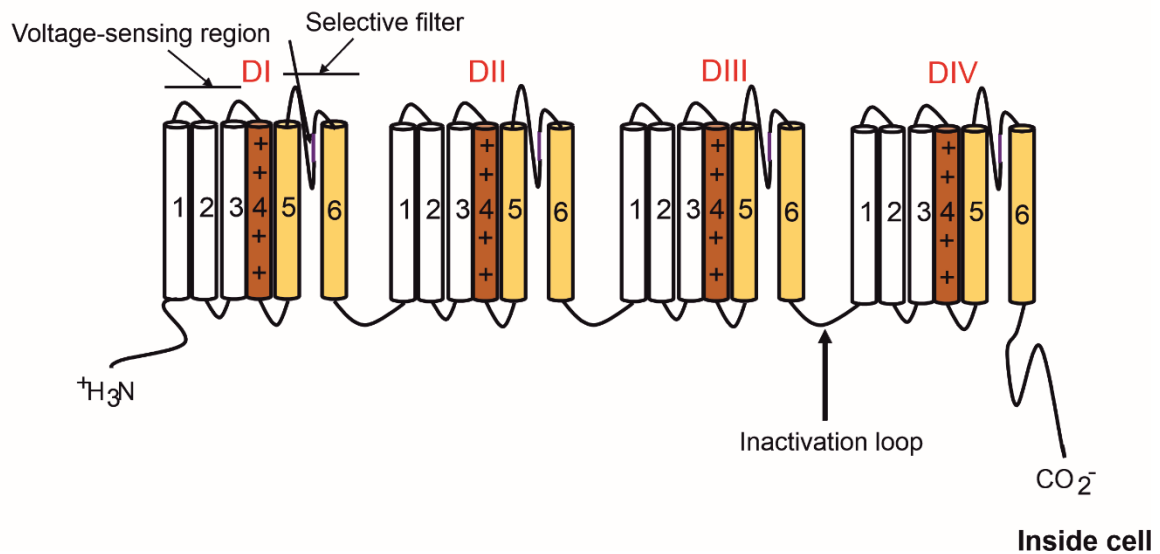


Figure 1-5. Voltage-gated sodium channel

The voltage-gated sodium channel consists of four domains and each domain containing six transmembrane alpha-helices (S1-S6). S1-S6 represents the main functional subunit of the channel. S1-S4 builds the voltage-sensing domain, with S4 acting as a sensor during voltage changes because of its charged residues. S5-S6 forms the pore conducting sodium channel and the selective filter. The inactivation loop that is required to close the channel during fast inactivation is localized between segment 6 (S6) of domain three (DIII) and segment 1 (S1) of domain four (DIV). Adapted from (*de Lera Ruiz et al. 2015*) [55]

1.7 Pharmacodynamics of antiarrhythmic drugs on Nav1.5 channel: Case of Lidocaine

According to their specific electrical effects on the myocardium, antiarrhythmic medications can be categorized into Vaughan Williams classes (I-IV) [64]. The requirements for classification include ion channel blocking (classes I and IV), receptor interaction (class II), and changes in electrophysiological parameters (class III) [65]. Ion sodium blockers such as the Nav1.5 channel blockers are mainly used for antiarrhythmic, antiepileptic or anaesthetic

therapy [55]. These drugs will block the channel and therefore suppress the spontaneous depolarization of the cardiac muscle cells. Studies of mutagenesis revealed that the binding site of these drugs is located on the S6 segments of the DI, III, and IV of the channel [66-68]. Nav1.5 channel binding sites and inhibition mechanisms are diverse [69]. However, F1760 (Phenylalanine at position 1760) localized at the S6 segment of the fourth domain has been described as an important binding site of class Ib antiarrhythmics drugs (AAD) [70], such as lidocaine, tocainide or mexiletine. Other studies reveal that T206 and F203 are also important binding sites of AADs [71]. Indeed, the class Ib drug will form with the phenylalanine residue tight cation- π interactions [72]. Cation- π interaction is a non-covalent bonding engaging a positively charged sidechain (Arg, Lys) to an anion (Phe, Tyr, Trp) building a strong interaction between the protein and the ligand [73, 74]. However, it has been demonstrated that compared to Arg, Lys form with the negatively charged sidechain a weaker interaction [75].

In opposition to class Ia and class Ic, the main property of class Ib AAD is to shorten the AP [76, 77] by blocking the sodium channel, which interacts weakly with the channel compared to class Ia and Ic [78]. AAD blocks the channel in a use-dependent block manner, which means that after the addition of the drug, the repetitive depolarization will initiate further blocks as illustrated in **Figure 1-6** [79]. The stability of the voltage-sensor segment S4 DIII-DIV has been described as fundamental for a high-affinity of the class Ib AADs (lidocaine) to the receptor, and this was regardless of the presence of the fast inactivation gate, whereby this latter is important to the channel to achieve its highest-affinity conformation [80]. Moreover, slow inactivation of the Nav1.5 channel has also been proposed as a mechanism of high affinity between lidocaine and the receptor on the channel [81]. Mutation of the channel might hamper the fast inactivation state promoting a disturbance in the AAD binding. Indeed, it has been postulated that for the drug to bind to the channel receptor, it needs to be in an open [82] or inactivated state [83, 84]. Indeed, in his review, *Dhein* revealed that for lidocaine to bind to the Nav channel, this latter should be in an open state allowing the drug to bind to the inactivated state of the channel [85]. Lidocaine will lose its affinity to the channel when this latter switches to its resting state, which causes the drug to detach from the channel. Despite all these findings, the blocking mechanism of sodium blockers is still elusive. Based on several experimental protocols, three distinct phenomena have been observed. The closed (resting) channel block is detected when channels are activated by infrequent membrane depolarizations; the frequency-dependent block which is related to a rise of the blocking effect when the stimulus frequency

is increased and, finally, the maximal block that occurs after a prolonged membrane depolarization inducing the steady-state inactivation of the channels [86].

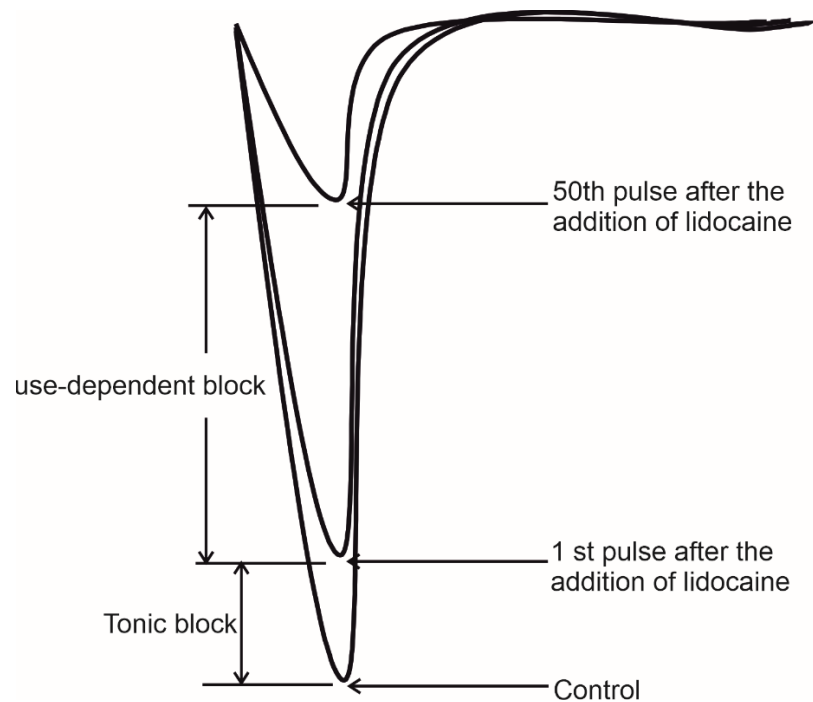


Figure 1-6. Picture of sodium current after a repetitive block by lidocaine.

Recordings show control I_{Na} and then I_{Na} after the drug was added for the 1st and 50th depolarizations of a pulse train. Holding potential, -140; Depolarizing step to 20 mV. (Adapted from Zipes *et al.* 2009) [79]

Although drugs of the same class share the same mechanism of action according to the classification of Vaughan-Williams [87], they might have different pharmacodynamics and pharmacokinetics. Indeed, it has been shown that the half-time of lidocaine elimination from the plasma is shorter when compared to mexiletine and tocainide [88], advocating that a rapid response is to be expected during treatment with this drug compared to its counterparts. However, this does not tell us much regarding the effectiveness of the drug. Therefore, in-vitro studies might further help to screen these drugs and further provide information on their safety for patients.

1.8 In-vitro studies of cardiac diseases

Heart diseases are disorders of the heart and blood vessels' functionality, which can be congenital or acquired. Numerous diseases can be listed: coronary artery disease and ischemic stroke [89], congenital diseases that can be due to channelopathies such as (LQTS, BrS, SSS, or CPVT), or a malformation of the heart [90]. The development of the cardiac tissue model is

a new technology used to investigate the pathophysiological mechanisms underlying numerous cardiac diseases using engineering human induced pluripotent stem cells (hiPSCs). The aim of modelling cardiac tissue (hiPSC-CMs) is to devise models that mimic human cardiac muscle cells and provide data that can be transferable to the clinic [91-93]. Moreover, hiPSC-CMs have enabled scientists as well as physicians to better comprehend the mechanism of action of different AADs, and therefore ameliorate the life condition of patients. Indeed, AADs can show considerable side effects in patients [94], which might even be fatal. Thus, tissue models are useful, not only for a better understanding of molecular, cellular, or physiological mechanisms involved in heart diseases but also help to develop and screen the side effects of potential drugs [94, 95]. However, this platform is still offering some challenges due to the inability of the cells to fully mimic the native adult cardiac cells. Moreover, the in-vitro model study cannot offer all the physiological properties of in situ cells.

1.8.1 Generation of human-induced pluripotent stem cells (hiPSCs)

Stem cells can self-renew and differentiate into all cell types such as neurons, macrophages, liver, kidney and myocytes. Due to this property of stem cells to differentiate into several cells which are necessary for ex vivo studies, *Takahashi and Yamanaka* have designed a protocol to bring back mature adult cells (mouse embryonic and mature fibroblasts) into their pluripotency state using four factors, *Act3/4*, *Sox2*, *c-Myc* and *Klf4* [96]. Later, they could prove that this technology is also applicable for human fibroblasts [97], which could differentiate into the three germ layers formed during embryonic development (ectoderm, mesoderm, and endoderm) and teratomas. These cells are of high importance in regenerative medicine because of their potential to retain the genetic background of the patients. Moreover, they offer a more precise comprehension of the disease mechanism in basic research compared to animal models, which are different in their physiology and could not be efficiently transferred to humans. HiPSCs also solved the ethical problem linked with the decimation of human embryos (**Figure 1-7**) [98].

Nevertheless, the practical use of the cells in clinical application is controversial due to the oncogenesis of some transcriptor factors such as *c-Myc*. HiPSCs have been primarily reprogramed using a retroviral or lentiviral vector system, which is described to be an inefficient and slow procedure [99, 100]. In addition to this, it is not adequate for the safety of the DNA because of the mutagenesis linked to its application. *Nakagawa et al.* have proposed another method omitting the c-Myc retrovirus [101] and this protocol offers a low efficiency in cell reprogramming despite the high quality of obtained iPSC cells. Therefore, other tools

have been proposed to deliver the transcription factors in the cells among which we have: transient plasmid, synthetic mRNA, and purified recombinant protein from *Escherichia coli* [102]. Indeed, *Huangfu et al.* could prove that using DNA methyltransferase and valproic acid (VPA) inhibitors might considerably improve the efficiency of the reprogramming, and this without the introduction of *c-Myc* [99]. Other reprogramming protocols based on small molecules as well as transdifferentiation have been studied and proposed to be more accurate and efficient compared to other protocols [103].

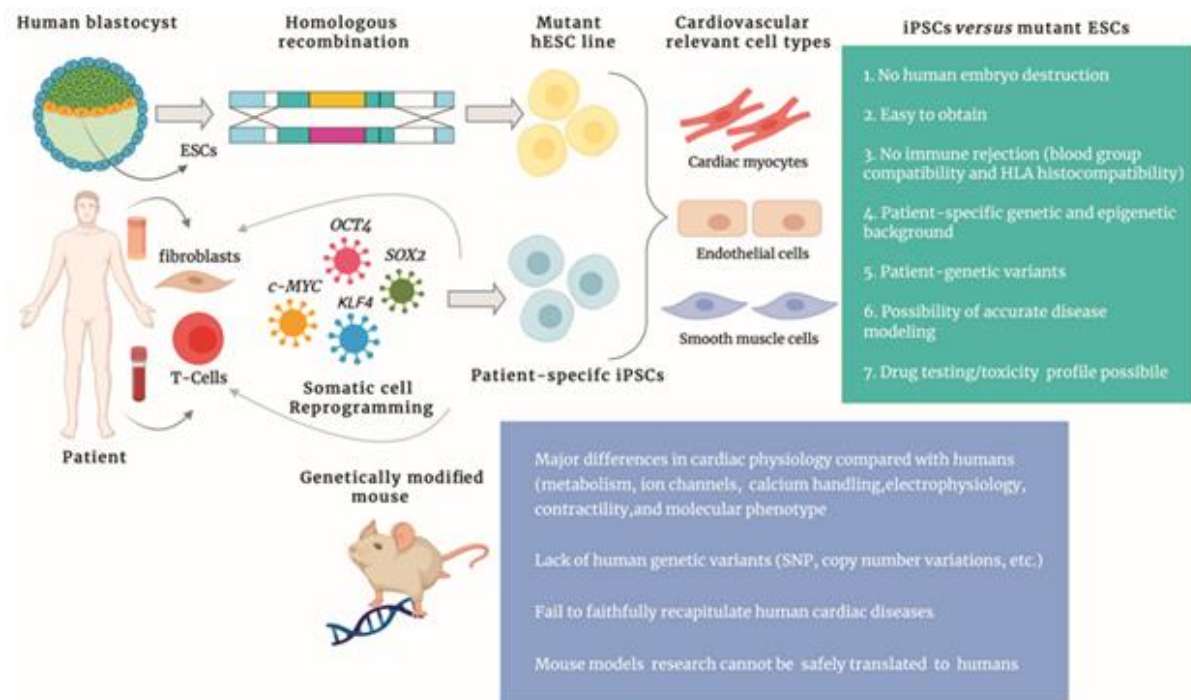


Figure 1-7. Advantages of induced pluripotent stem cells (iPSCs) over mutant embryonic stem cells (ESCs) and genetically modified mouse models

Embryonic stem cells (ESCs) originated from human embryos while induced-pluripotent stem cells are obtained from reprogrammed adult somatic cells such as skin fibroblasts, peripheral blood cells, urine epithelial cells, etc. Contrary to ESCs, iPSCs are easy to obtain and they also resolve the moral dilemma associated with the killing of human embryos. They maintain the genetic make-up of the person from whence they were produced preventing an immunological reaction. In comparison to the mouse model, studies with iPSCs can be safely translated to humans and constitute a trustworthy source of transplantable cells due to their human origin (*Parrotta et al. 2020*) [98].

1.8.2 Differentiation of hiPSCs into cardiomyocytes and functional properties

hiPSC-derived cardiomyocytes have enabled scientists as well as physicians to better access the pathophysiology underlying cardiac diseases. The differentiation of hiPSCs into hiPSC-CMs is based on the activation and the inhibition of the wingless (Wnt) signalling using, for

example, the small molecule CHIR and different Wnt inhibitors [104, 105]. The role of Wnt signalling has been described in **Figure 1-8** below [106]. Thus, Wnt is necessary to diminish the cell's pluripotency and support mesendodermal commitment when differentiating hiPSCs. To achieve this effect, the Wnt activation should be properly monitored as speculated by the latter author.

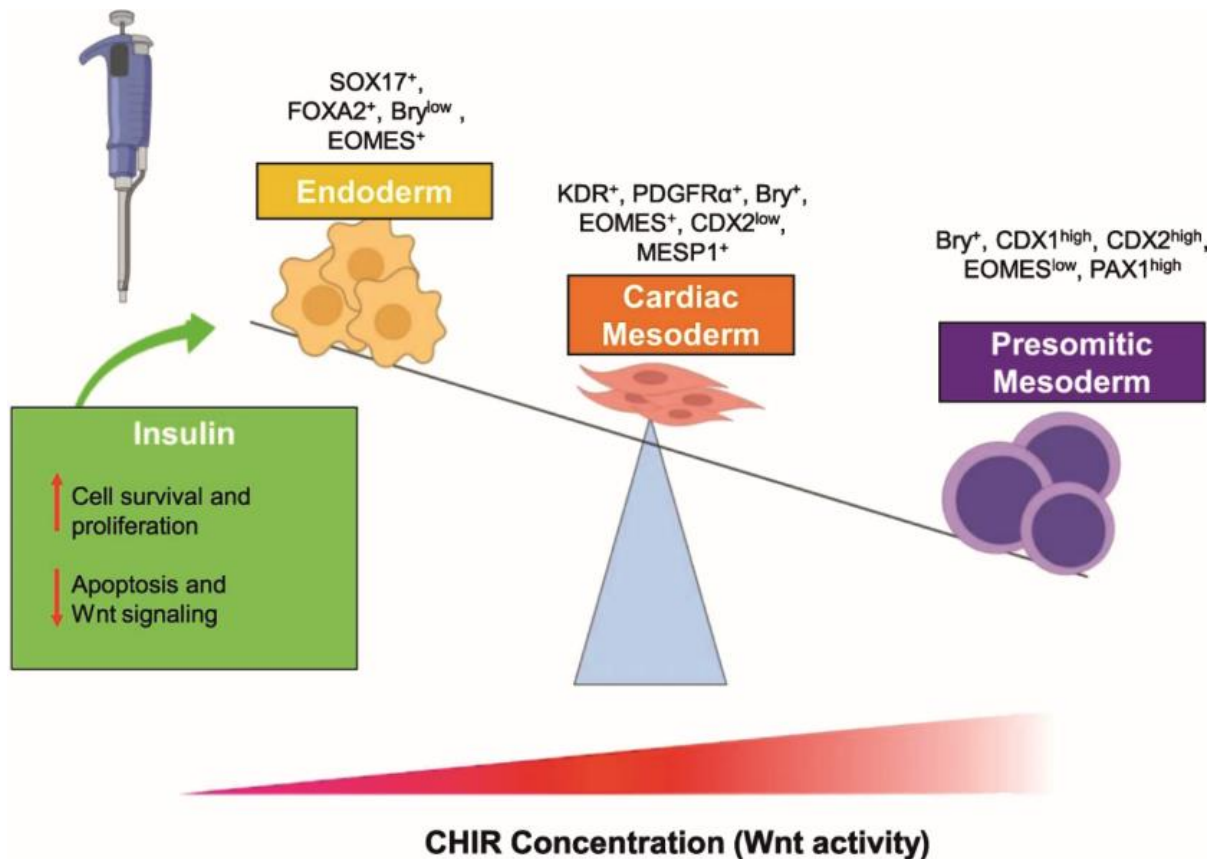


Figure 1-8. Deciphering role of Wnt signalling in cardiac mesoderm and cardiomyocyte differentiation from Human iPSCs: four-dimensional control of Wnt pathway for hiPSC-CMs differentiation

The role of Wnt signalling in hiPSC-CM differentiation. Wnt signalling is required to reduce pluripotency, limit endodermal specification (SOX17, FOXA2) and promote mesendodermal (Bry, EOMES) commitment in differentiating hiPSCs; however, excessive Wnt activation directs the cells toward the paraxial/presomitic mesoderm lineage (CDX1, CDX2, PAX1). The Gi(I/M)Wi protocol enables researchers to balance these antagonistic effects of Wnt activity for maximum cardiac mesodermal specification and hiPSC-CM yield by adjusting the CHIR initiation and maintenance doses for different hiPSC lines (e.g., hciPSCs or hdiPSCs) and culture systems (e.g., monolayer or suspension), or to incorporate other factors such as insulin, which increases cell survival and proliferation but partially limits Wnt activity (Zhao *et al.* 2019) [106].

To date, different protocols have been proposed to improve the maturity and the purity of cardiomyocytes, representing one of the limitations of the studies of disease models in-vitro. Prolonged cell culture, co-culture, electrical or mechanical excitation, and chemical

modulation have been proposed as a means of overcoming the immature phenotypes [107]. *Lewandowski et al.* for example demonstrated that, compared to day 20, day 40 cardiomyocytes highlight some features of adult cardiomyocytes in molecular as well as physiological aspects [108]. Moreover, *Biendarra-Tiegs* and collaborators previously demonstrated a clear difference in ion channel expression as well as in electrophysiology of hiPSC-CMs between D12 and D40 (**Figure 1-9**) [109]. Mechanical stretch used in terms of the mechanical stimulus also showed promising results in pluripotent stem cell-derived cardiomyocytes (PSC-CMs) maturation [110]. However, all the above-mentioned techniques still need to be improved to reach a level that is acceptable for clinical use.

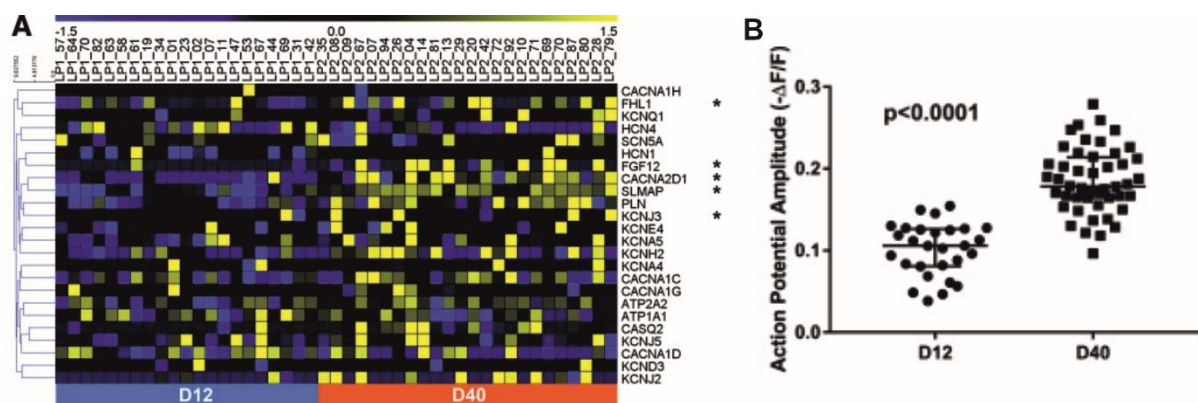


Figure 1-9. Maturation of hiPSC-CMs clearly revealed differences in several ion channel regulators and cardiac-derived cells' electrophysiology properties

A, Heatmap representation of expression patterns for representative electrophysiology- and calcium handling-associated genes in cardiomyocytes. Genes with significantly different expressions ($\log_2\text{FC} > 2$ and $P < 0.05$) between days 12 and 40 are marked with an asterisk. **B**, AP amplitude evaluated from D12 and D40 populations before submission for sequencing. P values were calculated by either a student's t-test or Mann–Whitney U test. Data are reported as median \pm interquartile range. (*Biendarra-Tiegs et al. 2019*) [109].

Adherent cell culture and 3D differentiation are distinct protocols used to produce derived cardiomyocytes with >90% purity [104]. Metabolic selection such as glucose deprivation is one of the techniques that has been used to date to provide cardiomyocytes with high efficacy [111, 112]. Nonetheless, these protocols give a mixed population of cardiac cells subtypes: atrial-like, ventricular-like or nodal-like [113], which represent another barrier to clinical application. Despite all these challenges, human-induced pluripotent stem cells-derived cardiomyocytes (hiPSC-CMs) represent a good tool to investigate the molecular spectrum and access the pathophysiology of cardiac diseases because, compared to animal models, they can mimic cardiac functionality in a suitable way [114]. Moreover, ion channels that are implicated

in the process of AP generation and regulation have been stated in those cells [115]. hiPSC-CMs are also a powerful tool for drug discovery and toxicity [116] that might be helpful to improve personalized therapy (**Figure 1-10**) [117].

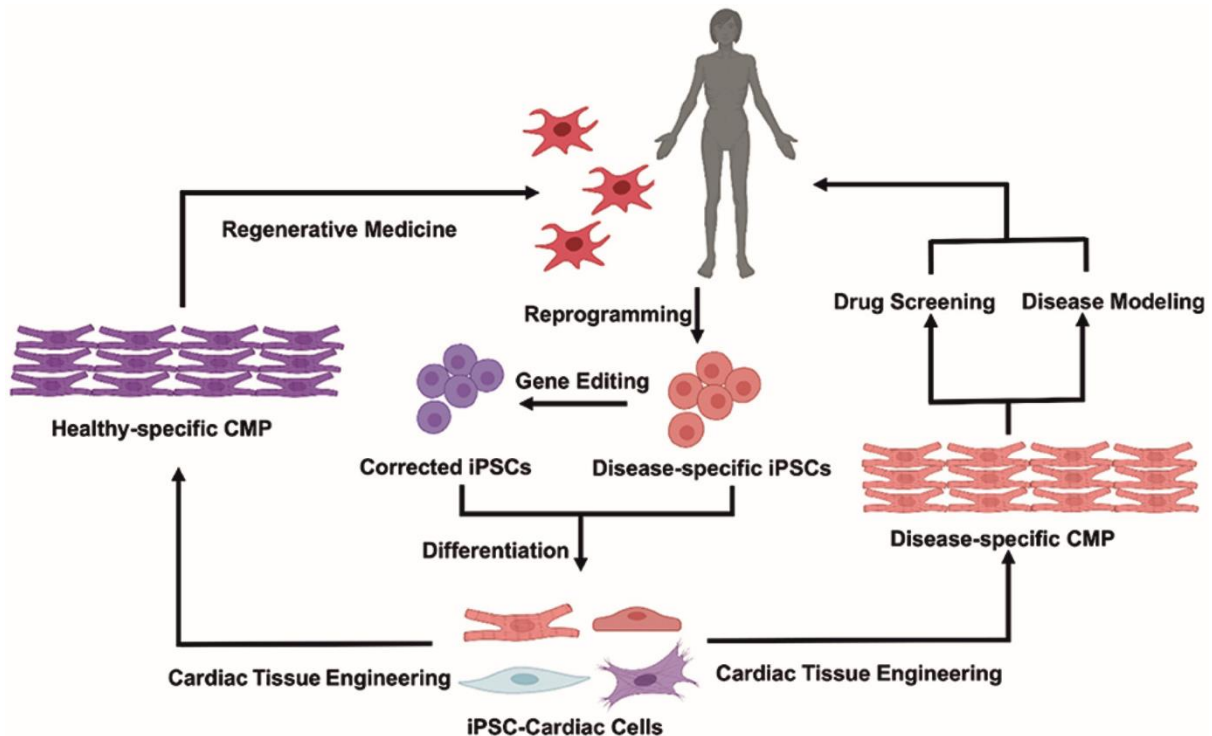


Figure 1-10. Cardiac tissue engineering and its applications.

Patient-specific iPSC can be derived by reprogramming somatic cells from the patient, in healthy vs. diseased states, and used to generate a variety of functional cardiovascular cells. The incorporation of cells within specifically tuned 3D biomaterial systems will enable the fabrication of the human cardiac muscle patch (hCMP) that could be used either in a variety of in vitro applications [drug screening and disease modelling (Right)] or as a cardiac patch for in vivo regenerative therapies (Left) (Wang *et al.* 2021) [117].

1.9 Channelopathies associated with cardiac dysfunctionality: the case of LQTS3 and BrS

1.9.1 Long QT Syndrome type 3 (LQTS3)

LQTS represents a possible cardiac cause of some cases of sudden infant death [118]. LQTS is a congenital disease characterized by a prolonged QT interval displaying the underlying marker for the disease. Nevertheless, studies have shown that QT intervals can overlap between LQTS patients and healthy individuals, and T-wave morphology could help physicians to ameliorate patients' diagnostic [119] and classify LQTS subtypes [120]. LQTS prevalence is estimated to be 1:2000 [121] live births. Among all the LQTS subtypes, types 1, 2, and 3 are the more common forms found in the population [122], with LQTS3 representing the more

lethal form [123]. Sodium channel mutation (*SCN5A*) is the main cause of LQTS3, causing a gain-of-function of the channel, and it appears that mutations underpinning LQTS3 are the only ones that may link sinus bradycardia to cardiac events [124]. The disability of the Nav to inactivate hampers the repolarization [125], which prolonged the AP.

Most *SCN5A* mutations are missense mutations found in Nav1.5 areas that are involved in fast inactivation, such as the cytoplasmic loops between the S4 and S5 segments, or in regions stabilizing the fast inactivation like the C-terminus [126]. Therefore, mutation at this site of the channel might explain the delay from channel inactivation as well as AP prolongation observed during LQTS3, and in some cases trigger mechanism of arrhythmia, such as early afterdepolarizations (EADs) occurred [127]. Some studies have demonstrated that some polymorphisms such as H558R could rescue the disease phenotype and allow a proper Nav current [128]. In fact, in their study *Ye and his associate* used different clones carrying an *SCN5A*-M1766L mutation and observed that the clone carrying the polymorphism H558R present a normal current. Moreover, H558R could restore the defect current to normal when co-expressed in another clone carrying the *SCN5A*-M1766L. However, the restoration of the pathologic phenotype by H558R is not applied to all mutations. Indeed, another study revealed that the polymorphism H558R did not have a significant impact on the *SCN5A*_E1784K phenotype [129]. These studies show the complexity of the disease physiology due to the different phenotypes associated with the several mutations, rendering the diagnostic and the therapy of LQTS3 more challenging.

Contrary to other congenital LQTS, LQTS3 therapy is based on sodium channel blockers [130, 131]. Blockers of the sodium channel able to block both the late (I_{NaL}) and the fast sodium (I_{Na}) inward current could be useful for patients presenting both gain-of-function and loss-of-function of the channel [132]. Beta-blockers have also been proposed as drug candidates for LQTS3 but the outcome was contradictory, and the author related these controversial findings to the genotype background of the patients [133] suggesting that drug therapy should be patient-specific. Patients that are not responding to drug therapy can receive an implantable cardioverter-defibrillator through surgical intervention which is not without any risk, or which can also present some disadvantages in the future [131].

1.9.2 Brugada Syndrome (BrS)

BrS is highly prevalent in Asia [134]. This rare disease mainly affects more men than women [135], in which the latter risk of arrhythmic events appears to also be less [136]. Three types

of BrS have been described, whereby only type one is considered the true form of the disease characterized by an ST-segment elevation in the right precordial leads of the electrocardiogram (ECG) [137]. This is its distinctive ECG pattern, which can occur spontaneously or be revealed by medicines [138]. Nevertheless, the electrocardiographic features of BrS are age-dependent and might only be detectable in subjects above 5 years of age [139]. *SCN5A* gene mutation is the main cause of BrS leading to the loss of function of the Nav1.5 channel [140]. Contrary to LQTS3, many mutations in BrS cause sodium channel truncation due to a frameshift in the DNA sequence by the premature appearance of a stop codon [79]. This suggests that loss of function of the channel could be associated with a reduced expression of the sodium channel. However, missense mutations leading to BrS showed that loss of function of the Nav channel is associated with defective protein trafficking at the cell surface [141, 142]. In some cases, the reduced ion current might reflect the fast inactivation of the channel or altered channel kinetic during AP [143, 144]. However, the magnitude of the electrophysiological anomalies in BrS is largely determined by the patient's genetic background [145]. This might explain the uncertain pathophysiological outcome arising during the disease.

Improper repolarisation or depolarisation [146] or an aberrant neural crest expression during right ventricular outflow tract (RVOT) [147] has been proposed to explain the cellular mechanism that occurs during BrS (**Figure 1-11**). Indeed, according to the repolarization theory, the BrS phenotype is principally caused by variable APD shortening across the myocardial wall. The depolarization theory, on the contrary, states that arrhythmogenesis is caused by a slower upstroke of phase 0 and a subsequent decrease in the conduction velocity (CV) of the AP [148]. This latter author also proposed that the third mechanism occurring during BrS is due to structural abnormalities of the RVOT, which consequently increase the current-load mismatch. Nonetheless, further studies need to be done to truly understand the pathophysiology underpinning the disease.

BrS therapy is based on anti-arrhythmic drugs and implantable cardioverter-defibrillator (ICD) for patients at risk of repetitive sudden cardiac death after drug therapy [146]. RVOT epicardium ablation is another therapy that has been developed to treat patients exposed to frequent ICD-shocks [149]. However, the risk of events in BrS is not genuinely understood. Indeed, different subtypes of the syndrome may exist with varying levels of arrhythmic risk, and identifying them may result in better care for BrS patients [150].

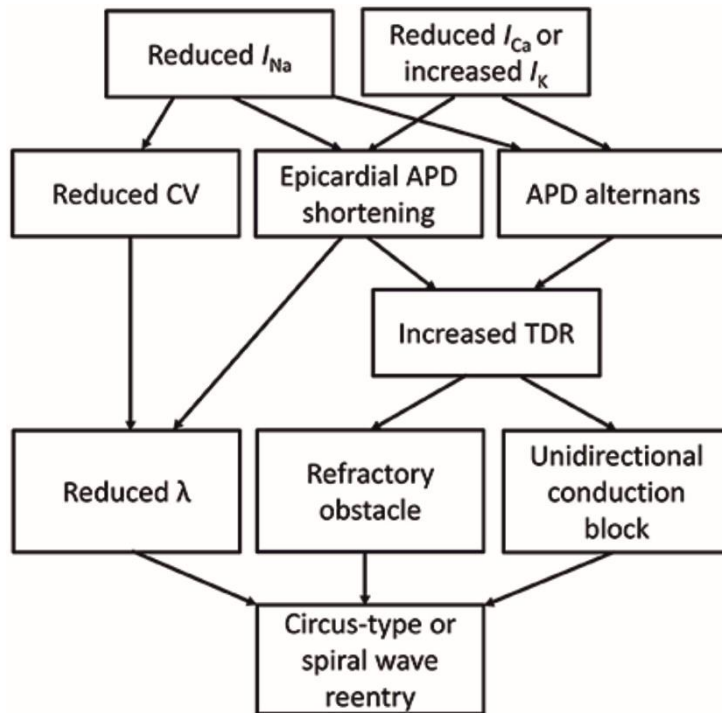


Figure 1-11. Molecular and electrophysiological mechanisms underlying arrhythmogenesis in Brugada syndrome.

CV (Conduction Velocity); APD (Action Potential Duration); TDR (Terminal Density Reversal). (*Elizari et al. 2007*) [147]

1.9.3 Overlapping phenotype between LQTS3 and BrS

SCN5A gene mutation is the main cause of LQTS3 and BrS leading to a gain-of-function and loss-of-function of the Nav1.5 channel, respectively [124, 140] with varying penetrance. As both diseases share the same main gene, the possibility of overlapping phenotypes is not excluded. This hypothesis has been validated by *Grillo et al.* [151]. Indeed, using the ECG of 25 patients they were able to demonstrate that in some subjects carrying the *SCN5A* mutations, a clinical coexistence between LQTS3 and BrS phenotype was observed, an observation which was further validated after flecainide administration. Subsequent studies further support the hypothesis of overlapping phenotype between BrS and LQTS3. Indeed, using derived cardiomyocytes from both mice and human cells carrying *SCN5A*^{1798insD/+} and *SCN5A*^{1795insD/+}, respectively, *Davis et al.* could show that the mutations recapitulate the existence of an overlapping phenotype between both diseases [152].

Four years after this study, *SCN5A*-E1784K has been further described as a causative mutation for an overlapping phenotype [153]. Indeed, patients carrying this mutation could show a QTc prolongation, but functional analysis of cells harboring the mutation presents a decreased Na^+

current density characteristic to BrS. Many other mutations associated with mixed syndromes have been further published [61], showing additional complexity in the pathological mechanisms linked with both diseases. As a result of this complexity, it could be that LQTS3 and BrS are alternative manifestations of the same problem. Therefore, further investigation to develop a better therapy for patients harboring those mutations is required.

1.10 Aim of study

Very little is known on the gene expression involved in the mechanism of ECC related to *SCN5A* mutation during LQTS3 and BrS. Moreover, some studies have demonstrated an overlapping phenotype between both pathologies rendering the mechanisms underlying both diseases very complex, and it has been revealed that drug therapy might differ from patient to patient. Thereby, in the present study, we aim to use derived cardiac muscle cells of a healthy individual and LQTS3 as well BrS patients to access the regulation of gene expression associated with the functional activity of cardiomyocytes in both situations: healthy and patient-derived CMs. We also aim to functionally characterize the cells using methods such as calcium imaging, MEA analysis and patch-clamp.

During our study, we interpret the following questions:

- Does the *SCN5A* mutation affect other gene expressions involved in the mechanism of cardiac muscle cell contractility, and how is the calcium transient regulated during the diseases compared to the control? As gene expression is switched during the maturation of *in-vitro* CMs differentiation, we postulate that CMs maturation affects the result outcomes between the control and the disease models. Moreover, cell sheets are different from single cells in their constitution, and we therefore also try to find out if using these two types of cells can affect the data interpretation.
- Another line-up of the study was to better understand the phenomenon of overlapping phenotype between BrS and LQTS3. Therefore, we ask ourselves that if the phenotype is present, how could it manifest at a molecular as well as at a functional level?
- Due to the heterogeneity in the mechanisms associated with *SCN5A* mutation and the different responses to antiarrhythmic drugs by patients, the third point of our study was to access the efficacy or proarrhythmic effect of antiarrhythmic drugs on LQTS3 derived cardiomyocytes.

2 Materials and Methods

2.1 Materials

Cell culture plates, the cryotube vials and coverslips (22x22 mm, 12x12 mm) were from Becton Dickson Labware, USA and Thermo Fisher, Germany. The centrifuges tubes (15 ml and 50 ml), the pipettes, the cell strainers (40 μ m) and bacterial dishes (10 cm, 6 cm) were obtained from Greiner-bio-one and Sarstedt/ Germany. The FACs tubes and the sterifix (0.2 μ m) were supplied by Corning, Mexico, and B. Braun Melsungen AG, Germany, respectively. The Pasteur pipettes and the syringe (5, 10, and 20 ml) originated from VWR.com and BD Discardit™ II/ Germany. The RNase/DNase free microtubes and pipettes tips were provided by Axygen, USA; Nerbe plus, Germany and Gilson, Axygen. The safe seals (0.5, 1.5, 2 ml) respectively came from Biozym Diagnostic, Germany; Sarstedt, Germany and Eppendorf, Germany.

2.2 Laboratory equipment

The equipment used during this study are listed on the following table.

Table 2.2.1 List of equipment

MEA 1060-Inv-Bc amplifier	Multi-Channel Systems, Germany
Multi-Channel output fA60SBC	Multi-Channel Systems, Germany
Temperature controller TCO2	Multi-Channel Systems, Germany
Centrifuge 5430	Eppendorf, Hamburg, Germany
Multifuge 1S-R	Heraeus Instruments,
Centrifuge 5417 R	Eppendorf, Hamburg, Germany
IEC CENTRA CL2 Centrifuge	Thermo Fisher, Germany
7500 fast real-time PCR System	Thermo Fisher, Germany
1000 Touch Thermal cycler	Bio-Rad, Germany
BD FACSCanto™ II	BD Biosciences, Canada
Fluorescence power manager	CONRAD, Germany
Nanodrop 1000	PeqLab, Germany
Sterile work bench Lamin Air HB 2448	Heraeus Instruments
Sterile work bench HERA Safe	Thermo Fisher, Germany
HERACELL 240i C02 incubator	Thermo Scientific, Germany
Microscope Axiovert 25	Zeiss, Germany

Microscope Axiovert 200M	Zeiss, Germany
Microscope IX50	Olympus
Microscope IX81	Olympus
Laser set up	Olympus, Japan
Manual manipulator	Märzhäuser Sensotech, Germany
ApoTome	Zeiss Werk, Germany
GFL Waterbad	ProfiLab24.com, Germany

2.3 Reagents

The listed reagents were used for the cell culture

Table 2.3.1 List of reagents

Company	Thermo Fisher/ Invitrogen, Germany
Reagents	Catalogue number
E8	A1517001
RPMI 1640 W/ Glutamax-I	61870010
RPMI 1640 (- Glucose)	11879
DPBS (-/- Mg ²⁺ , Ca ²⁺)	14190169
WFI H2O	A1287302
DMSO	14190-094
Vitronectin (rhVTN-N)	A14700
RevitaCell supplement (100x)	A2644501
B-27 Supplement, minus Insulin	A1895601
TrypLe	12605010
DMEM/Nut.Mix.F-12/Glut-I	31331093
Penicillin-Streptomycin	15140122
Fluo-4	F14201
Monoclonal troponin T mouse IgG1 (1:100)	MS-292-P1
Alexa Fluor 555 anti-mouse IgG1 (1:1000)	A21127
Alexa Fluor 488 anti-rabbit IgG (1:1000)	A11034
ProLong Gold Antifade-Reagent	P36966
SuperScript VILO™ cDNA Synthesis	11754-050
Platinum SYBR Green qPCR	11733-046

PureLink Genomic DNA Mini Kit	K1820-01
Macherey-Nagel™ NucleoSpin™ Gel and PCR Clean-up Kit	740609.50
O'gene ruler DNA ladder	SM1173
Electrophoresis buffer	B49
Company	Qiagen, Germany
Qiazol	79306
Rneasy Mini Kit (250)	74106
Rnase-Free Dnase Set	79254
	Bio-RAD, Germany
Ethidium Bromide	1610433
Company	LC Laboratories
CHIR99021	C-6556
	Selleck chemicals
Wnt-C59	S7037
	Roth, Germany
Roth-Immuno Block solution (1:10)	A151.1
Di-sodium hydrogen phosphate	T876,1
Sodium chloride	3957.1
	Goldbio.com, USA
Agarose LE	A-201-500
	Merck, Germany
Sodium Dihydrogen Phosphate Monohydrate	106340500
	New England BioLabs (NEB), England
6X-loading dye	B7024S
	Sigma, Germany
Sodium DL-lactate	L4263
Caffeine Anhydrous	C-0750
L-ascorbic acid 2-phosphate	A8960-5G

	monoclonal α -actinin mouse IgG1 (1:800)	A7811
	Polyclonal Cx43 rabbit 1:400	C6219
	Triton-X_100 (0.25%)	T8787
	Nucleus Stainer Bisbenzimidazole – Hoechst (1:2000)	B2261
	AppliChem	
	Chloroform pure	A0642, 1000
	From the Neurophysiology Institute	
	Tris-Waschbuffer	

2.4 Media and Buffers

Table 2.4.1 RPMI media for Differentiation (100 ml)

Media/Compound	Amount	Final concentration
RPMI 1640 + Glutamax supplement	98 ml	-
B-27 supplement, minus insulin	2 ml	-
L-ascorbic acid 2-phosphate	100 μ l (50 mg/ml)	50 μ g/ml
Penicillin-Streptomycin	1 ml	100 U

Table 2.4.2 RPMI media for purification (50 ml)

Media/Compound	Amount	Final concentration
RPMI 1640 (minus Glucose)	49 ml	-
L-ascorbic acid 2-phosphate	50 μ l (50 mg/ml)	50 μ g/ml
Sodium DL-Lactate	0.925 μ l/ml	5 mM
Penicillin-Streptomycin	0.5 ml	100 U

Table 2.4.3 Tyrode's solution for Ca^{2+} Imaging

Compound	Amount in mmol/l
NaCl	140
KCl	5.4
MgCl ₂	1

Table 2.4.4 Agarose gel' preparation

Chemical	Amount
Ultrapure Agarose	0.8 g
VE water	100 ml

(The mixture was boiled in a microwave to ensure the solubility of the chemical)

Sodium pyruvate	2
CaCl ₂	1
Glucose	10
HEPES	10

(Tyrode's solution was adjusted for a pH of 7.4 with NaOH at room temperature (RT) and stored at 4°C)

Table 2.4.5 TAE buffer (50x)

Chemical	Amount
Tris	242 mg
EDTA	18.61mg
Glacial acetic acid	57.1 ml
DDI H ₂ O	1000 ml

Table 2.4.6 Tris-wash buffer (10x)

Compound	Amount
Trizma-Base	60.5 g in 700 ml Aqua distillate
Aqua distillate	1000 ml

(The preparation was adjusted for a pH of 7.6 with 2 N hydrochloric acid and a solution of NaCl and kept at RT)

Table 2.4.7 4% Paraformaldehyde

Compound	Amount
Di-sodium hydrogen phosphate	137.99 mg
Sodium dihydrogen phosphate monohydrate	141.96 mg
Sodium chloride	58.44

(The compounds were dissolved in 1000 ml Bidistillate water at 50-60 °C with the help of a magnetic stirrer, and the preparation was adjusted for a pH of 7.4 with 1 N NaOH)

2.5 hiPSCs culture

hiPSCs were kindly provided by the Saric group. The cells were cultured on 6 well or 3cm plates and passaged when they reached 80-90% confluency. For the cells' dissociation, we used the dissociation reagent TrypLE (Thermo Fisher, 12605-010). The cells were washed once with DPBS (-/-Mg²⁺, Ca²⁺), and 0.5 ml of TrypLE was added to the cells, which were incubated with the reagent for about 3 to 4 min at RT, after which a proportional amount of the E8 media (Thermo Fisher, A1517001) was added to the cells to stop the enzyme reaction. We collected the cells in 15 ml falcon tubes and centrifuged them at 1000 RPM for 2 min. The supernatant was absorbed with the help of a Pasteur pipette and resuspended in 1 ml media. We pipetted the cells up and down 3 to 5 times to obtain the desirable colony size and replated them on vitronectin (Thermo Fisher, A14700) or a matrigel (Corning; 354248) coated plate at a final concentration of 5µg/ml or 10mg/ml, respectively. The cells were replated in a final volume of

1.5 ml to 2 ml E8 media in such a way that they will reach the desired confluency within 4 to 5 days. To improve the cells' survival, 10 μ l of RevitaCell (Thermo Fischer, A26445) was added to the cells after replating. We distributed the cells to the entire surface of the plate through an up-and-down, left and right movement and replaced them in an incubator at 37°C with 5% CO₂. Media was changed every day until the next passage.

2.6 Differentiation of hiPSCs to hiPSC-CMs

Cells were passaged as described above. After centrifugation and resuspension in the E8 media, the cells were up-and-down pipetted about 10 to 14 times to obtain the desired cell size, which is a very important step to obtain a successful differentiation. We replated the cells either on 3cm plate dishes or six-well plates in a density that will reach the desired confluency of 70-80% within 2 to 3 days. When the confluency was reached, we replaced the culture media with the differentiation media (RPMI+Glutamax+50 μ g/ml LAA+B27-insulin) supplemented with CHIR99021 (LC Laboratories, G611) for the first 48 hours of differentiation. The concentration of CHIR99021 varied from cell line to cell line (5 μ M for NP0016-C3; 6 μ M for NP0134-26B; 8 μ M for NP0040-8) in an end volume of 3 ml in each well. After 48 hours, the media was replaced with RPMI media supplemented with Wnt inhibitor (Selleck Chemicals, S7037) at the end concentration of 2 μ M in 3 ml media, and the cells were further incubated for another 48 hours to stop the gastrulation. On the fourth day of differentiation, the medium was changed and replaced with the normal differentiation media. The media was changed every 2 days and beating activity could be observed on day 6 of differentiation for NP0040-8 (control cell line) and NP0134-26B (BrS cell line) and day 8 or day 9 for NP0016-C3 (LQTS3 cell line). Glucose starvation was performed on day 9 or 12 dependent on the time of beating activity appearance, and the cell was maintained in the purification media for 4 days (RPMI minus glucose+50 μ g/ml LAA+B27-insulin+5mM Sodium DL-lactate). We maintained the cardiomyocytes in the differentiation media until further used. The schematic illustration of the protocol is described in the figure below.

Day 20-25 and day 40-45 were determined as the early and late stages, respectively. The cellular, molecular and functional analysis were performed at both stages of differentiation.

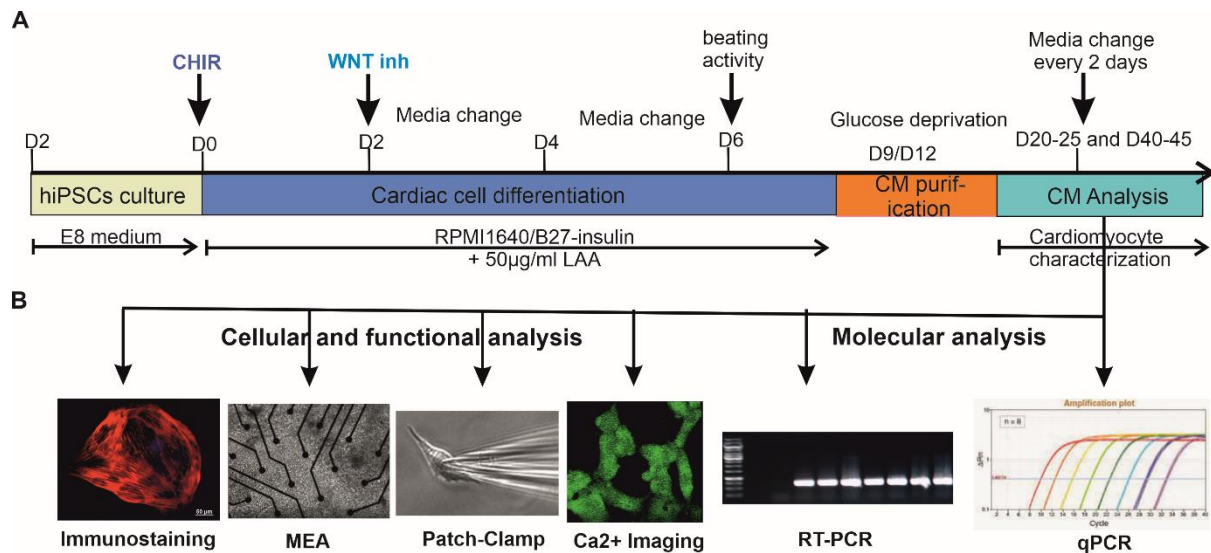


Figure 2-1. Schematic illustration of human cardiac muscle cells differentiation and characterization

A, Schematic protocol of hiPSC-CMs differentiation. Briefly, the cells were replated as small clusters 2 days before differentiation. The small molecules CHIR and WntC59 were used to initiate and stop the gastrulation. Beating activity could be observed on day 7 of differentiation and glucose deprivation was performed for 4 days, after which the cells were further cultured for different characterization. Cardiomyocytes were characterized at a different stage of differentiation at the cellular, molecular and functional levels with the different illustrated methods (**B**). (LAA=L-Ascorbic Acid; inh =inhibitor; CM= Cardiomyocyte)

2.7 HiPSC-CMs dissociation

Cells were dissociated with either TrypLE or collagenase B, according to the experiments. Collagenase B was used when preparing cells for the patch-clamp experiment, and TrypLE was used for cardiomyocytes (CMs) dissociation intended for other functional characterization. Before the dissociation, the cells were washed twice with DPBS (-/- Mg^{2+} , Ca^{2+}). For dissociation, we added 0.70 ml to 1 ml of TrypLE to the plate and incubated the cells in an incubator at 37°C with 5% CO_2 for about 7 to 10 min. For FACS analysis, this incubation time was increased to allow a better dissociation into single cells. After this incubation time, the same volume of differentiation media was added to the cells to stop the enzyme reaction. We then collected the cells in a 15 ml tube and centrifuged them for 2 to 3 mins at 1000 RPM. After centrifugation, the supernatant was removed, and the cells were resuspended in 1 ml differentiation media. 10 μ l of RevitaCell (Rock inhibitor) was added to the suspension, which was pipetted several times to obtain single cells. We filter the cells using a 40 μ m filter and count the living cells with the help of the trypan blue. The desired number of cells were replated for further experiments. For dissociation with collagenase B, the cells were previously washed as described above, 0.5 ml of collagenase B was added to the plate, and the cells were incubated

for 30-35 min at 37°C with 5% CO₂. After 15 to 20 min incubation time, we triturated the cells with a 1 ml pipette and incubated them for another 15 or 10 min. The cells were again gently triturated several times after incubation to obtain single cells and the reaction was stopped with the differentiation media at the same volume of collagenase B. Single cells were replated on glass coverslips for patch-clamp analysis.

2.8 Immunostaining

For this experiment, the cells were dissociated 3 to 4 days before and replated in a density of 35×10^3 to 50×10^3 CMs on a 12x12 mm coverslip placed in a 24 well plate. Coverslips were previously coated with 10 mg/ml matrigel or 40 µg/ml fibronectin. The cells were allowed to attach to the coverslip without media change for 48h. On the third or fourth day, the cells were washed and fixed with 4% paraformaldehyde (PFA) for 20 min at RT. The fixed cells were maintained in 0.5 ml DPBS at 4°C until staining. Immunostaining could be performed directly, or the cells could be kept at 4°C for several days until further use. During immunostaining, we used the Tris-Wash-Buffer (1:10) for all washing steps. Before permeabilization with triton x (0.25% triton-x-100, T8787, Sigma), the cells were washed once, and the cells' permeabilization was performed at RT for 15 mins. The cells were washed 6x with Tris-wash-buffer, and for each washing step, we incubated the cells with the buffer for 5 min to optimize the staining. To avoid unspecific binding sites, we blocked the cells with the blocking reagent (Rot immuno-block solution 1:10, A151.1, Roth) for 120 mins. For single or double staining, the first antibodies (monoclonal alpha-actinin mouse IgG1 1:800, A7811 Sigma; monoclonal troponin T mouse IgG1 1:100, MS-292-P1, Thermo scientific; the polyclonal Cx43 rabbit 1:400, C6219, Sigma) were added to the preparation and incubated overnight at 4°C in the cold room in the dark. The next day, we repeated the 6x washing step with a 5 min incubation time and added the second antibody (Alexa Fluor 555 anti-mouse IgG1 1:1000, A21127 Invitrogen) for a single staining or (Alexa Fluor 488 anti-rabbit IgG 1:1000, A11034 Invitrogen) for the double staining. We used the nucleus stainer Hoechst at this step (1:2000) and incubated the cells for 2h at RT in the dark. After the incubation time had elapsed, we repeated the washing step and prepared the microscope slide with ProLong Gold Antifade, on which the coverslips were mounted. During this step, it is advisable to use a drop of the ProLong Gold and avoid forming bubbles when placing the coverslip, and, if bubbles are formed, remove them with a pipette tip. The preparation is either stored in a cardboard box at 4°C or the cells are directly analysed on the apotome.

2.9 FACs analysis of hiPSC-CMs

For FACs analysis, the cells were dissociated with TrypLE as described in **section 2.7**. We started the experiment with at least 0.5×10^6 cells. For the staining, an appropriate number of cells was distributed in 15 ml tubes and centrifuged for 2 mins at 1200 rpm at RT. The supernatant was discarded and 0.5 ml of 4% PFA was given to the detached cells, which were transferred in 1.5 ml Eppendorf tubes and incubated for 15 min at RT. The preparation was then centrifuged at 4°C and 0.5 ml of permeabilization and blocking buffer (0.5% Triton x-100 in 0.5% BSA) was added to the cells and incubated for 10 min at RT. All the other centrifugation steps were done at 4°C at the same speed and for the same duration. After blocking, the cells were centrifuged and resuspended in 100 µl staining buffer (0.1% Triton x-100 in 0.5% BSA). 1:50 dilution of the first antibody was given to the suspension (mouse monoclonal Troponin T IgG2a; Santa Cruz Biotechnology) and incubated overnight in the cold room in the dark. The following day, 1ml of washing buffer (0.5 % BSA) was added to each tube and centrifuged, after which cells were stained with the second antibody (1:1000 or 1 µg/ml Alexa Fluor 555 Goat anti-mouse IgG1; Invitrogen) previously resuspended in 100 µl washing buffer, and incubated for 30 min in the dark at RT. The cells were washed and resuspended in 0.25 ml washing buffer, filtered and FACs analysis was performed with FACs Aria II. Data were analysed with FlowJo7.

2.10 gDNA extraction

Cells were cultured and maintained in the E8 medium. When reaching the desired confluency, they were passaged with TrypLE as described in **section 2.5**. The supernatant was removed, and the cells were resuspended in 200 µl DPBs (-/- Mg^{2+} , Ca^{2+}). The genomic DNA isolation was performed following the mammalian cell lysate protocol from Thermo Fisher (cat no. K1820-01) and the extracted DNA was directly used for PCR analysis or stored at -20°C until further use.

2.11 PCR sequencing

The stock concentration of 100 µM was prepared for each primer after the manufacturer's instructions in nuclease-free water. For the working solution, a 1:10 dilution of each primer was performed (80 µl H₂O + 10 µl forward primer + 10µl reverse primer). The Master Mix preparation for one sample was made as follows: 2 µl diluted primers + 12.5 µl PCR Mix + ~100 ng gDNA + 2 µl DMSO to avoid gDNA binding. The samples were distributed in PCR tubes and completed with H₂O for a final volume of 25 µl. The PCR was performed under the following conditions (Initial denaturation: 95°C for 5min, Melting: 95°C for 45 s, Annealing:

58°C for 40 s, Extension: 72°C for 30 s for 34 cycles. Final elongation at 72°C for 5 min and the end of the reaction was set at 4°C). The 5 µl PCR product was then run on 0.8% agarose gel with 1 µl of 6X-loading dye (B7024S, NEB) at 90mV for 40 min in 1x TAE (see section 2.4 for TAE composition) electrophoresis buffer (B49, Thermo Fischer). 7 µl of O'gene ruler DNA ladder (SM1173, Thermo Fischer) was also loaded onto the gel for band size detection. The gel was then stained with ethidium bromide (BIO-RAD, 1610433) and observed under UV light using Royal Bio-Imaging System – Intas Gel iX Imager (Royal Biotech, Ltd, Germany). For PCR sequencing, after the PCR run was finished, the PCR product was purified using Macherey-Nagel™ NucleoSpin™ Gel and PCR Clean-up Kit (Thermo Fisher; 740609.50) according to the manufacturers. The DNA concentration was measured via Nanodrop ND-1000 Spectrophotometer (Thermo Scientific) and the samples were prepared for sequencing (1 µl sequencing primer (1:10 dilution) + 250 ng PCR product + 7 µl RNase free water). The product was sent for sequencing and the data was analysed with the BioEdit software.

Table 2.11.1 PCR primers and sequencing primers designed for Mutation detection

LQTS3 mutation	V240M
Primer sequence	For: 5'- GGGGGTCATGCTCTGAGTATGTGTTGTC - 3' Rev: 5'- GGGATCAGGCAGGGCTTGAACAGC - 3' Sequencing primer: 5' TCCACACCCATGCCATATATTTG - 3'
BrS mutation	Q646R
Primer sequence	For: 5'- GTGATATGTGTAGCTTCCTGACCACACTC - 3' Rev: 5'- CAGGCCAGATGTGGGAGTATTTGGG - 3' Sequencing primer: 5'- CAGGAGAGAACAAGCTGAAACAGATG - 3'

2.12 RNA isolation for gene expression profiling

hiPSCs and hiPSC-CMs (day 20 and day 40) were harvested in 1.5 ml Eppendorf tubes and centrifuged at RT at 1000 or 1200 rpm for 2 min. The cells were washed once with 1 ml DPBS (-/- Mg²⁺, Ca²⁺) at 4°C, and the pellet was resuspended in 700 µl to 1 ml Qiazol (Qiagen, 79306). The cells were stored at -80°C or were directly used for RNA isolation. For the isolation, we triturate the cells 8 to 10 times with the help of a 5 ml syringe. 200 µl of chloroform was added to the lysate, vortexed and kept at RT for 5 min. The cells were then centrifuged for 15 mins at 12500 rpm at 4°C. RNA was isolated using the Rneasy Mini Kit from Qiagen (catalogue no. 74106). The clear phase (supernatant was collected without touching the middle layer) was collected in 1.5 ml tubes, adjusted with an equal volume of 70%

pure cold ethanol and the solution was mixed by gentle up and down movement. Approximately 750 µl of the solution was applied to the columns and centrifuged for 20 seconds (s) at 12500 rpm at RT. We discarded the filtrate, and the step was repeated until the solution was completely used. The other centrifugation steps following were done at RT at 12500 rpm. 350 µl of RW1 buffer was applied to the columns and centrifuged for 20 s, the filtrate was discarded and 80 µl of DNase mixture was applied (10 µl DNase + 70 µl RDD buffer from the RNase-Free DNase Set from Qiagen; Catalogue no. 79254) to the columns and incubated for 15 min. After the incubation, the columns were washed with RW1, the filtrate was discarded and the columns were washed twice with 500 µl RPE buffer and centrifuged for 15 s and 20 s, respectively. The columns were shifted to a new 2 ml collection tube and spun for 1 min. They were transferred to 1.5 ml Rnase/Dnase-free Eppendorf tubes for RNA collection. For this step, 25 to 27 µl of nuclease-free water was added to the centre of the columns without touching the membrane (the nuclease-free water was previously warmed at 37°C for better RNA extraction). The preparation was incubated for 15 min and spun down the columns for 1 min at RT. The collected RNA was directly placed on ice and the quantity as well quality verification was done via the Nanodrop.

2.13 Protocol for cDNA synthesis

For cDNA synthesis, we used the SuperScript VILOTM cDNA synthesis kit from Life Technologies (catalogue number, 11754-050). The master mix of samples was prepared without RNA. For a single reaction, the following amounts of reagents were needed: 4 µl 5X VILOTM reaction Mix, 2 µl 10X SuperScriptR Enzyme Mix, the desired volume of RNA (1µg) and the desired volume of RNase-free water to complete the reaction to 20 µl. The preparation was gently mixed and incubated for 10 min at 25°C for primers extension, followed by the cDNA synthesis for 60 min at 42°C. The reaction was terminated at 85°C for 5 min and the cDNA product was directly placed on ice to stop the reaction. The cDNA was diluted with 280 µl RNase-free water and stored at -20°C for future use.

2.14 RT-PCR protocol with Platinum SYBR Green qPCR SuperMix-UDG

SYBR Green was previously prepared (12.5 ml Platinum SYBR green qPCR superMix-UDG + 50 µl ROX reference Dye) and stored at -20°C in the dark. A mixture of 5µM of forward (For) and reverse (Rev) primers working solution was prepared (10 µl For + 10 µl Rev + 200 µl RNase-free water) and stored at -20°C. Each gene was run as technical triplicates during the experiment. The master mix for a single reaction was prepared as follows: 10 µl SYBR Green, 1 µl primer working solution, 7 µl RNase-free water, and 2 µl cDNA. For triplicate reaction,

the master Mix was prepared without cDNA, and 18 µl of the preparation was distributed in the desired wells of the MicroAmp™ Fast optical 96 wells plate (Thermo Fisher, 4346907), and 2 µl of the cDNA product was added later to complete the reaction to an end volume of 20 µl. The experiment was run with the ABI 7500 fast mode programme (stage 1: 50°C for 2 min for the denaturation; stage 2: 95°C for 2 min for the primer annealing; stage 3: 95°C for 3 s for every cycle (40 cycles) corresponding to the primer extension and the reaction was terminated at 60°C for 30 s). Data analysis was validated with the 7500-software version 2.3.

Table 2.14.1 Designed primers for qPCR

The primers were designed with the help of SnapGene and the following online tool:

https://eu.idtdna.com/PrimerQuest/Home/Details/0_4

Sequence ID	Product Size (bp)	Gene (Human)	Primer sequence
NM_001035.3	97	RyR2	For: 5'-GCTGATGATCGGGATGACTATG-3' Rev: 5'-CCCAGACATTAGCAGGTTCTT-3'
NM_000719.7	104	Cav1.2	For: 5'-TCGTGGGAAAGGTGGTAAAG-3' Rev: 5'-GTGGCCTCTTTGCTGAATTG-3'
AF261085.1	102	GADPH	For: 5'-CAAGAGCACAAAGAGGAAGAGAG-3' Rev: 5'-CTACATGGCAACTGTGAGGAG-3'
NG_007866.2	94	TNNI3	For: 5'-TACTTAGGCATCCAGGGTAGAG-3' Rev: 5'-TCAGAGGTTAGGGTCTCTTCTT-3'
NM_000024.5	83	ADRB2	For: 5'-GCCTCTGCCTGCTCTAAATA-3' Rev: 5'-GGACCTGACTGGAAAGGTATAG-3'
NM_000684.3	104	ADRB1	For: 5'-GTGGAAGATGGGTGGGTTAG-3' Rev: 5'-GCTGGTAGTGTGTTCTCTGTT-3'
NM_005477.3	101	HCN4	For: 5'-AATGAGGTGCTGGAGGAGTA-3' Rev: 5'-TGGAGGAGGATGGAGTTCTT-3'
NG_007556.1	101	TNNT2	For: 5'-GCCTCTGCCTGCTCTAAATA-3' Rev: 5'-GGACCTGACTGGAAAGGTATAG-3'
	133	SCN5A	For: 5'-CCCAAACAATTCCTGCTCCCT-3' Rev: 5'-TGACGATGATGCTGTCTGAAGA-3'

2.15 Multi-electrode Array (MEA) Experiment

The MEA experiment was performed with a 60 electrodes MEA plate. Electrode spacing was 200 µm and the diameter of each electrode was 30 µm. The recording of the extracellular potential was performed at a rate of 2 kHz in a standard differentiation media.

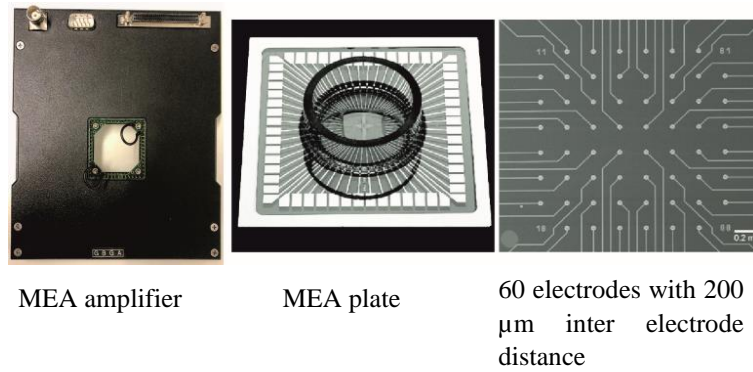


Figure 2-2 Part of the Set up for field potential (FP) recording

The amplifier, a typical MEA culture dish and the 60 electrodes grid are represented on this figure. Scale bar: 0.2 mm

The cells were replated as clusters on the MEA plate three to five days before measurement, allowing proper cells' attachment to the electrodes. The field potential recordings were made on days 20-25 and days 40-45 of differentiation corresponding to the early and late stages, respectively. Before measurement, the air-conditioner inside the room was switched off, and the cells were measured on a plate warmed at 37°C. Each MEA plate had an end volume of 0.5 ml during measurement, and we recorded each drug concentration separately. The data were converted using the MC-DataTool and further analysed via Origin version 7, CorelDraw 2020 and software developed in our institute for statistical evaluation of the QT interval, the amplitude and the FP rate.

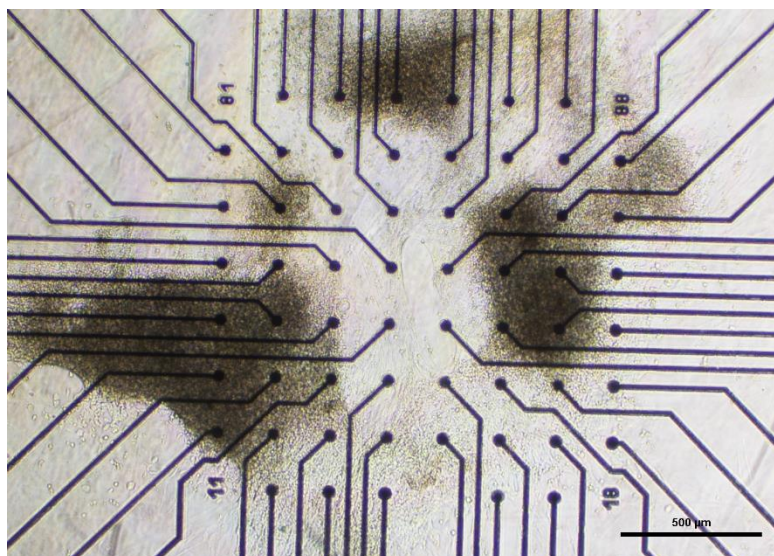


Figure 2-3 Example of beating human cluster attached on a MEA plate.

The plate was coated with 10 mg/ml Matrigel 2 hours before the cell replating or left overnight. The cluster was maintained in RPMI/B27-insulin+50 μg/ml LAA. The picture was taken with a 4x objective.

2.16 Calcium Imaging

Dissociated cardiomyocytes were replated as single cells on a previous matrigel (10 mg/ml) or fibronectin (40 µg/ml) coated coverslip (22x22 mm). The cells were incubated at 37°C with 5% CO₂ for 2 to 3 days, after which measurements were performed. To perform the imaging, the coverslip was mounted on a cell chamber and cells were stained with the Fluo-4, AM-ester from Life Technologies at an end concentration of 5 µM (5 µl of the dye + 995 µl MilliQ water or WFI water). The cells were incubated with 0.5 ml or 1 ml of the dye for 30 mins at RT in the dark. After this time, the cells were washed twice with 1 ml of 1% Tyrode's solution (**see section 2.16**) and maintained in 0.5 ml differentiation media during measurement. Calcium transient was first recorded at a baseline, and for recording with caffeine, 20 µM of caffeine was prepared in 2 ml tubes and 0.5 ml of the compound was applied to the cells during recording for a final caffeine concentration of 10 µM. For all measurements, good beating cells were selected (region of interest, ROI) for data analysis. Data were analysed using the following software: FV-1000 Olympus, sigmaPlot 8.0, and CorelDraw 2020.

N.B: All cell cultures were performed under sterile conditions.

3 Results

3.1 Culture of hiPSCs in a xeno-free and feeder-free system

Xeno- and feeder-free systems were developed to support the transfer of in-vitro studies to the clinic. Studies revealed that E8 media efficiently supports hiPSCs expansion in a xeno-free system [154]. Moreover, the extracellular matrix vitronectin and matrigel are a feeder-and-Xeno-free system that has shown effectiveness in hiPSCs expansion [154-156]. This system, therefore, renders the transfer of in-vitro studies to the clinic feasible. During our study, both extracellular matrices were used for hiPSCs proliferation, and the cells were cultured in the Essential 8 (E8) media. The three cell lines: NP0040-8 (control cell line), NP0016-C3 (LQTS3 cell line carrying a missense mutation C7718>A, p.V240M on the exon 7 of *SCN5A*) and NP0134-26B (BrS cell line carrying a heterozygous mutation in the exon 13 of *SCN5A*, c.1936delC, p.Gln646Argfs*5) grew and expanded successfully as shown in **Figure 3-1**. Cell culture was kept at 37°C with 5% CO₂ and passaged each 4 to 5 days.

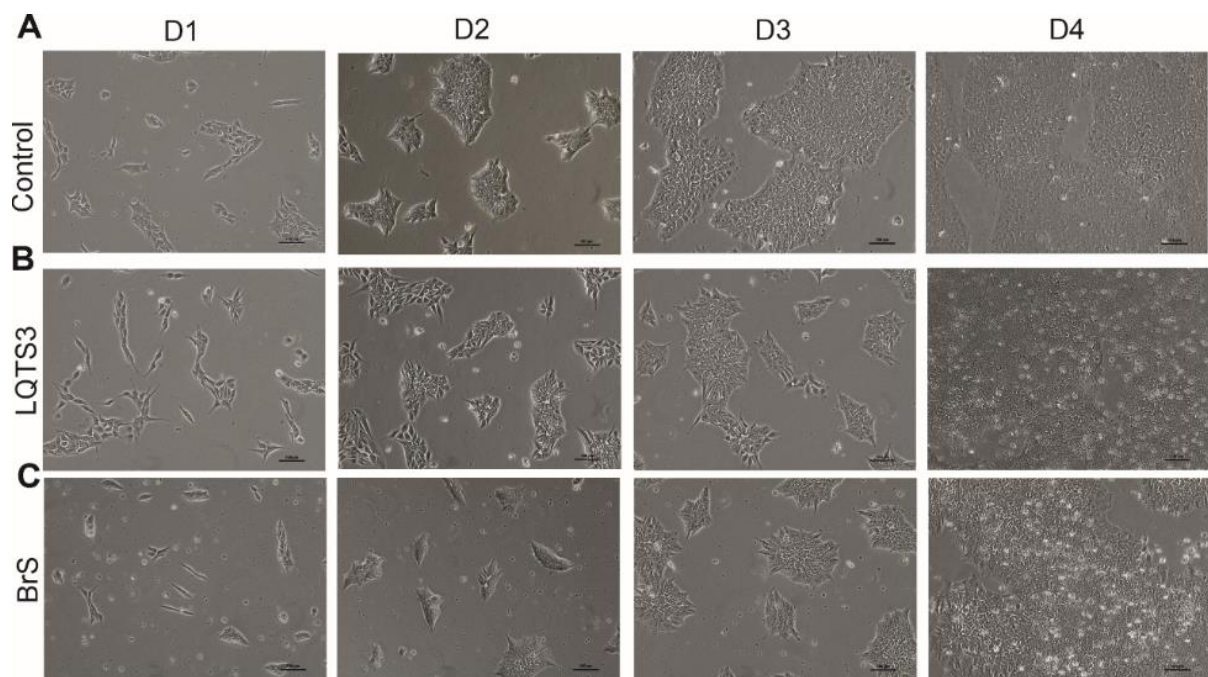


Figure 3-1. hiPSCs culture in E8 media

A-C Illustrates representative pictures of cells' proliferation from a control subject, LQTS3 and BrS patients in E8 media, respectively. We passaged the cells every 4 or 5 days and maintained them in an incubator at 37°C with 5% CO₂ and the media were changed every day. The pictures were taken with the 10x objective.

3.2 High effectiveness of cardiomyocytes differentiation with RPMI supplemented with ascorbic acid

To access the pathophysiological mechanism underlying our disease models, we needed to differentiate the stem cells into cardiomyocytes for further molecular, cellular as well as functional analysis. Previous studies showed that small molecules such as CHIR99021, which is a GSK3 inhibitor, and WNT inhibitors such as Wnt-C59 are effective for cardiac differentiation [157]. Additionally, designed cardiomyocytes differentiation protocols revealed that promoters of cardiac progenitors such as ascorbic acid could enhance cardiac differentiation effectiveness [158, 159]. Therefore, we developed our protocol based on these findings as illustrated in **Figure 3-2A**. Using the healthy control cell line, we illustrated an example of cell structure before and after induction of gastrulation (**Figure 3-2B**). The three cell lines have been successfully differentiated into cardiomyocytes. The characterisation were performed on day 20 and revealed that cells appropriately express sarcomere' markers troponin T (green) and alpha-actinin (red) (**Figure 3-2C**), whose organization is primitive within this unit. FACS analysis showed that after cell purification almost 90% of cells are cardiomyocytes (**Figure 3-2D**) showing the effectiveness of this protocol.

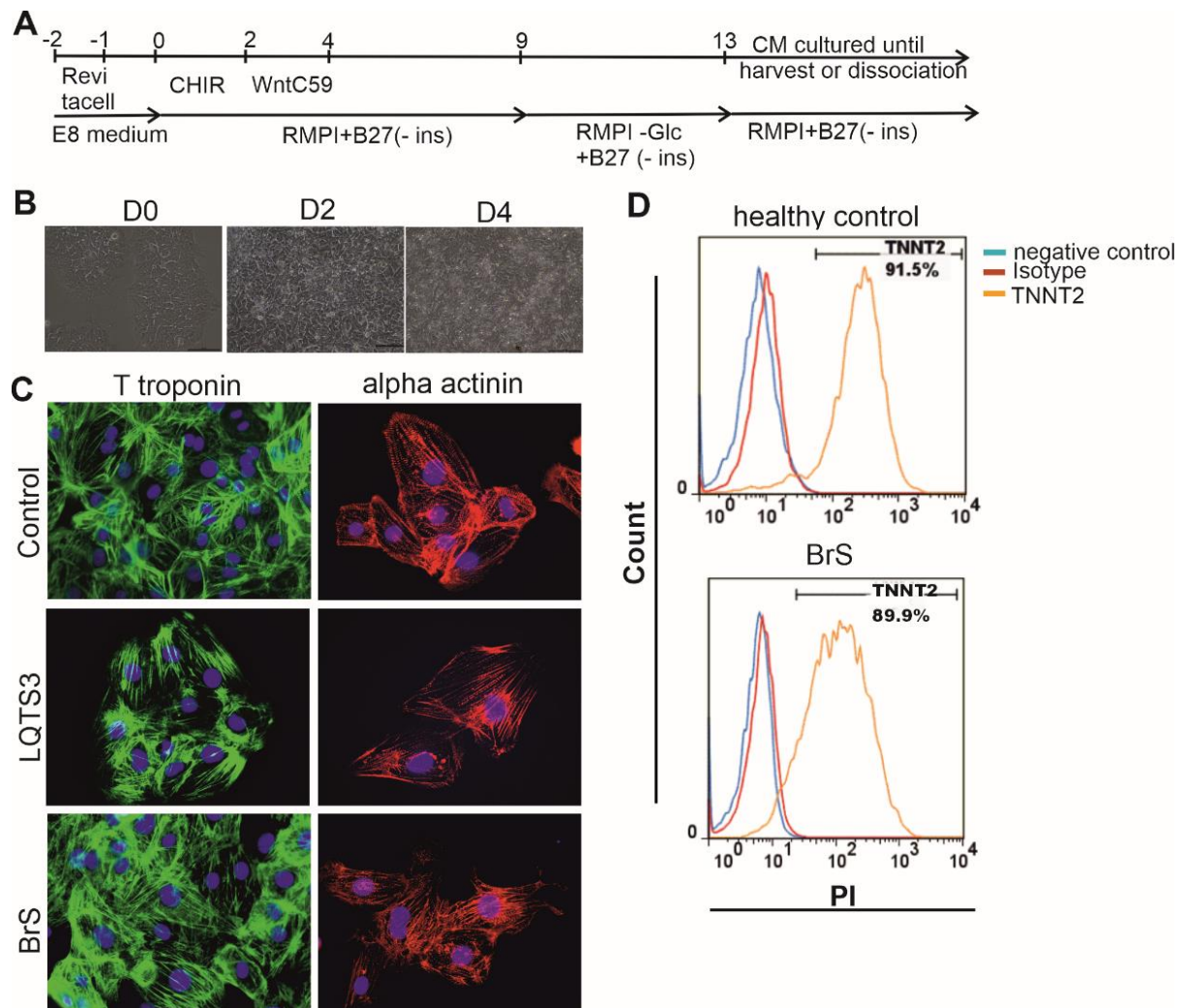


Figure 3-2. hiPSC-CMs differentiation and characterization.

A, Illustrates a schematic protocol of cardiomyocytes (CMs) differentiation. **B**, example of cell structure before and after induction of gastrulation using the healthy control cell line picture of day 0 to day 4 of differentiation corresponding to the day before gastrulation induction (D0), the day after the gastrulation (D2), and the day after inhibition of the Wnt pathway (D4). **C**, Representative illustration of T troponin and alpha-actinin staining of each cell line (scale bar = 50μM). **D**, FACS analysis revealed that almost 90% of CMs are obtained after CMs purification. Results represent at least 2 biological replicates.

3.3 Characterization of the sarcomere and connexin 43 organization at a late stage of differentiation between the control and the disease models

To compare sarcomere organization at the late time point vs the early time point, further staining for alpha-actinin was performed at day 40 as illustrated in **Figure 3-3A**. Compared to the early stage illustrated in **Figure 3-2C** above, the sarcomere organization at a late time point shows better myofibrils alignment, supporting the hypothesis of cell maturation in long-term culture. It was difficult to identify any difference in the structure of the contractile units of the cardiac muscle cells between the control and patient-derived cardiomyocytes. We, therefore,

hypothesized that this unit might not be affected by the mutation. However, additional characterization is required to make a proper statement.

LQTS3 and BrS are both associated with electrical disturbance, and a recent study has raised the hypothesis of a probable delocalization of connexin (Cx43) within the intercalated discs during BrS [160]. Therefore, to go further with this speculation, double staining of CMs using alpha-actinin and Cx43 was performed. Contrary to the previous hypothesis, disturbance in Cx43 alignment in BrS CMs (**Figure 3-3B**) could not be identified, which is also true for LQTS3-derived cardiac cells, indicating that mutation related to these pathologies might not have a direct impact on Cx43 distribution within the cells. We also localized Cx43 in the nucleus' surroundings in all cell types.

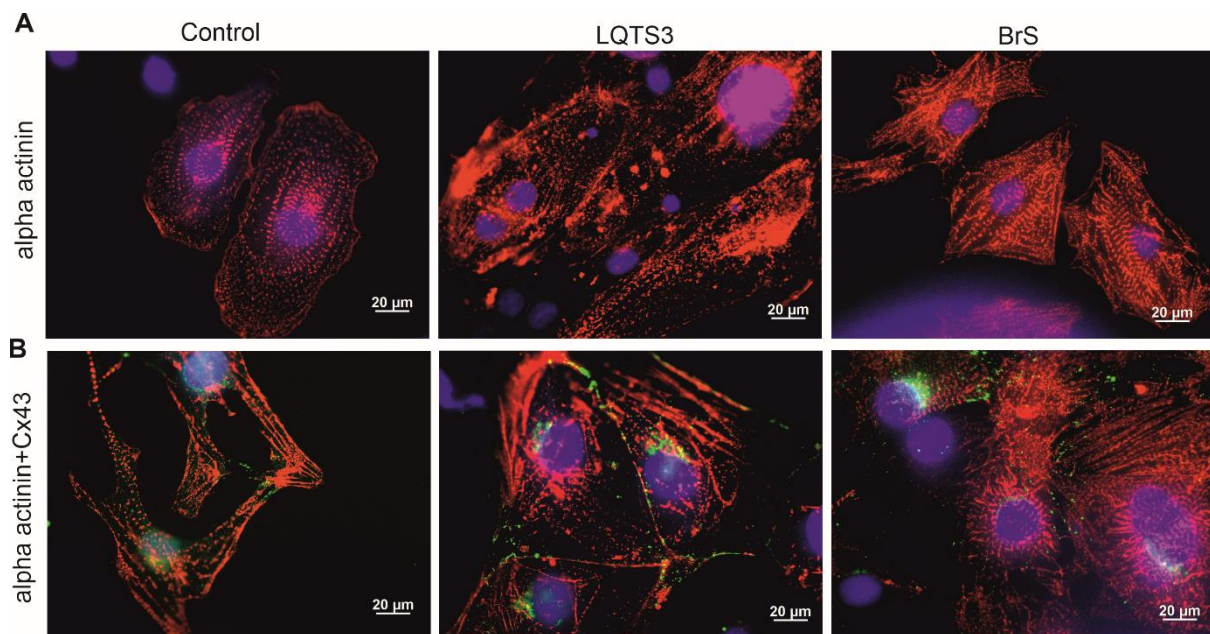


Figure 3-3. Characterization of cardiomyocytes and distribution of Cx43 within the cells.

A, Sarcomere organization of a healthy subject (control), an LQTS3, and a BrS patients CMs. **B**, Present Cx43 distribution in the healthy control and the disease models cell lines showing Cx43 alignment within the intercalated discs and the end-to-end interdigitations. Pictures were taken with 60x oil objective and scale bar: 20 μm.

3.4 Validation of the disease mutations.

A skin biopsy-derived fibroblast from male subjects suffering from LQTS3 and BrS was cultured and reprogrammed by the Saric group from the Institute for Neurophysiology at the University Hospital of Cologne. The cell line was indicated as NP0016-C3 for LQTS3 and NP0134-26B for BrS. The latter were sequenced and cryopreserved for further use by the same group. Studies could demonstrate that gene expression, pluripotency markers as well as karyotype are maintained during hiPSCs cryopreservation [161, 162]. However, validating the

existence of these mutations in this present study removes any doubt about their existence. The sequence analysis showed that the LQTS3 patient effectively carries a point mutation (c7718>A, p.V240M) on exon 7 of the *SCN5A* gene (**Figure 3-4**).

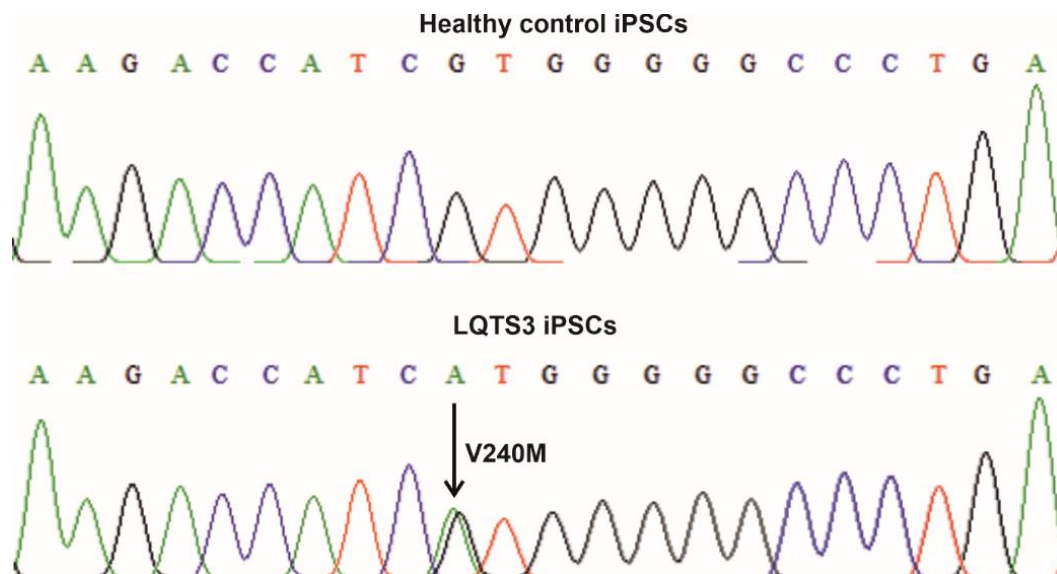


Figure 3-4. Validation of LQTS3 Mutation

Illustration of the wild-type sequence of *SCN5A* gene from healthy control and LQTS3 patient. The heterozygous mutation c.718G>A, V240M was identified on the exon7 of the *SCN5A* sequence gene of the patient.

The frameshift in the sequence of the BrS patient was observable on the exon 13 (**Figure 3-5**) as previously published [163, 164]. Thus, we could further validate the existence of the disease-driven mutations on these cell lines.

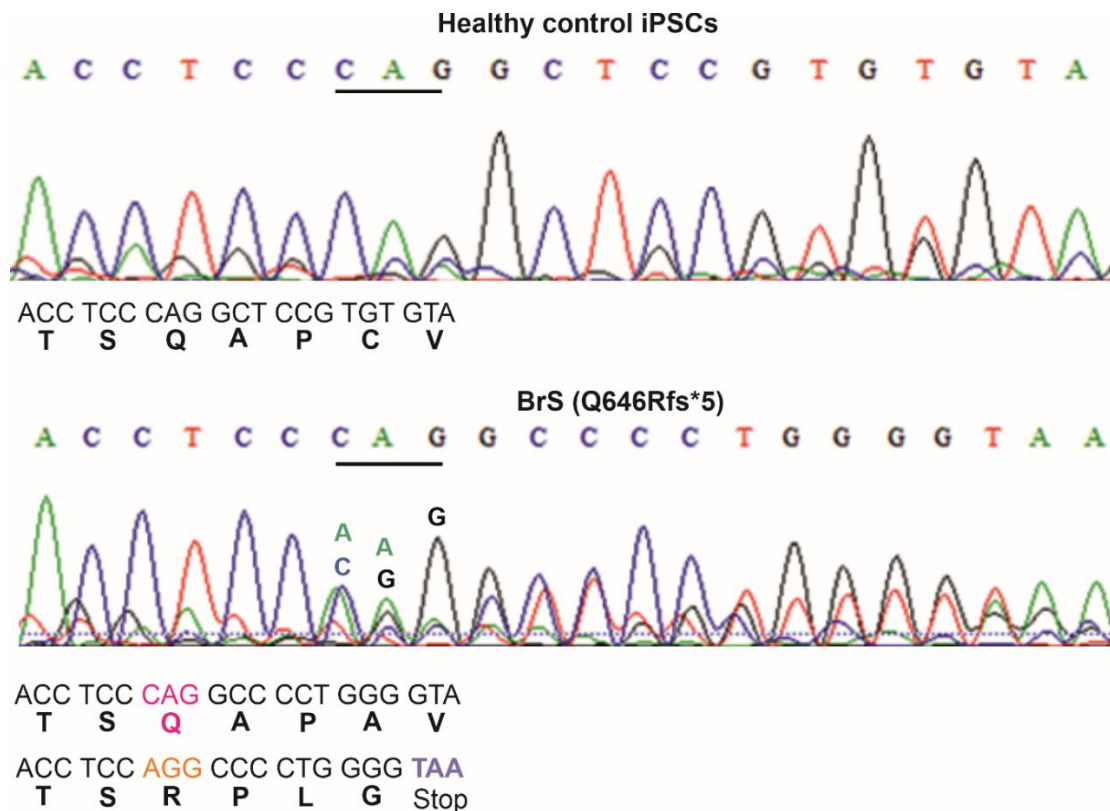


Figure 3-5. Validation of BrS mutation

BrS mutation carries c.1936delC heterozygous mutation at the exon13 of the cardiac sodium channel. The deletion of the nucleotide prematurely introduces the stop codon (TAA) in the sequence.

3.5 Gene expression profiles between healthy control and disease models

Transcriptomic analysis helps researchers investigate the whole transcriptome of an organism, which provides information on how genes are regulated characterizing the organism's biology [165]. Two methods are used for this aim: namely next-generation sequencing (NGS) and microarray technology [165, 166]. The latter has been used for gene profiling characterization during this study. To date, molecular mechanism related to LQTS3 and BrS is still elusive. Principal component analysis (PCA) provides a platform for the overview and first interpretation of large data sets [167, 168]. Additionally to the PCA, hierarchical clustering subsequently allows the grouping of data sets based on their expression profiles that further help for the first data investigation [169]. With the same goal of having a broad overview of the gene expression profiling on healthy control and patients, we performed a transcriptomic analysis and performed with the data a PCA as well as hierarchical clustering. For this purpose, the RNA was sequenced at different time points: day 0, day 20, and day 40 of differentiation. The PCA shows us that at day 0, the gene-level expressions profile between the healthy control and the disease models are close (**Figure 3-6A**). This result is further confirmed by the

clustering of the different cells group in that same condition (**Figure 3-6B**). However, differentiated cells present a difference in gene expression between the early and late stages of the same cell group that could be related to the difference in cell maturation. A clear difference was noticed between the different cell lines showing that gene expression profiles differ considerably among them.

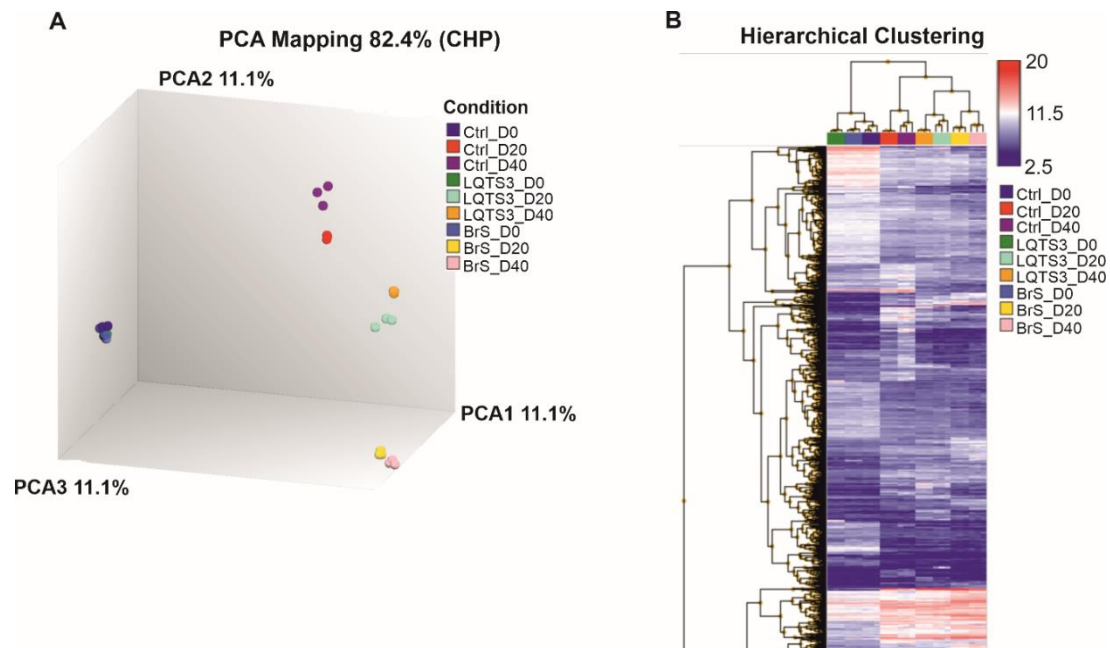


Figure 3-6. PCA and hierarchical clustering

A, Illustration of the principal component analysis (PCA) of cells at different time points. **B**, Hierarchical clustering of the different cell groups. Both present less difference in gene expression between cell lines at D0, but in differentiated CMs differences were observed between cell lines. The gene marker expression was run in triplicate for each condition.

3.6 Genes expression regulation in LQTS3 and BrS compared to the control

Disturbance in the mechanism of depolarization and repolarization has been elucidated during LQTS3 and BrS. However, very little is known regarding the expression profile of the genes involved in this mechanism during the pathology. Therefore, with this study, we aimed to identify the regulation of some key genes that are involved in the mechanism of cardiac physiology during LQTS3 and BrS compared to the healthy control. Gene expression levels obtained from the transcriptomic analysis were considered up- or downregulated when gene level was > 2 or < -2 , respectively with $p > 0.05$. Data analysis shows us that some genes are expressed only at a late time point of differentiation (day 40) but not at day 20 as shown on **Figures 3-7A** and **3-7B**. This observation highlights the need to use an advanced stage of maturation of cardiomyocytes during gene profiling studies. Moreover, genes such as *RyR2*,

CasQ2, and *PLN* that are involved in the mechanism of excitation-contraction coupling, although dysregulated during both conditions (early and late stages), show changes in gene expression level in the two conditions (D20 & D40 CMs), which further underline the impact of cell maturity on gene expression. Gene profiling also demonstrated that the T-type calcium channel gene, L-type calcium channel gene, and its β -subunits are dysregulated in disease models. The *TNNI3* gene is upregulated in the two disease models when compared to the control (**Figure 3-7B**). Interestingly *SCN5A* was downregulated in CMs derived from the LQTS3 patient and upregulated in BrS CMs. In both disease models, the hyperpolarization-activated funny current gene (*HCN4*) and the beta-adrenergic receptor *ADRB2* genes are upregulated which might portray a dysfunction in the heart rate. The T-type calcium channel gene (*CACNA1G*) was upregulated in LQTS3-derived cells. The dysregulation of some of those genes was further validated via qPCR (**Figures 3-7C & 3-7D**). We therefore postulated that during LQTS3 and BrS genes involved in the proper function of the heart are dysregulated.

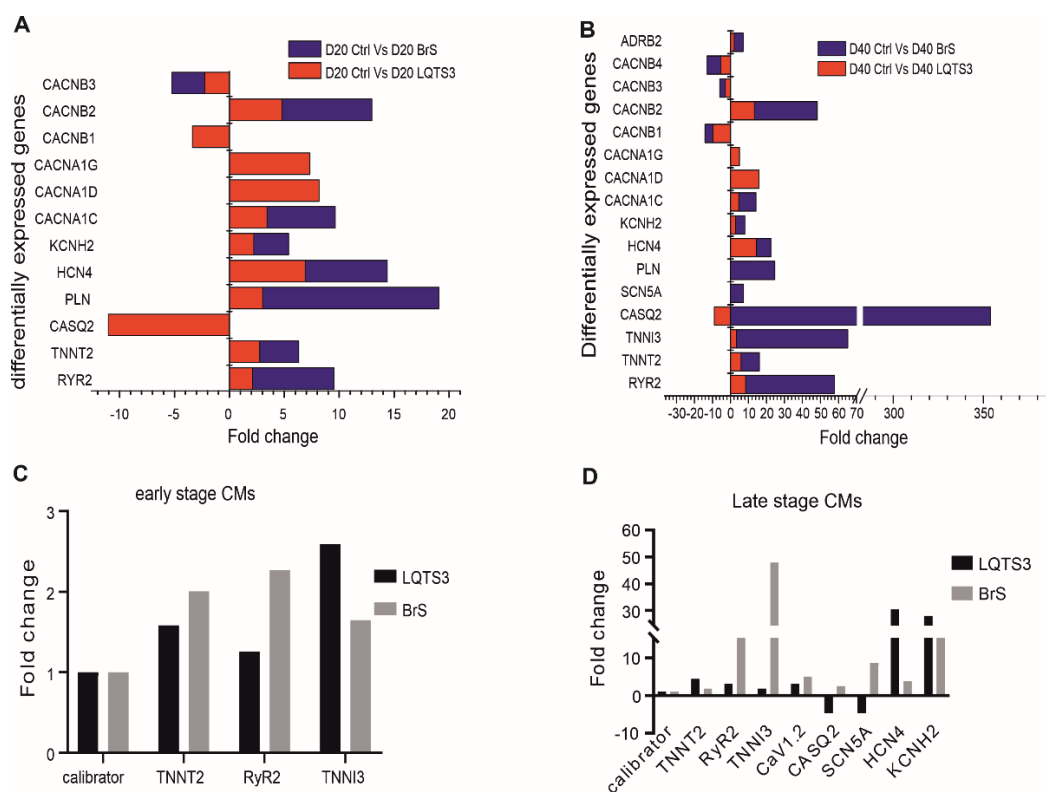


Figure 3-7. Gene-level expression and qPCR validation

A-B, Illustrates gene-level expression between the control and the disease models at different time points early stage (D20) and late stage (D40) of differentiation. Disease models (LQTS3 and BrS) harbour a dysregulation in genes involved in the regulation of ECC, CICR mechanism as well as in cell repolarization. Gene dysregulation was further validated by qPCR (**C-D**) and GAPDH was used as a positive control. Chip and qPCR experiments were run as technical replicates.

3.7 Gene ontology analysis of healthy and defective cardiomyocytes

Cardiac defects can be detectable at a prenatal stage [170, 171]. Therefore, performing the gene ontology (GO) of cardiomyocytes from a healthy subject and patients could tell us if during cardiomyogenesis any abnormal features or pathways will differ from the control. For this analysis, positive regulation of genes at day 40 CMs of each cell line has been compared to their day 0 counterpart corresponding to the pluripotent stage. Genes were plotted in the Metascape analysis tools for functional enrichment analysis. The first 20 sets of gene functions have been selected for our analysis. Functional processes analysis of CMs from the healthy subject and patients revealed that genes involved in heart morphogenesis and heart development are highly regulated and, although gene enrichment shows a positive regulation of cell adhesion in both disease models, this process is more enriched in the control cell line, which also shows a high regulation of cell junction organization (**Figure 3-8A-C**). Other pathways such as head development are also present in all cell lines, which might originate from the use of the B27-supplemented in the differentiation media.

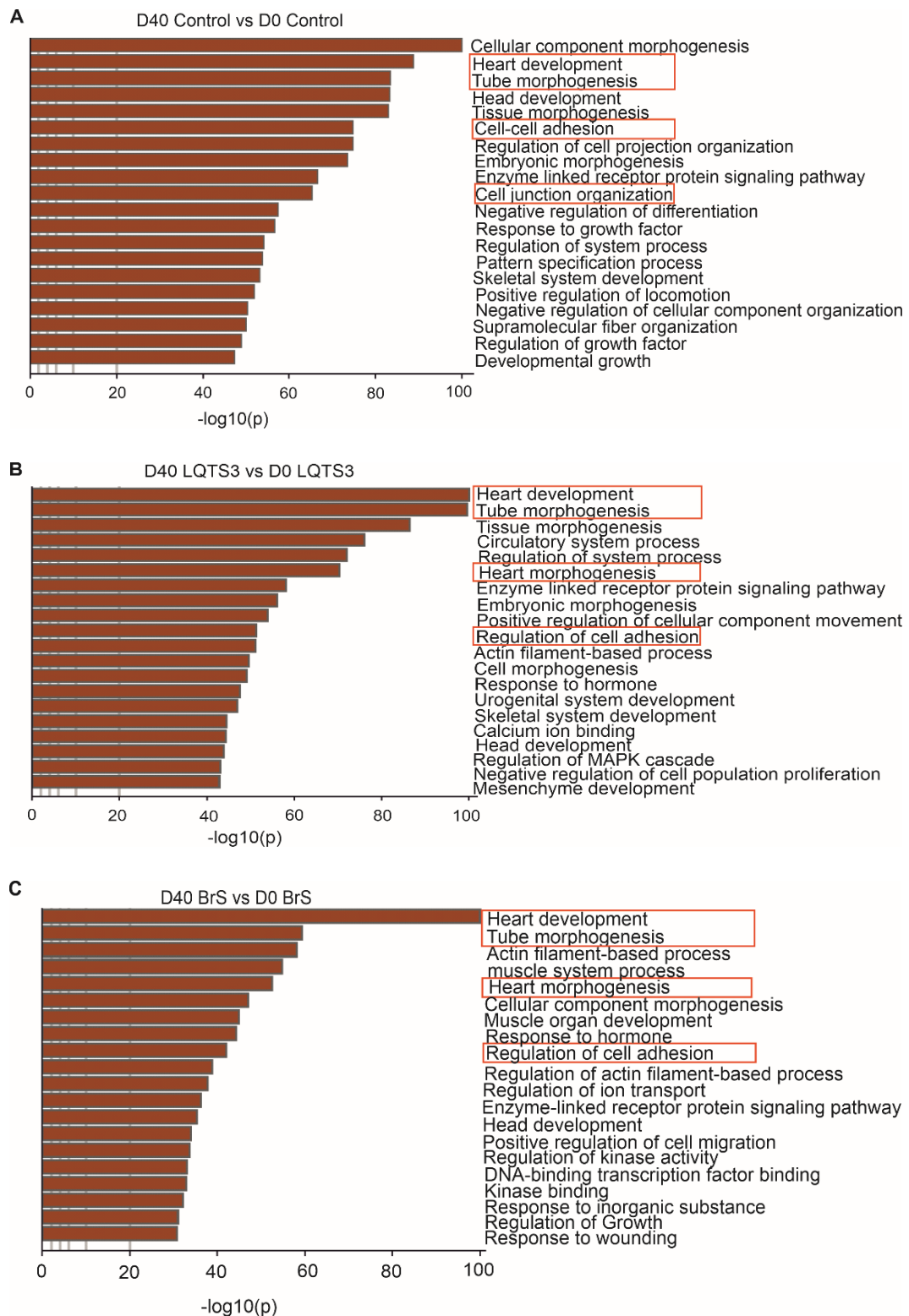


Figure 3-8. Gene ontology analysis.

A-C Represents the gene ontology of derived CMs obtained from the healthy control and LQTS3 as well BrS patients, respectively. The health control shows a higher enrichment in cell-cell adhesion and cell junction organization compared to both patients. Genes involved in the heart development and heart morphogenesis are high regulated in all cell lines. For enrichment analysis, we considered the gene prioritization by evidence counting (GPEC) with $p \leq 0.01$.

3.8 Field potential recording in healthy and disease cardiomyocytes: QTc analysis

Multielectrode Array (MEA) has extensively been used due to its high throughput recordings to access cardiomyocytes' activity by evaluating the field potential rate or QTc interval [172]. Therefore, the device was used during our study to record field potential (FP) and access the difference in QTc between the early stage and late stage of maturation of cardiomyocytes within the same cell line. The results show that the cardiomyocyte of the control subject and the BrS patient present a significant difference in QTc interval between both time points of differentiation (**Figure 3-9A and 3-9B panels a & b**). Moreover, the control cell line presents a lower amplitude at the early stage of differentiation that is statistically significant, reflecting the immaturity of cardiomyocytes on day 20 in contrast to day 40 (**Figure 9A panel c**).

Comparing the QTc interval between the control and LQTS3 cardiomyocytes, we detected a significant prolongation of the QTc interval in the LQTS3 CMs (**Figure 3-9C panels a & c**), revealing the existence of the disease phenotype in this cell line. The comparison was only possible at an advanced time point of differentiation (D40 – D45). Elevated T-wave was also identified on LQTS3 CMs characteristic of the disease phenotype. This observation points out the importance of using late time point CMs to study the different features that are associated with cardiac pathology during in-vitro research.

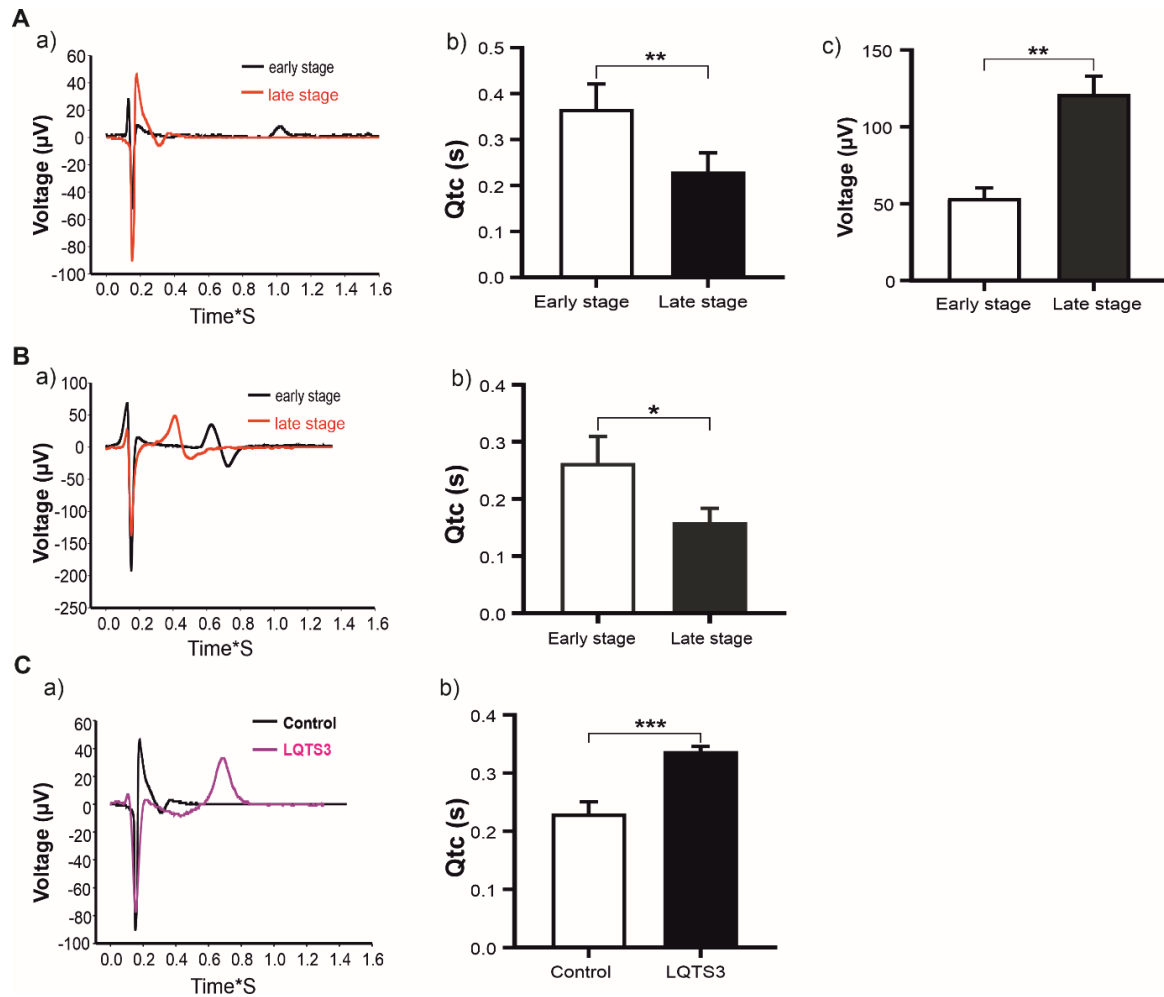


Figure 3-9. QTc evaluation between healthy control and LQTS3 CMs and between early and late stages cardiomyocytes

A-B, Represent the field potential traces of the healthy control and BrS derived cardiomyocytes respectively showing a statistically prolonged QTc interval at the early stage (days 20-25) compared to its late-stage (days 40-45) counterpart. The late stage of the healthy CMs showed an improved cardiac contraction amplitude. **C,** QTc elapsed time is prolonged in the LQTS3 disease model compared to the healthy control. The experiments were performed at 37°C and each experiment represents at least 3 biological replicates. QT was corrected to QTc according to the formula of Fridericia and Hodges. ** represents $P < 0.005$, *** $P < 0.0005$.

3.9 Lidocaine effect on LQTS3-derived cardiomyocytes

Lidocaine which belongs to class 1b of antiarrhythmic drugs has been used to reduce the QTc prolongation induced during tracheal intubation [173]. However, it has also been used on patients underlying the LQTS3 phenotype to correct the functional abnormality of the heart [174]. In this study, pharmacological lidocaine range as well as non-clinical range were used. Using lidocaine's clinical range on hiPSC-CMs derived from LQTS3 patients, we observed that this drug failed to restore the QTc to normal. On the contrary, it further prolonged it in a

concentration-dependent manner as illustrated in **Figures 3-10A panel a and 3-10B panel a**. Moreover, with concentrations above the pharmacological range, the QTc interval could not be restored either (**Figure 3-10A panel b and 3-10B panel d**). At 20 μM the drug tends to increase the FP rate with a statistical significance, but it does not increase the amplitude of cells (**Figure 3-10B, panels b & c**). However, at higher lidocaine concentrations (30 μM – 50 μM) the voltage significantly decreases which might reflect the toxicity of the drug at these concentration ranges (**Figure 3-10B, panel f**). Moreover, at these latter concentrations, the cells' activity was significantly increased in a concentration-dependent manner (**Figure 3-10B, panel e**).

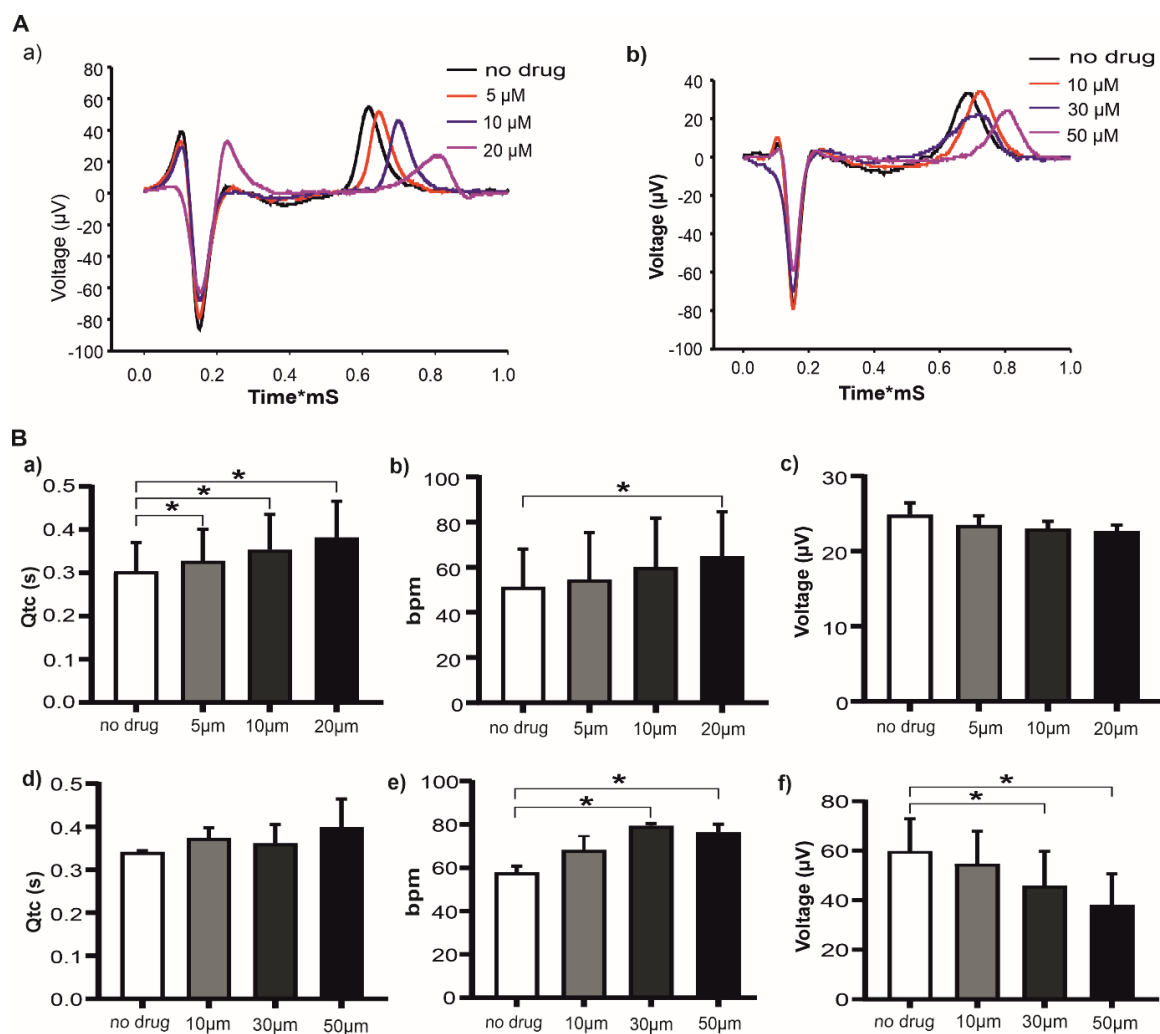


Figure 3-10. Effect of lidocaine on LQTS3-derived cardiomyocytes.

A, Representative illustration of lidocaine treatment on LQTS3-derived cardiomyocytes at clinical and nonclinical concentrations. In both cases, lidocaine failed to restore the QTc interval to normal. **B**, Statistical representation of lidocaine effect on the QTc, the FP rate and the amplitude of LQTS3 CMs. The study was carried out at 37°C and n represents a minimum of 3 biological replicates. * $P < 0.05$. non-treated (no drug) and treated cells are compared.

3.10 Field potential comparison between healthy control and disease models in different maturation time points

Bradycardia phenotype observed during LQTS3 has been correlated to age [175]. In BrS patients as well, this phenotype is responsible for the phenomenon of SCD that occurs at rest [176]. Therefore, to identify this phenotype in-vitro, FP recording was performed at different stages of cardiomyocyte maturation. Using derived cardiomyocytes from LQTS3 and BrS patients at D20 – D25 of differentiation, we observed that the pathological phenotype could be observed on LQTS3 CMs but not on BrS CMs (**Figure 3-11A panels a-c and 3-11B panel a**). However, at a more mature stage (D40 – D45) the phenotype appeared in both disease models (**Figure 3-11A, panels d - f**) with statistical significance (**Figure 3-11B, panel c**) when compared with the control. This suggests that during the characterization of derived cardiac cells in-vitro, it is important for the cells to reach a certain threshold of maturity to mimic what could occur or what is occurring in-vivo. Moreover, at the early stage of differentiation, the amplitude of contraction was significantly increased in BrS cardiac cells compared to the control, while in the late stage of differentiation, the amplitude between the control and BrS CMs did not show a difference (**Figure 3-11B panels a and b**).

We also observe that at the late time point of differentiation, CMs generally exhibit a higher amplitude in all cell lines compared to their early-stage counterparts (**Figure 3-11B, panels b and d**) further characterizing a better setup of ion channels involved in the mechanism of cardiac cell contractility.

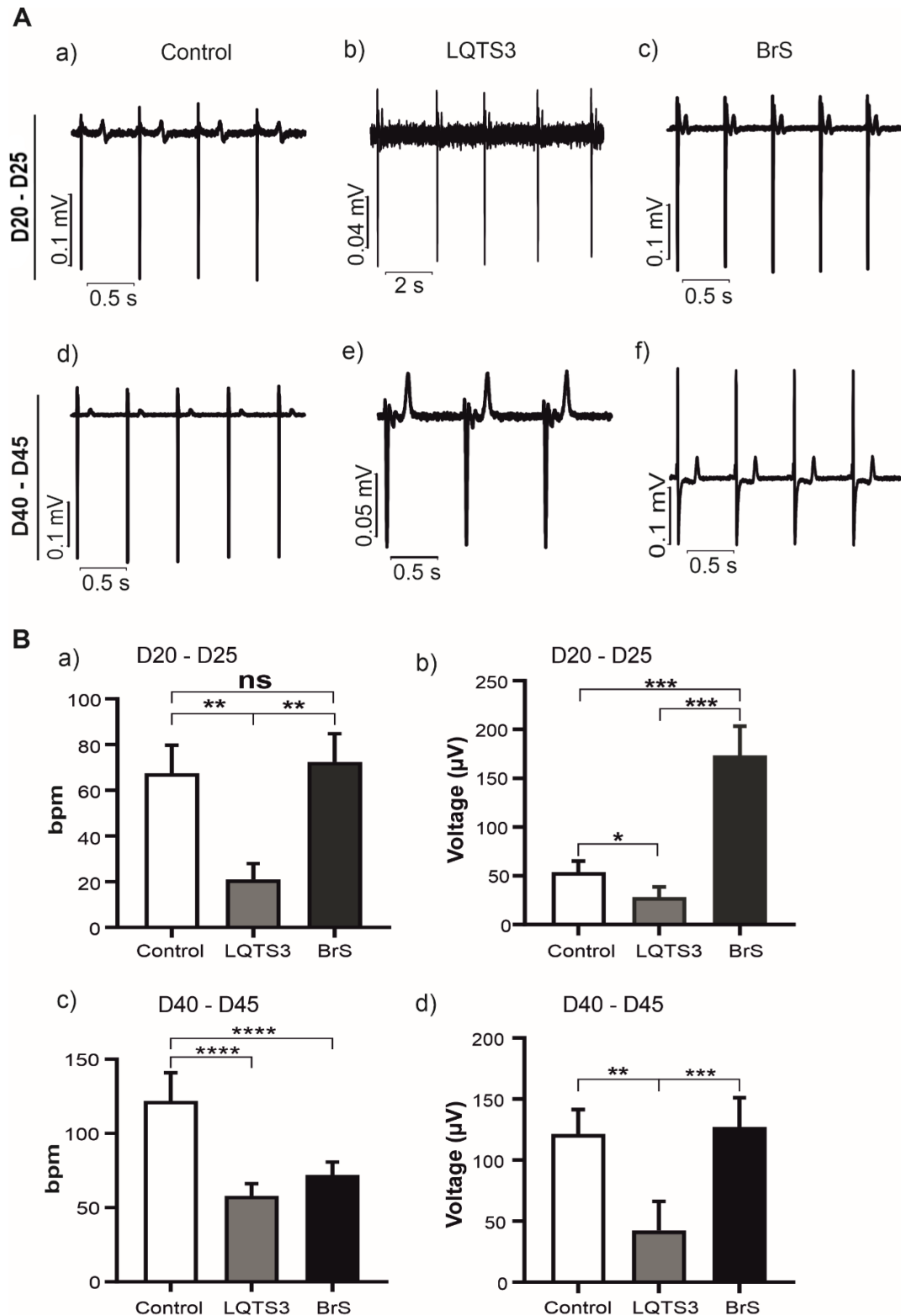


Figure 3-11. Amplitude and field potential rate of control cell line and disease models

A, Representative field potential traces of control, LQTS3, and BrS cardiomyocytes. **B**, Statistical results of FP rate and amplitude differences between the control and both disease models obtained from the recorded FP (n represents at least 3 biological replicates). The experiment was performed at 37°C. * $P < 0.05$, ** $P < 0.005$, *** $P < 0.0005$. Comparison is made between control vs disease models or LQTS3 vs BrS.

3.11 Calcium transient measurement for field potential rate evaluation on cell sheets

Another technique of measuring FP rate is through the evaluation of calcium transient during calcium imaging with the help of calcium indicators. Although showing some limitations and disadvantages, this technique further helps in the understanding of disease mechanisms. Performing the experiments with CMs at both stages of differentiation, we were able to observe that, compared to the control, patient-derived CMs present a reduced cells' activity (**Figure 3-12 A & B**) and the result was statistically significant (**Figure 3-12 C & D**). Moreover, CMs of patients tend to present more signs of arrhythmia during measurement than the control. We also observed that, at the early stage, cells of the healthy subject have a reduced activity compared to the late stage, while in BrS-derived cardiomyocytes, the opposite was observable (**Figure 3-12C panel left and right** respectively) pointing out the importance of cell maturation during in vitro studies to mimic what might occur in vivo.

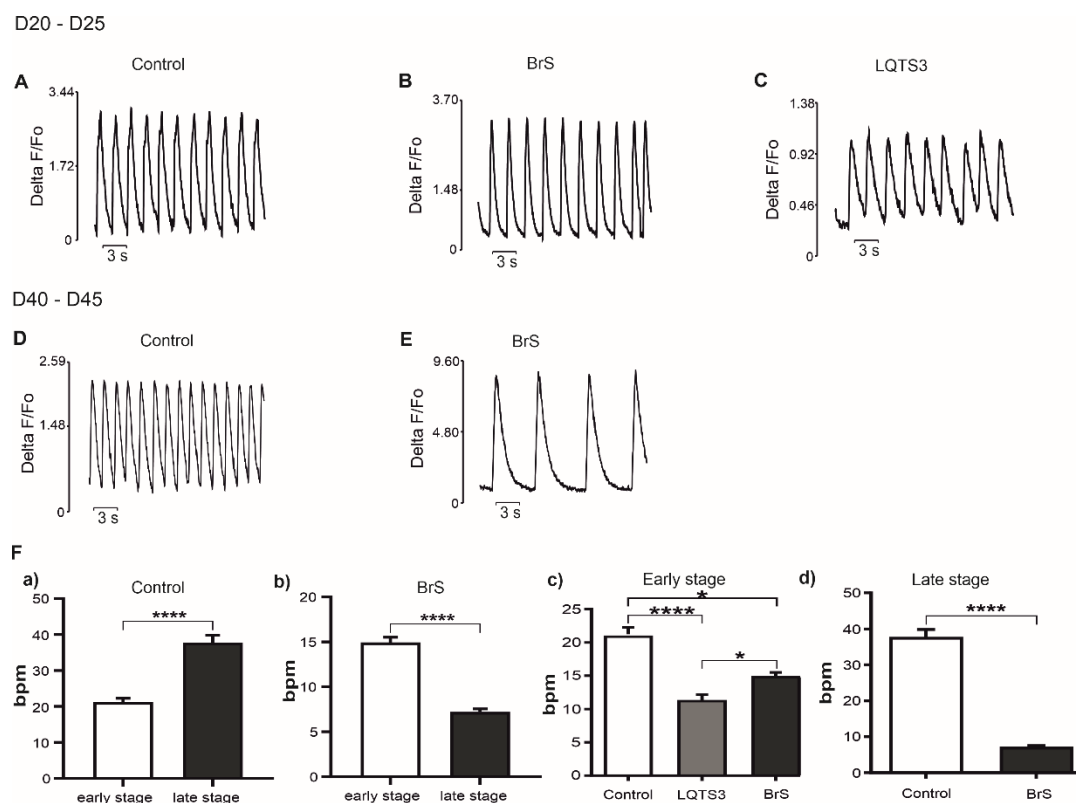


Figure 3-12. Calcium transient in control and patient derived cardiomyocytes

A-E, Field potential traces of derived cardiomyocytes from a healthy subject, BrS, and LQTS3 patients at the early and late stages. **F**, Statistic quantification of the FP rate between the healthy control and the disease models at the early and late stages. n=19 for LQTS3 CMs. n=80 and n=42 for the healthy control at early and late stages respectively. n=42 and n=52 for BrS CMs at early and late stages respectively. This study was done at RT (22°C to 24°C). *P<0.05 and ****P<0.00005.

3.12 Calcium transient measurement for field potential rate evaluation on single cells CMs

To further validate the difference in FP rate between the cells of the healthy control and the patients, we performed the experiment with single cells to obtain the results on both dimensions (single cell and cell sheets). Indeed, fluorescence imaging can be performed with different cell types: clusters, sheets, or single cells [177]. The aim of performing this analysis with both cell types was to evaluate the impact of those on the data interpretation. The study was done with days 20-25 and days 40-45 cardiomyocytes corresponding to the early and late stages, respectively. The results show that compared to the control, the bradycardia phenotype is observable in disease models at all stages of differentiation with a statistical significance (**Figure 3-13 A, B, D**). We also noticed that within cell lines, no difference in FP rate was noticeable between the early and the late time point of differentiation as is the case for the control and LQTS3 cell lines (**Figure 3-13 C panels left and middle**). However, a difference was observable in the BrS cell line (**Figure 3-13 C, panel right**).

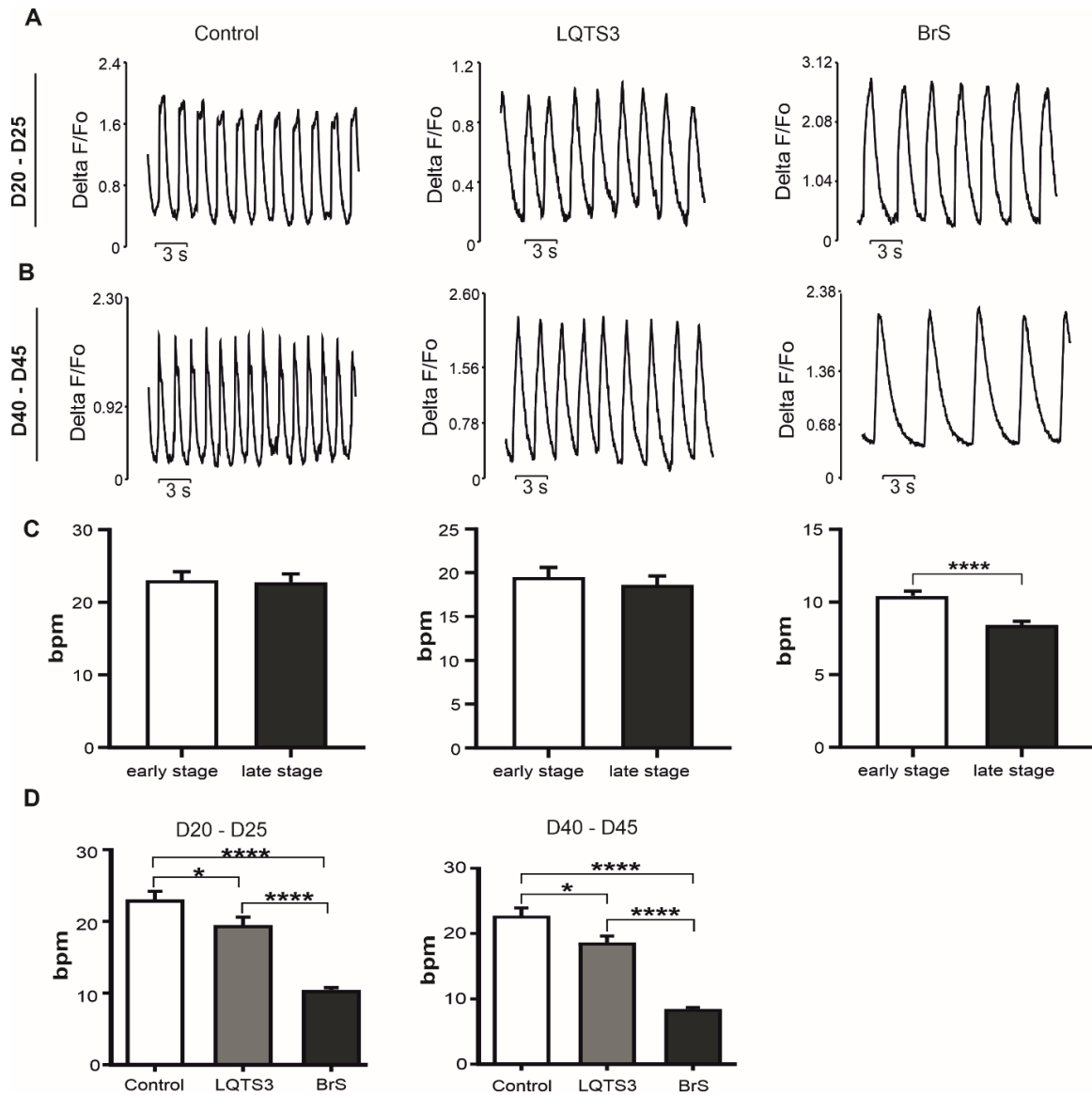


Figure 3-13. Evaluation of field potential rate using single cells

A-B Representative traces of FP from the control and the disease models. **C**, Statistical representation of the early and late stages CMs between the same cell lines. Compared to the control, the activity of the cells is reduced in both disease models (**D**). $n = 49$ and $n = 60$ for the control at the early and late stages of CMs respectively. $n = 61$ and $n = 28$ for LQTS3 CMs at the early and late-stages respectively. $n = 131$ and $n = 131$ for BrS-derived CMs at early and late stages respectively. The experiment was run at RT between 22°C to 24°C. * $P < 0.05$ and **** $P < 0.00005$.

3.13 Comparison of the field potential rate between early and late stages CMs in single cells and cell sheets

Cardiomyocytes analysis using single cells (SC) or cell sheets (LC) may influence cardiomyocytes characterization. Therefore, for our study, we used both cell types at different time points of differentiation to compare the FP rate outcome between both. The result analysis

shows that within cell lines, using single cells or cell sheets significantly impacts the FP rate (**Figure 3-14 A-C**). In the control cell line, for example, we observed that using cell sheets resulted in an increase in cell activity at the late stage of differentiation whereas in BrS this activity is reduced compared to the SC equivalent. At the early stage, on the other hand, cardiomyocyte activity is increased in BrS cell sheets compared to the single-cell counterpart, whereby in the LQTS3 disease model, the adverse result was obtained. These observations showed that during disease model investigation the type of cells that are used could influence the interpretation of the FP rate.

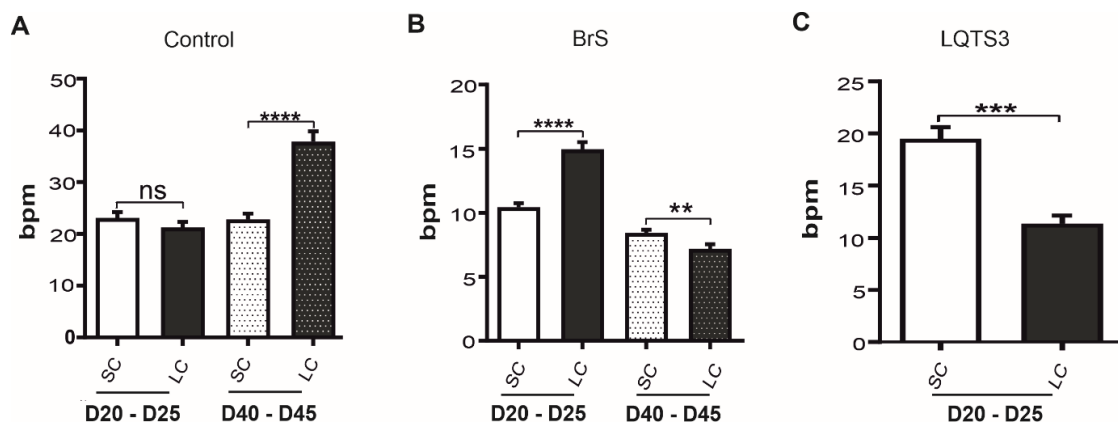


Figure 3-14. Field potential rate comparison between single cells and cell sheets

A-B, Represents the quantification of cells' activity between single cells (SC) and cell sheets (LC) in distinct maturation time points of the control and BrS cell lines respectively. Differences in FP rate were observable between two cell types within the same cell line. **C**, Early-stage CMs of LQTS3 display a difference in the FP rate between single cells and cell sheets. The number of measured cells for each individual was as followed: $40 \geq N \geq 130$. Data was recorded at 22°C to 24°C RT. ** $P < 0.005$, *** $P < 0.0005$, **** $P < 0.00005$, *ns*=non significant.

3.14 Cardiomyocyte calcium transient in healthy control and disease models

Calcium plays a key role in the mechanism of ECC. Therefore, improper calcium transient could be subject to dysfunctional cardiac functionality. Accordingly, a defect in calcium homeostasis has been observed during LQTS3 [178] and BrS [179]. To verify this hypothesis with our disease models, calcium imaging was performed using single cells or cell sheets at different maturation time points. At a single-cell level, there was likely no difference observable in the calcium transient of the control and the BrS cell line at the early stage. However, at this stage, LQTS3 CMs already present signs of arrhythmias (**Figure 3-15A**). At the late stage, both disease models present an impaired calcium transient compared to the control characterized by a prolonged Ca^{2+} transient in LQTS3-derived CMs and an appearance of trigger activity (EADs) in BrS-derived CMs (**Figure 3-15B**). Indeed, it takes a long time for

LQTS3 CMs to return to the baseline whilst most of BrS CMs show signs of trigger arrhythmia, illustrating a defective cardiac functionality. Using cell sheets, we could further validate the abnormal cardiomyocyte functionality in the LQTS3 model. Interestingly, by using this cell type, it was possible to observe impaired Ca^{2+} homeostasis in BrS CMs at the early stage, highlighting the importance of considering the type of cell used during in-vitro studies of cardiac diseases (**Figure 3-15C**).

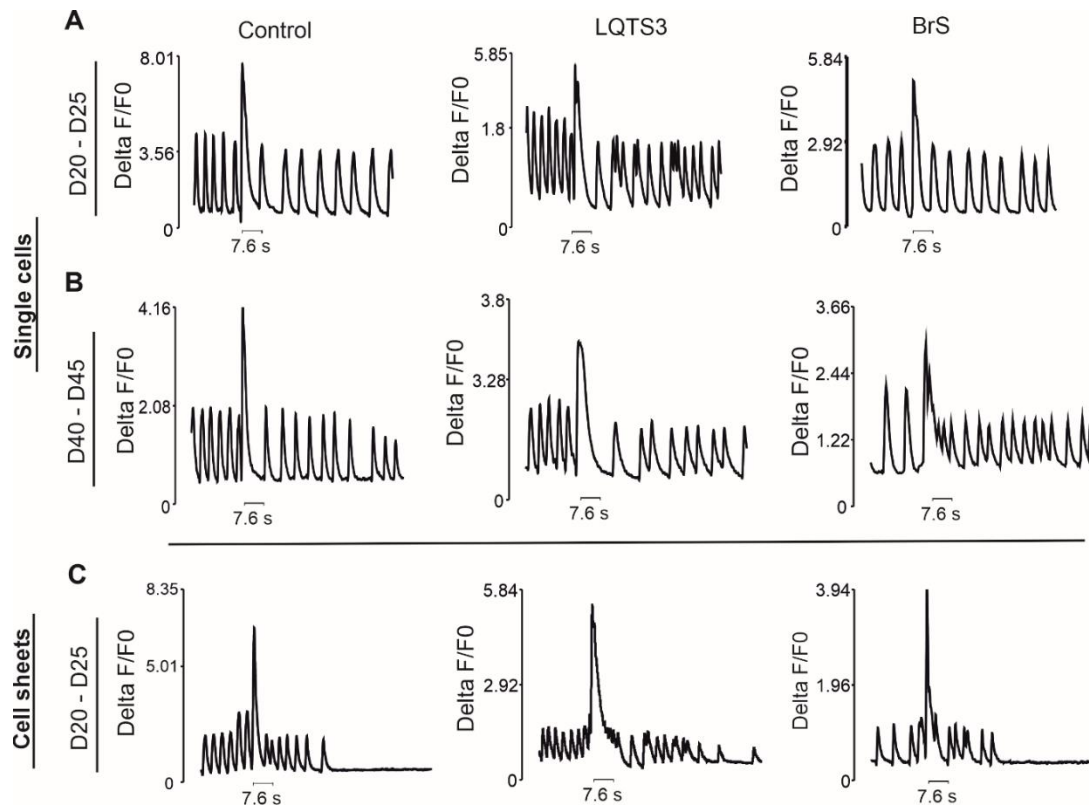


Figure 3-15. Calcium transient in healthy control and disease models

A-B, Representative traces of calcium transient on control and patient derived CMs at early and late stages of differentiation at single cells level. Patient-derived CMs show a disturbance in calcium homeostasis. **C,** Calcium homeostasis between healthy control and disease models at the early stage of differentiation using cell sheets. Both disease models show an abnormal calcium transient (FPD). The experiments were done at RT (22°C to 24°C).

3.15 Time to 50% relaxation in healthy and unhealthy cardiomyocytes

To further access the calcium transient in healthy control and disease models, the time of 50% calcium decay has been evaluated. Indeed, this analysis provides additional information regarding the halftime of cardiomyocytes' relaxation in healthy control and disease models. The experiment was run with single cells and cell sheets at distinct cardiomyocytes maturation time points and the results show that data interpretation can be affected by the kind of cells that

have been used and the time point of maturation. Indeed, single cells analysis shows that the halftime extrusion of the calcium from the cytosol lasts longer in LQTS3 CMs compared to the control, while no difference was noted between the control and BrS-derived cardiomyocytes at the early stage of maturation (**Figure 3-16A**). However, at a more mature stage (D40 – D45), the analysis of the single-cell revealed that the half time of Ca^{2+} removal is delayed in either disease model (**Figure 3-16B**), indicating that cell maturity is important for the functional characterization of disease models. Moreover, by comparing this time in cardiomyocyte's from early and late stages within cell lines, we observed a significant reduction in this time in the healthy control and BrS at the late stage (**Figure 3-16C**), further showing the maturation of the cells at day 40 compared to day 20 of differentiation. In the case of LQTS3, this time also tended to be reduced at day 40, although this reduction was not statistically significant. Using linked cells, we observed that at the early stage (D20 - D25) of differentiation, both disease models could show a prolonged half time of Ca^{2+} extrusion as illustrated (**Figure 3-16D**). Additional comparison of the half time of Ca^{2+} removal between single and linked cells revealed that this time could change significantly depending on the type of the cells used (**Figure 3-16E**), which could explain the occurrence of inadequate Ca^{2+} extrusion in both disease models at the early stage when using cell sheets.

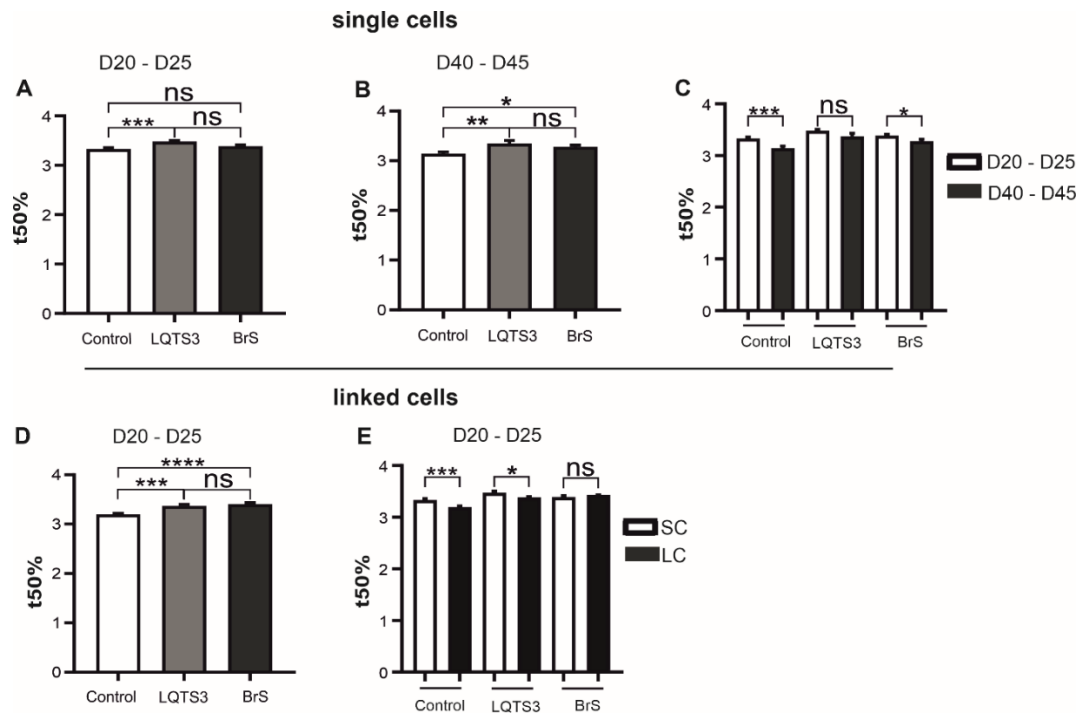


Figure 3-16. T50% of calcium extrusion in healthy control and disease models

A-B Represents respectively the statistical analysis of 50% Ca^{2+} decay in control and disease models at early and late-stage at the single cells level. Delay in $[\text{Ca}^{2+}]$ -related fluorescence decay is detected in the two disease-related cardiomyocyte populations at the late stage of CMs. **C**, A difference in the time elapsed to extrude half of the Ca^{2+} from the cytosol differs between both stages of maturation. Using cell sheets, a prolonged fluorescence decay could be identified at the early stage in both disease models (**D**). **E**, Illustrates the difference of half time of Ca^{2+} extrusion between single cells and cell sheets within the same cell line. The study was performed at RT between 22°C and 24°C. * $P < 0.05$, ** $P < 0.005$, *** $P < 0.0005$, **** $P < 0.00005$, *ns*=nonsignificant.

4 Discussion

4.1 Culture of hiPSCs in a xeno-free and feeder-free system

Cardiovascular diseases are acquired or congenital heart disorders representing one of the main causes of morbidity and mortality worldwide [180, 181]. LQTS3 and BrS are congenital channelopathies caused by a mutation in the *SCN5A* genes leading to a gain-of-function and loss-of-function of the channel respectively [182]. Pathophysiological mechanisms characterizing both diseases are still elusive and require more investigation.

Thanks to the novel technology using reprogramming factors to drive differentiated cells into stem cells, scientists have been able to generate human-induced pluripotent stem cells (hiPSCs), which constitute a valid in-vitro model for diseases and drug discovery. Therefore, to conduct in-vitro experiments that will be beneficial for clinical application, different hiPSCs culture protocols have been developed to obtain a culture deprived of animal supplements in a xeno- and-feeder-free system [183-185]. Indeed, despite maintaining a normal phenotype in a prolonged culture, it was shown that culturing hiPSCs on mouse embryonic fibroblast (MEFs) and human dermal fibroblasts (HDFs) could be problematic for the transfer of in-vitro study into a clinical approach, due to cell contamination [186]. Therefore, cell culture in a xeno-free and feeder-free system has gained scientists' interest. Thus, for our cell culture, the same system was used. We cultured our hiPSCs in the E8 media from Thermo Fisher and used either vitronectin or matrigel as an extracellular matrix for cell' plating, which offers a xeno-free and feeder-free system [187, 188]. The culture of our cell lines in this system was successful and up to 50 cell passages could be performed with successful differentiation showing the accuracy of the media and the extracellular matrix to preserve the cell's pluripotency in a long-time culture. Nevertheless, we also observed that proper handling during cell passage is required to maintain cell quality and viability. Indeed, we noticed that an appropriate cell passage is a crucial step for good differentiation.

4.2 High effectiveness of cardiomyocytes differentiation with RPMI supplemented with ascorbic acid

To date, many protocols based on monolayer culture using small molecules such as CHIR99021, Activin A, BMP4 and Wnt inhibitors such as IWP2, IWR1, or Wnt-C59 [189-191] have been proposed for cardiomyocytes differentiation for further scientific investigation and cell therapy. *Burridge et al.* for example showed that incubating hiPSCs in a chemically defined media supplemented with an appropriate concentration of CHIR99021 for two days

followed by another two days of cell treatment with Wnt-C59 could give up to 90% CMs after purification [189]. Moreover, studies have shown that ascorbic acid is an effective enhancer of cardiac differentiation via the promotion of cardiogenesis [192, 193]. Therefore, we adapted our protocol of differentiation based on these previous findings. We used the same small molecules as *Burridge* and the same incubation time as described in **Figure 3-2A**, but a different media composition made of RPMI+glutamax supplemented with B-27-insulin, and we maintained the ascorbic acid in the media to promote cardiac differentiation and maturation as previously described [159]. After cardiomyocytes purification through glucose starvation for 4 days, cells were characterized at day 20 by immunohistochemistry to assess troponin T and alpha-actinin expression. In all cell lines, both markers were considerably expressed and revealed cross-striated organization, although primitive. FACS analysis further revealed that up to 90% of cells were TNNT2 positive showing the efficiency and the robustness of this protocol.

4.3 Late-stage characterization of the sarcomere and connexin 43 organization between the control and the disease models

The sarcomere organization is important to assure and maintain the proper functionality of the heart [11, 194]. Although primitive in *in-vitro*-derived cardiac cells, their characterization using sarcomeres' markers are crucial to validate the quality of the cardiomyocytes. In all our cell lines, we were able to identify the establishment of this cardiac unit, whose arrangement is already taking place at the early stage of differentiation. Nevertheless, when comparing the late-stage CMs to early-stage CMs, we observed a better alignment of myofibrils, an observation that was also made by *Pioner and associate* on their long term hiPSC-CMs culture [195]. Therefore, long-term culture promotes the maturation of CMs. However, additional experiments are necessary to assess the organization of this cell unit in disease models which will help to bring more insight in the pathological mechanism underlying LQTS3 and BrS.

To understand the disturbances occurring during heart failure, studies related to gap junction expressions and organization were conducted. Cell-to-cell communication in the heart is mostly assured by Cx43, which expression can be impaired or improperly distributed in an abnormal heart [196-199]. Moreover, a study on mutated mice mimicking the BrS phenotype revealed impaired conduction velocities and a probable delocalized Cx43 from the intercalated discs [160] raising the hypothesis of delocalized Cx43 arrangement during BrS. During our study, we could not observe a displacement of Cx43 within the intercalated discs of CMs derived from the BrS patient suggesting that disturbance in the electrical coupling during BrS might not be

a consequence of Cx43 defects. This observation align with the finding of *Li et al.* who used hiPSC-CMs as well [200]. However, the latter author described a probable reduction of the Cx43 protein in BrS CMs, which is similar to the finding of *Nademanee and collaborators* [201]. Indeed, performing an in-vivo study using ablated epicardial of the right ventricular outflow tract (RVOT) of BrS patients, the author shows that Cx43 could be reduced in those patients. This suggests that the reduction of this protein in a heart of a BrS patient may be the reason for the abnormal conduction velocity observed and not the dislocation of the protein within the intercalated discs. Cx43 also seems to be properly distributed within the sarcomere in LQTS3 cardiac cells, but just as in the case of BrS, additional analysis such as the protein quantification should be accessed to obtain supplemental information. Furthermore, looking for Cx43 and SCN5A interaction could bring more insight in the understanding of arrhythmia occurring during both diseases. Indeed, it has been speculated that electrically altered sick hearts frequently exhibit decreased excitability and reduced expression of gap junctions [202] with unknown impact on the heart functionality. Moreover, a recent study showed that the overlap and interaction of Cx43 and SCN5A is reduced in BrS CMs compared to the control CMs [200], which required further investigation.

The immunostaining also revealed that Cx43 can be localized in the nucleus in all cell types. Indeed, it has been shown that the presence of Cx43 at this site of the cell, as well in the mitochondria, has a cardioprotective effect and is also involved in cell growth regulation and differentiation [203] showing the multifunction of connexins in cells.

4.4 Validation of the disease mutations.

HiPSCs derived from a skin biopsy of a healthy donor and patients were reprogrammed and cryopreserved by the Saric group at the University Hospital of Cologne. More details regarding those cell lines can be found online (<https://hpscreg.eu/>) under UKKi011-A, UKKi008-A, and UKKi030-C, respectively. The gene sequencing performed during this study could further validate the existence of the V240M mutation responsible for the LQTS3 as previously reported [163]. The frameshift mutation 1936delC has also been identified and revealed that this mutation leads to the insertion of a premature stop codon in the sequence of the *SCN5A* gene. A previous study associated with this BrS mutation further supports our finding [164]. Therefore, in this study, we were able to prove that the mutations that drove both diseases: LQTS3 and BrS are present on the respective cell line, which allowed us to continue with the characterization of the cardiac cells.

4.5 Gene expression profile between healthy control and disease models

To date, the molecular mechanisms related to LQTS3 and BrS are still elusive and require further investigation. During this study, we aimed to discover whether gene mutation could also impact the expression of other genes involved in cardiac functionality. For the gene expression analysis, we performed transcriptomic analysis of each cell line at distinct differentiation time points: day 0, day 20, and day 40 corresponding to hiPSCs, the early and late stages of cardiomyocytes, respectively. The principal component analysis (PCA), as well as the hierarchical clustering, show that gene expression between all cell lines at day 0 of differentiation is likely the same, whereas, for differentiated cells, both graphs present differences in gene expression between cell lines and within cell lines at different time points of maturation. Although genes at day 20 and day 40 of the same cell line are distinctly expressed due probably to the difference in cell maturation, the difference in gene-level expression was more pronounced between CMs of the healthy control and the disease models, as well as between the two disease models. These differences could be directly related to the non-identical genetic background of the subjects while some differences could be associated with the disease. Due to this observation, we decided to do an in-depth investigation by looking at genes that could be differentially expressed focussing our attention on genes that are involved in the mechanisms of cardiac excitability and contractility.

4.6 Genes expression regulation in LQTS3 and BrS compared to the control

LQTS3 and BrS are associated with an electrical disturbance of the heart. Although some functional aspects are well studied, very little is known on the molecular level. Therefore, during our study, we tried to identify genes that might present differences in regulation and paid attention to some key genes that are directly involved in the mechanical as well as functional properties of the heart. In the first approach, we evaluate the *SCN5A* gene expression in BrS and LQTS3 CMs. Interestingly *SCN5A* was up regulated in BrS CMs, a result that was further validated by qPCR. However, even though the transcriptomic analysis could not provide any information regarding *SCN5A* expression in LQTS3 CMs, qPCR analysis shows that this gene is downregulated compared to the control. This result outcome might be controversial to the sodium channel functionality described to date for both diseases, namely gain-of-function and loss-of-function during LQTS3 and BrS, respectively [182, 204]. However, this controversy may be explained by the discrepancy that can be found between gene expression at the mRNA and the protein level [205], suggesting that to make a proper conclusion of our observation we required the data of this gene at the protein level. Indeed, it has been postulated

that loss-of-function of the channel associated with BrS is related to the synthesis deficiency of the channel [206], which further supports the hypothesis of deficiency of the channel at the protein level. This hypothesis is also supported in this study by the introduction of a premature stop codon in the sodium channel sequence due to the frameshift mutation as shown in the BrS sequence. Down-regulation of *SCN5A* in LQTS3 cardiac cells could also be associated with an existing overlapping phenotype between LQTS3 and BrS. Indeed, a mixed phenotype between LQTS3 and BrS has already been published in earlier studies [129, 207], where our hypothesis of mixed phenotype displayed by the *SCN5A*-V240M mutation.

Gene profile analysis also displayed a dysregulation in the genes involved in the mechanical and functional activity of the heart, and some of those genes were further validated by quantitative PCR (qPCR). LTTCs have diverse functions: initiation of the mechanism of excitation-contraction coupling, regulation of the action potential duration (APD), and gene expression [208]. In both disease models, *CACNA1C* that codes for the CaV1.2 calcium channel was upregulated, and dysregulation of the *CACNA1D* gene encoding for CaV1.3 calcium channel was additionally observed in LQTS3 derived CMs. Overexpression of LTCCs in LQTS3-derived CMs has already been described in a previous study [178]. Moreover, dysregulation of LTTCs has also been signaled during heart failure [209], suggesting that dysregulation of these genes during LQTS3 and BrS may affect the calcium transient and impact cardiac contractility. Moreover, functional analysis revealed that on patient derived CMs, L-type calcium channels fail to be properly inactivated [210]. However, the current density was not increased. The transcriptomic analysis also showed that beta subunits (*Ca_vβ*) genes are dysregulated in both disease models. In fact, previous studies have already showed their importance in the mechanism of excitation-contraction coupling (ECC) [211, 212]. Additionally, previous studies revealed that *Ca_vβ* may play an important role in calcium current density [213, 214]. In this study we observed a downregulation of *Ca_vβ1*, *Ca_vβ3*, and *Ca_vβ4* in both disease models compared to the control, and an upregulation of the *Ca_vβ2* gene. Indeed, among all the *Ca_vβ* subunits isoforms, *Ca_vβ2* is the most common form found in the human adult heart [215] and also the only subunits to form the L-type voltage-dependent Ca^{2+} channel (L-VDCC) [216]. During their study, the latter authors speculated that *Ca_vβ2* is impaired in mice with heart deficiency, which could raise the importance of this protein in the regulation of calcium trafficking. A previous study also supported the hypothesis of regulation of LTCCs activity through *Ca_vβ2* [217]. However, a recent study speculated that *Ca_vβ* subunits are not indispensable for ECC but are essential for proper modulation of the β-adrenergic stimulation

[218]. Thus, understanding the role of these subunits might further help to understand the pathological mechanism associated with BrS and LQTS3.

Low voltage-activated calcium channels also known as T-type calcium channels are implicated in several physiological functions [219]. It was speculated that the faculty for this channel to be activated under low membrane depolarization is beneficial for the cells during certain physiological events [220]. However, studies revealed that, although not directly involved in the phenomenon of ECC, the T-type Ca^{2+} channel might play a role in cardiac diseases [221-223]. Indeed, T-type Ca^{2+} channels are mainly expressed in fetal heart [224] and studies have demonstrated that in a failing heart, fetal genes could be reactivated and contribute to cardiac dysfunctionality [225]. Moreover, studies postulated that in pathological hearts the channel resurface [226]. Indeed, our experimental study revealed that the *Cav3.1* gene persists in CMs derived from LQTS3 patients, which may point out the pathologic feature of those cells. However, we are still sceptical regarding this hypothesis, due to the fetal-like type of CMs produced in-vitro on the one hand and the protective cardiac effect of its channel in another hand [227]. Therefore, further research is required to determine the importance of this channel in LQTS3 disease. Additional genes such as *RyR2*, *CASQ2*, and *PLN* encoding proteins that are involved in calcium regulation were also dysregulated in both disease models. Among those genes, some have already been associated with SCD by a previous report [228]. Furthermore, other studies demonstrated that proteins that are tightly bound to Ca^{2+} store and Ca^{2+} release from the SR are dysregulated during both LQTS and BrS, which could explain the impaired contractile function of the heart during both channelopathies [229-231] due to an impaired Ca^{2+} load in the SR. However, supplemental studies are needed to additionally provide a deep understanding of the molecular pathology underlying LQTS3 and BrS.

Further analysis of the gene-level expression between the healthy control and heart insufficient patients revealed that in both pathological CMs, β 2-adrenoreceptor (*ADRB2*) is upregulated. Although β 1-adrenoreceptor (*ADRB1*) is the main cardiac receptor involved in the modulation of the heart rate and cardiac contractility, it has also been suggested that *ADRB2* may play a role in this above-mentioned mechanism [232]. This finding supports the hypothesis that compromised heart rate could be associated with dysfunctional adrenergic receptors. That β 1-adrenoreceptor is not expressed at day 40 of differentiation might reflect the immature phenotype of the cells compared to the native human ventricular cardiomyocytes. Indeed, a previous study showed that on day 30 of differentiation, *ADRB2* is highly expressed and only

on day 60 a transition of downstream signalling to ADRB1 occur [233], explaining the absence of the expression of this gene in our experiment.

To gain a deeper insight into the features that can influence the proper function of the heart during LQTS3 and BrS, we examined the *HCN4* gene expression, which plays an important role in cardiac automaticity. The result showed that in both disease models, this gene is upregulated. A recent study indicates that overexpression of this gene impairs calcium homeostasis and increases arrhythmia events [234]. Therefore, it might also play a role in arrhythmia events occurring in LQTS3 and BrS patients.

It is important to notice that some genes could only be expressed at a late stage of maturation (D40-D45) and, although some genes could be expressed during both time points of differentiation, differences in the degree of expression were observed, noting the importance of reaching a threshold of maturity during in vitro study of cardiovascular diseases. However, because of the differences in genetic background between individuals, it would have been appropriate to perform a CRISPR-Cas9 on both disease models to correct the mutation and compare the obtained data to the corrected cell lines. We are also aware that using single-cell RNA analysis may bring deeper comprehension of the functional unit by profiling gene expression of each cell types present in the differentiated cell culture, helping to provide more accurate data. Nevertheless, these results provide us with an approach to what is taking place during BrS and LQTS3 on the gene expression level. It is important to note that these results may not apply to all LQTS3 or BrS CMs, since different mutations could drive distinct disease outcomes correlated to varying degrees of the same disease's phenotypic expression as also previously described during CPVT [235].

4.7 Gene ontology analysis of healthy control and defective cardiomyocytes (BrS & LQTS3)

By performing the gene ontology (GO) of cardiomyocytes from healthy subjects and patients, we were able to learn whether there are any aberrant features or pathways that deviate from the norm during cardiomyogenesis. During BrS for example, a defect in electrical conductivity is observed [236, 237]. An impaired electrical conductivity could be the result of a delay and lower cell-to-cell communication. Using the bioinformatics tool of *Zhou et al* [238] we established the gene ontology (GO) of the 20 more enriched processes of healthy and defective CMs and observed that all the cell lines display a positive regulation of cell adhesion, whereby the expression score in healthy CMs was higher than in both disease models, suggesting that

cell-cell communication might be reduced in disease models. The high regulation of the tube-and-heart morphogenesis pathways erased the probability of structural abnormalities of the heart during LQTS3 and BrS in this study, which further supports prior statement [239-242]. Thus, the hypothesis of a cardiac defect related to ion channel dysfunction during LQTS3 and BrS is the most likely cause of arrhythmic disorders occurring during both diseases.

Interestingly we notified that in all cell lines, genes that are involved in head development are enriched in cardiomyocyte populations. The presence of these genes might result from the use of the B-27 supplement in the differentiation media. Indeed, B-27 has been designed to support neuronal cultures by improving cell survival and cell differentiation [243, 244]. Thus, although important for a successful cardiac muscle cell differentiation, the supplement might also enrich the cardiomyocytes population with genes that enter the establishment of head development. This suggests that protocols for cardiomyocyte differentiation should be improved.

4.8 Field potential recording in healthy and disease cardiomyocytes: QTc analysis

It is known that prolonged cell culture improves the maturation of CMs in-vitro to more adult-like cells [245] characterized by a better contractile apparatus of the cells, elongated cell types, and an improved cell functionality [246]. During our study, we were able to align with this hypothesis. Indeed, when comparing early and late stages CMs from the healthy control and BrS patient, we observed that field potential duration (FPD) was significantly increased on day 20 of differentiation compared to day 40. Moreover, the amplitude of CMs contraction in the control was considerably increased at the late time point of differentiation, which can be linked with a better expression of genes involved in the mechanism of ECC, and therefore, the contractile apparatus of the cells. All these observations support the hypothesis that prolonged in vitro culture of CMs increase their maturity. Indeed, a previous study has shown that the long-term culture of CMs may favour the adult-like CMs through a switch in gene expression over time [247], during which sarcomere may present a more mature phenotype and therefore better regulate cell functionality [248]. This might be the reason why the long QT phenotype was observable at day 40 of differentiation and not earlier in LQTS3-derived cardiac cells, suggesting that for in-vitro characterization of pathophysiological features related to heart failure, CMs need to reach a certain maturation threshold. The study of *Knight et al.* further supports this statement. Indeed, with the aim to model cardiac hypertrophy, they developed a platform that will enable the obtaining of CMs in a more mature-like phenotype for a better characterization of the disease [249]. Overall, these observations tell us that during in-vitro

characterization of a disease or healthy model, a certain threshold of CMs maturity is required to have a better approach to data interpretation. In addition of showing a prolonged QTc, LQTS3 CMs also showed late-onset T-waves which is characteristic in LQTS3 patients [250]. The observation was further confirmed by the study of *Horigome et al.* who use the ECG of different LQTS3 patients to perform some geometric morphometries on the T-wave [251]. Since the QTc phenotype was observable after FP measurement, we tried to correct the phenotype using the class Ib anti-arrhythmic drug lidocaine during MEA recording.

4.9 Lidocaine effect on LQTS3-derived cardiomyocytes

HiPSC-CMs offer a potential paradigm for drug safety testing in the preclinical stage [252]. The MEA system has been widely used because of its high-throughput platform to access the safety and the pro-arrhythmic action of drugs [172]. Class Ib anti-arrhythmic drugs such as lidocaine, mexiletine have shown their effectiveness in shortening the QTc interval in LQTS3 patients [123, 253, 254]. Using both: clinical concentration range (5uM -20uM) [255] and nonclinical concentrations on cardiomyocytes derived from the LQTS3 patient, lidocaine treatment failed to restore the QTc interval. On the contrary, it further increases it in a concentration-dependent manner, suggesting that for this patient this drug is ineffective and could be life-threatening. Although lidocaine failed to restore the QTc interval to normal, it did increase the FP rate concentration-dependently, a result that confirmed the study of *Abramovich-Sivan et al.* [256]. *Müller-Edenborn et al.* additionally showed that lidocaine can improve the heart's contractility in ischemic mouse models revealing that lidocaine plays a role in the contractile function of the heart [257]. However, Lidocaine did not change the amplitude of the CMs at pharmacological concentrations. Nevertheless, at concentrations above this range, the amplitude of the cells significantly decreased in a concentration-dependent manner indicating the toxicity of the drug at these concentrations.

4.10 Field potential comparison between healthy control and disease models in different maturation time points

Low beating activity which is also known as bradycardia is one of the main characterizations of LQTS3 and BrS, which is involved in the phenomenon of SCD occurring during sleep in both diseases [258]. To access the FP rate between a healthy subject and LQTS3 and BrS patients, the FP of derived cardiomyocytes obtained from these patients was recorded. The result showed that compared to the healthy control, cells from patients present a low beating activity rate with statistical differences. However, at the early stage of differentiation (D20-D25), the phenotype could not be detected in BrS-derived CMs, which highlights the

importance of reaching a certain threshold of CMs maturation for the characterization of cardiac disease models features during in vitro studies. Moreover, we also observed that the time of maturation affects the interpretation of the contractility amplitude between the control and unhealthy cardiomyocytes. Indeed, at the early stage of differentiation, BrS CMs showed a high amplitude compared to the control, while late-stage CMs do not show a difference between both cell lines. This result could be interpreted by the less organization, the reduction, or the absence of some channels involved in the mechanism of cell contractility at day 20 of differentiation compared to day 40. In the LQTS3 model, however, the amplitude was reduced compared to the control at both stages. Reduced amplitude observed in these cells could be directly associated with the *SCN5A* gene mutation. Indeed, impaired sodium current (I_{Na}) can affect the refractory period allowing another AP to be generated while the cells have not fully repolarized, inducing a delayed depolarization resulting in a smaller cell contraction amplitude [29]. This theory of re-entry during LQTS3 due to slow I_{Na} channel inactivation resulting in small AP amplitude and prolonged AP has been reported [259], suggesting that defect I_{Na} affects the AP upstroke affecting the cardiac contractility.

Another explanation for the low voltage in cell contraction could be associated with *CASQ2* dysregulation in those cells. Indeed, the *CASQ2* gene whose protein buffers Ca^{2+} in the SR is downregulated in LQTS3 CMs. Hence, we hypothesized that one of the mechanisms involved in the cell's contractility reduction may be the reduction of calcium stored in the SR, impairing, the availability of Ca^{2+} during the phenomenon of ECC. In fact, a study on rats demonstrated that a reduction in *CASQ2* levels severely reduces the amplitude of Ca^{2+} [260]. In BrS CMs, on the contrary, no statistical difference in the voltage was observable between those cells and the CMs of the healthy donor. This could suggest the existence of a compensatory mechanism in those cells to adjust the amplitude of contraction of the cells, or it could also be that at this stage of differentiation it is not possible to access the changes on this parameter with the MEA recording.

4.11 Evaluation of the sodium current in healthy control and disease models through patch-clamp technique

Electrophysiology is essential to investigate the functionality of the heart and discover dysfunctional mechanisms occurring in a failing heart. Several tools such as patch-clamp, Multi-electrode array (MEA), sharp-electrode, and fluorescence microscopy have been used to elucidate the different pathological features that could take place during cardiac diseases [261].

Patch-clamp was developed in the 1970s [262] to measure the ionic currents that flow through a single cell channel and, therefore, provide information regarding the quantity of current that passes through a cell's membrane. Using single cardiomyocytes of BrS we were able to show that in those cells, the current was decreased compared to the control (data obtained by Nour Katnahji, working group of PD Dr. Jan Matthes, Centre for Pharmacology). This result supports the hypothesis of loss-of-function of the Nav channel associated with BrS and validates the affiliation of the c.1936delC mutation to BrS as previously published [263]. Thus, we further support the hypothesis that frameshift mutation in BrS leads to synthesis deficiency of the Nav channel reducing the I_{Na} during AP. Another hypothesis could be related to channel trafficking defect toward the membrane [264]. However, the latter has been mainly associated with missense mutations driven BrS [141, 142].

Patch-clamp analysis of LQTS3 cardiomyocytes, on the contrary, showed us that p.V240M might be associated with a mixed phenotype between LQTS3 and BrS. Indeed, the I_{Na} current was reduced in those cells (data obtained by Nour Katnahji, working group of PD Dr. Jan Matthes, Centre for Pharmacology). Moreover, in LQTS3 cells, we also observed a reduction of Nav channel availability and a positive shift of activation characteristic of loss-of-function of the channel [265]. Additionally, a prior study conducted with patient derived CMs carrying the same mutation showed that the current density can be reduced in those cells compared to healthy derived CMs [163]. Moreover, the qPCR analysis revealed that *SCN5A* is downregulated in those cells. Indeed, LQTS3 is normally linked with a high Na^+ current and therefore upregulation in the *SCN5A* gene [266]. Therefore, we speculated that the V240M mutation is associated with an overlapping phenotype between LQTS3 and BrS. The overlapping phenotype has already been mentioned between LQTS3 and BrS in prior reports [129, 151-153]. In fact, during their study, the authors demonstrate that patients carrying the heterozygote mutation *SCN5A*-E1784K present a long QT phenotype characteristic to LQTS3, but a reduced I_{Na} characteristic of BrS, which is associated with a loss-of-function of the channel and which matches our observation [152]. The existence of an overlapping phenotype could also explain the inefficiency of lidocaine treatment on those cells. In fact, a recent study revealed that mexiletine, which is the same class of antiarrhythmic drug as lidocaine, could rescue the overlapping phenotype observed in an LQTS3 patient [267], suggesting that for this patient this treatment might be more suitable. However, this hypothesis needs some verification because therapy with a Nav channel blocker could present some genotype-phenotype

dependency. Indeed, studies revealed that under LQTS patients, life-threatening arrhythmias are more likely to occur in a gene-specific manner [268].

4.11 Calcium transient evaluation in healthy control and disease models

The main mechanism relating to electrical excitation and mechanical contraction in cardiomyocytes is CICR [269]. A method for measuring contraction and calcium simultaneously using the fluorescent dye Fluo-4 has been reported [270, 271]. Therefore, in the context of our study, we used this tool to access the perturbed Ca^{2+} that has been described in LQTS3 and BrS. The experiments were carried out with single cells and cell sheets. The use of cell sheets revealed that the bradycardia phenotype can be identified in both disease models at a relatively early stage of differentiation (D20 – D25), which is further pronounced at a more mature stage of differentiation (D40 – D45). This observation indicates a better expression of genes involved in the contractile function of the heart at this latter stage of differentiation. Using single-cell, we also concluded that a low beat frequency is associated with LQTS3 and BrS and that this observation was true for both early and late-stage CMs. Therefore, whether single cells or cell sheets are used during calcium homeostasis to access the beating activity between control and patient derived CMs might not influence the interpretation of the results. However, the use of single cells is preferred by scientists, as the cell sheets could contain distinct types of CMs such as ventricular, atrial or nodal types, which can be problematic for the understanding of the pathophysiology of the disease. Nevertheless, the use of cell sheets could add to the understanding of the mechanisms related to the diseases, as under physiological conditions, cardiomyocytes are communicating together via gap junctions. Therefore, using protocols that could pilot the cardiac cell differentiation in ventricular cell type will be beneficial for this study.

Comparing the FP rate obtained from MEA recording with calcium transient field potential between the control and disease models, we were able to observe a difference that might be associated with the difference in temperature during both experiments. Indeed, during the MEA measurement that was carried out at 37°C, no difference in FP activity was noticeable between the control and BrS cardiomyocytes at the early stage of differentiation. Moreover, the cell activity of the control obtained from the calcium transient traces at RT is lowered compared to the value obtained with MEA, showing the influence of the temperature on cardiac activity. In fact, a study demonstrated that low temperature has a significant impact on cardiomyocyte beating activity [272] which further strengthens our statement. Thus, all these parameters should be taken into consideration when running the experiments and interpreting the data.

Using single-cell as well as linked cells to analyse the change of FP rate within the same cell line at different maturation time points, we observed that the types of cells used could significantly affect the interpretation of the cardiomyocytes' activity. Indeed, the single-cell analysis of the healthy control revealed that there is no difference in FP rate at the early and late stages of CMs but using cell sheets we observed a significant difference. Furthermore, comparing the FP rate of single-cell and linked cells at the same stage of differentiation additionally supports our speculation. Hence, the type of cell that is used during the functional analysis of cardiomyocytes could significantly affect the interpretation of the cardiomyocytes activity.

It was speculated that improper calcium transient might be associated with impaired CMs contractility during LQTS3 [178] and BrS [273]. In terms to go in-depth with this hypothesis, and relating our molecular findings with the cells' functionality, we accessed the intracellular Ca^{2+} homeostasis using 10 mM caffeine. Caffeine is known as a RyR2 agonist that triggers the mechanism of CICR [274, 275]. Thus, using it further contributes to the comprehension of the arrhythmic phenotype arising during LQTS3 and BrS. Using early-stage single-cell CMS, we observed that LQTS3 CMs mostly present signs of arrhythmia while the healthy control and the BrS cell line show a proper calcium flux. However, at the late stage of differentiation, calcium transient FP is prolonged in both disease models after caffeine treatment with BrS mostly showing signs of trigger activity. Moreover, the time to 90% of inactivation obtained during patch-clamp experiments additionally supports the existence of a prolonged AP (data obtained by Nour Katnahji, working group of PD Dr. Jan Matthes, Centre for Pharmacology). The phenomenon of trigger activity observed during BrS might be associated with both: impaired Na^+ transient and Ca^{2+} handling. Indeed, in **Figure 3-6B**, gene expression analysis showed that BrS CMs exhibit a high expression of *CASQ2* and *RyR2* genes whose proteins are responsible for Ca^{2+} storage in the SR and Ca^{2+} release, respectively, therefore regulating the cardiac muscle contractility. Moreover, *CASQ2* has been proposed as a possible regulator of RyR2 in Ca^{2+} release [276]. Therefore, abnormal cardiomyocyte contractility might be associated with Ca^{2+} overloaded in the SR, which is spontaneously released during the mechanism of ECC. This phenomenon might further lead to membrane depolarization hindering proper cell repolarization and causing the observed EAD phenomenon on those cells. The hypothesis of spontaneous Ca^{2+} release during EADs has been mentioned earlier by *Tse et al.* [277]. Moreover, repolarization theory that is based on the reduction of Na^+ current entry through the channel, which therefore impaired different currents such as the K^+ and the Ca^{2+} ,

which in turn affect the AP, has been proposed as one of the mechanisms occurring during BrS [278]. All these observations, from gene expression to calcium imaging, show that for this BrS-related mutation, the repolarization theory might be more speculative than the depolarization theory [279], and more study based on the Ca^{2+} or K^{+} current is needed to obtain supplemental information.

In LQTS3-derived CMs, the calcium transient was prolonged compared to the control which reflects improper Ca^{2+} homeostasis taking place in those cells. Studies performed in mice revealed that in mice harbouring the overlapping phenotype *SCN5A-1798insD/+*, the sodium current decay was reduced compared to the WT [280]. In the context of our study, we also obtained the same result after patch-clamp analysis, suggesting that the prolonged APD observed in this case could be linked to impaired degradation of the I_{Na} , which further prolonged the plateau phase of the AP. However, the gene expression analysis displays a downregulation of the *CASQ2* gene suggesting a likely impediment to Ca^{2+} accumulation in the SR. Although NCX also plays an important role in cytosolic Ca^{2+} extrusion that opposes Ca^{2+} accumulation in the SR [281], it may not compensate for the deficit of Ca^{2+} sequestration in the SR, whose storage is important for adequate cardiac contractile function. Indeed, several studies have shown that a decrease in the magnitude of the Ca^{2+} transient is associated with a reduced concentration of Ca^{2+} in the SR [282, 283]. Therefore, the low amplitude of contraction observed in cardiac cells derived from this LQTS3 patient may also be the result of less calcium leak from the SR during the ECC mechanism. Thus, reduced calcium stored by the SR could be associated here with reduced cell contractility amplitude observed during MEA recording.

As calcium transient was prolonged in both disease models, we also evaluated the half-time of calcium extrusion from the cytosol to further support our hypothesis. Analysis of the calcium transient at the late stage of CMs at the single-cell level demonstrated that the rate of Ca^{2+} removal from the cytosol is extensive in both defective CMs. However, at the early stage of differentiation, this defect in calcium homeostasis could not be validated in BrS, underlining the importance of cell maturity during in-vitro studies of cardiac diseases. Furthermore, a significant difference was mainly observed between the early and late stages of CMs from the same cell line when comparing the half time of cell relaxation, which decreases in the late stage of differentiation. This difference could be the consequence of the better expression of ion channels that are involved in the mechanism of contraction and relaxation of CMs. The fact that the elapsed time to remove calcium from the cytosol of patient-derived cardiac muscle cells is prolonged has already been proven by other studies [282, 284]. Using cell sheets, we

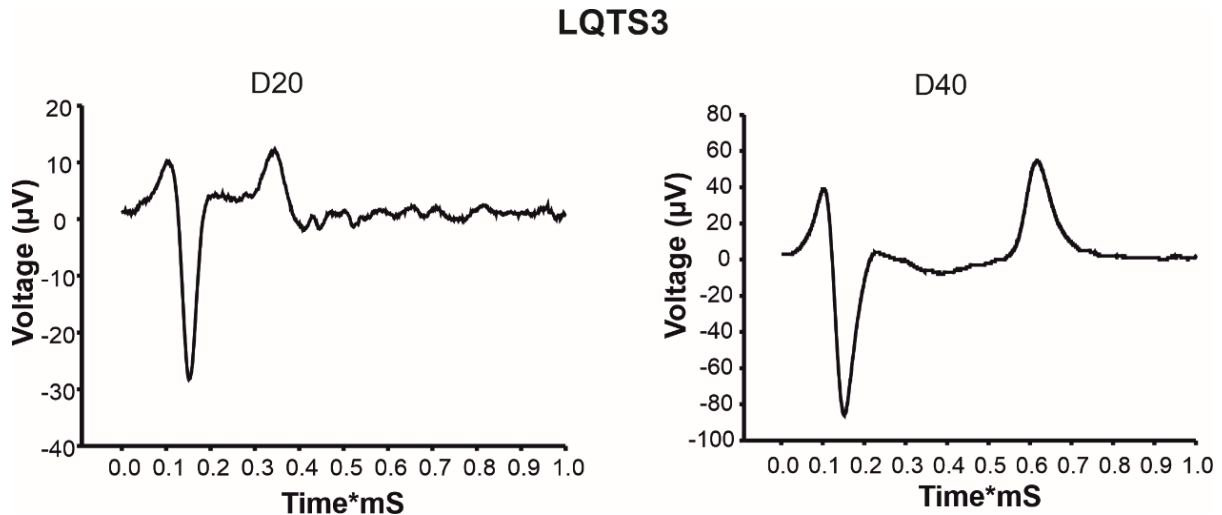
observed that at the early stage of differentiation, both disease models showed a prolonged halftime of Ca^{2+} extrusion compared to the control. Comparing both cell types (single cells and cell sheets) at the same differentiation time point, an important difference in this time was mostly detected within the same cell line, suggesting that the type of cells used to access cell functionality during disease models could affect the results' interpretation, and might need to be taken into consideration.

4.12 Conclusion

To bring more insight into the pathophysiological mechanisms underlying BrS and LQTS3, we engineered human-induced pluripotent stem cells-derived cardiomyocytes from a healthy donor as well as LQTS3 and BrS patients. The cells were further used for disease characterization at the cellular, molecular, and functional levels. The experiments were performed with different stages of CMs to evaluate the impact of cell maturation on cardiac myocyte physiology during *in vitro* studies of cardiac diseases. At the cellular level, we observed that Cx43 distribution within the intercalated discs is not disturbed in disease models compared to the control, suggesting that the electrical disturbance occurring during the two diseases is associated with channels defect. Indeed, numerous genes coding for proteins involved in the mechanisms of ECC and cardiomyocytes' contractility were dysregulated. However, the interaction between Cx43 and SCN5A requires further investigation. The molecular data as well as the patch-clamp analysis performed by our collaborator allowed us to hypothesize that V240M mutation might be associated with a mixed phenotype between LQTS3 and Brs. We also postulated that the inefficacy of lidocaine to restore the QTc interval to normal might result from the mixed phenotype that presents those cells. In BrS cardiomyocytes we were able to confirm the loss of function of the sodium channel associated with the mutation. The calcium imaging showed that in the two disease models, the Ca^{2+} transient is impaired, and the time corresponding to 50% of Ca^{2+} extrusion is prolonged. Additionally, BrS CMs mostly display signs of EADs. Using cardiomyocytes at distinct time points of maturation, we observed that a certain threshold of CMs maturity is necessary for the evaluation of disease phenotypes during *in-vitro* experiments. This study not only suggested a probable mixed phenotype between LQTS3 and BrS associated with the V240M mutation, but also provided more information about the gene dysregulation associated with both diseases. However, additional studies using the CRISPR-Cas9 technique as well the single-cell sequencing are necessary for better disease characterization, which will help to avoid the problem of differences in the genetic background, on the one hand, as well as the problem of mixed cardiomyocytes cell types during molecular analysis, on the other hand.

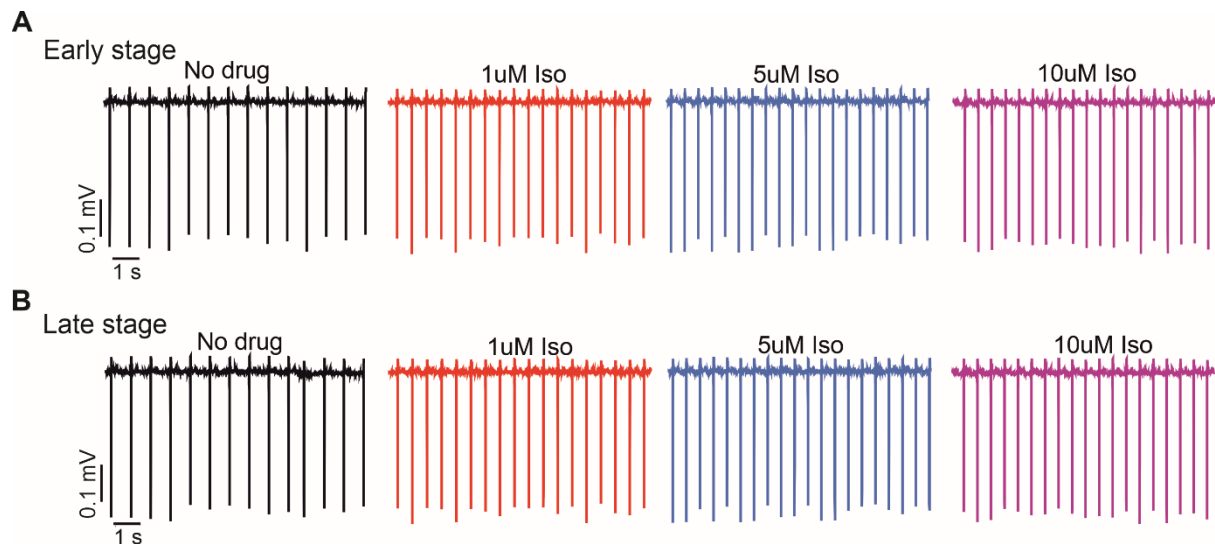
5 Appendix

A prolonged culture improved the maturation of human-derived cardiomyocytes and enable a proper disease characterization



Clusters were replated on the MEA plate three to five days before FP recording. D40 of differentiation illustrates a long QTc phenotype characteristic of LQTS3 whereas D20 cardiomyocytes could not display this phenotype.

The beta-agonist Isoproterenol (Iso) efficiently activates beta-receptors of derived cardiomyocytes.



A, representative traces of Iso on the early stage (D20-D25) of differentiation of derived cardiac muscle cells of a healthy subject. **B**, Illustration of the Iso effect on the late-stage (D40-D45) differentiation on derived cardiomyocytes of a healthy individual. In both cases, isoproterenol increases the cell' activity in a concentration-dependent manner.

6 References

- [1] A. Arackal, K. Alsayouri, Histology, Heart, StatPearls, Treasure Island (FL), 2022.
- [2] A. Saxton, M.A. Tariq, B. Bordoni, Anatomy, Thorax, Cardiac Muscle, StatPearls, StatPearls Publishing
- Copyright © 2022, StatPearls Publishing LLC., Treasure Island (FL), 2022.
- [3] N.J. Severs, The cardiac muscle cell, *Bioessays* 22(2) (2000) 188-99.
- [4] E.D. Canale, G.R. Campbell, J.J. Smolich, J.H. Campbell, Morphology of Cardiac Muscle, in: E.D. Canale, G.R. Campbell, J.J. Smolich, J.H. Campbell (Eds.), *Cardiac Muscle*, Springer Berlin Heidelberg, Berlin, Heidelberg, 1986, pp. 8-51.
- [5] A. Arackal, K. Alsayouri, Histology, Heart, StatPearls, Treasure Island (FL), 2021.
- [6] L.F. Santana, E.P. Cheng, W.J. Lederer, How does the shape of the cardiac action potential control calcium signaling and contraction in the heart?, *Journal of Molecular and Cellular Cardiology* 49(6) (2010) 901-903.
- [7] M.E. Zoghbi, P. Bolaños, C. Villalba-Galea, A. Marcano, E. Hernández, M. Fill, A.L. Escobar, Spatial Ca(2+) distribution in contracting skeletal and cardiac muscle cells, *Biophys J* 78(1) (2000) 164-73.
- [8] I. Rehman, A. Rehman, Anatomy, Thorax, Heart, StatPearls, Treasure Island (FL), 2022.
- [9] J.W. Calvert, D.J. Lefer, Chapter 6 - Overview of Cardiac Muscle Physiology, in: J.A. Hill, E.N. Olson (Eds.), *Muscle*, Academic Press, Boston/Waltham, 2012, pp. 57-66.
- [10] R.J. Laird, S. Irwin, Chapter 1 - Cardiovascular Structure and Function, in: S. Irwin, J.S. Tecklin (Eds.), *Cardiopulmonary Physical Therapy (Fourth Edition)*, Mosby, Saint Louis, 2004, pp. 3-38.
- [11] C. Crocini, M. Gotthardt, Cardiac sarcomere mechanics in health and disease, *Biophys Rev* 13(5) (2021) 637-652.
- [12] E. Braunwald, Structure and function of the normal myocardium, *Br Heart J* 33 (1971) Suppl:3-8.
- [13] J. King, D.R. Lowery, Physiology, Cardiac Output, StatPearls, Treasure Island (FL), 2021.
- [14] I. Rehman, A. Rehman, Anatomy, Thorax, Heart, StatPearls, Treasure Island (FL), 2021.
- [15] C. Pinali, H.J. Bennett, J.B. Davenport, J.L. Caldwell, T. Starborg, A.W. Trafford, A. Kitmitto, Three-dimensional structure of the intercalated disc reveals plicate domain and gap junction remodeling in heart failure, *Biophysical journal* 108(3) (2015) 498-507.
- [16] C.A. Walker, F.G. Spinale, The structure and function of the cardiac myocyte: a review of fundamental concepts, *J Thorac Cardiovasc Surg* 118(2) (1999) 375-82.
- [17] A. Saxton, M.A. Tariq, B. Bordoni, Anatomy, Thorax, Cardiac Muscle, StatPearls, Treasure Island (FL), 2021.
- [18] T. Hong, R.M. Shaw, Cardiac T-Tubule Microanatomy and Function, *Physiol Rev* 97(1) (2017) 227-252.
- [19] J.L. Greenstein, R. Hinch, R.L. Winslow, Mechanisms of excitation-contraction coupling in an integrative model of the cardiac ventricular myocyte, *Biophys J* 90(1) (2006) 77-91.
- [20] M. Ibrahim, J. Gorelik, M.H. Yacoub, C.M. Terracciano, The structure and function of cardiac t-tubules in health and disease, *Proceedings of the Royal Society B: Biological Sciences* 278(1719) (2011) 2714-2723.
- [21] S. Despa, F. Brette, C.H. Orchard, D.M. Bers, Na/Ca Exchange and Na/K-ATPase Function Are Equally Concentrated in Transverse Tubules of Rat Ventricular Myocytes, *Biophysical Journal* 85(5) (2003) 3388-3396.
- [22] T. Hong, H. Yang, S.S. Zhang, H.C. Cho, M. Kalashnikova, B. Sun, H. Zhang, A. Bhargava, M. Grabe, J. Olgin, J. Gorelik, E. Marban, L.Y. Jan, R.M. Shaw, Cardiac BIN1 folds T-tubule membrane, controlling ion flux and limiting arrhythmia, *Nat Med* 20(6) (2014) 624-32.
- [23] L. Sacconi, C. Ferrantini, J. Lotti, R. Coppini, P. Yan, L.M. Loew, C. Tesi, E. Cerbai, C. Poggesi, F.S. Pavone, Action potential propagation in transverse-axial tubular system is impaired in heart failure, *Proc Natl Acad Sci U S A* 109(15) (2012) 5815-9.
- [24] E.A. Woodcock, S.J. Matkovich, Cardiomyocytes structure, function and associated pathologies, *The International Journal of Biochemistry & Cell Biology* 37(9) (2005) 1746-1751.

- [25] A.H. Kashou, H. Basit, L. Chhabra, Physiology, Sinoatrial Node, StatPearls, Treasure Island (FL), 2022.
- [26] L.F. Santana, E.P. Cheng, W.J. Lederer, How does the shape of the cardiac action potential control calcium signaling and contraction in the heart?, *J Mol Cell Cardiol* 49(6) (2010) 901-3.
- [27] A.O. Grant, Cardiac Ion Channels, *Circulation: Arrhythmia and Electrophysiology* 2(2) (2009) 185-194.
- [28] M.S. Bohnen, V. Iyer, K.J. Sampson, R.S. Kass, Novel mechanism of transient outward potassium channel current regulation in the heart: implications for cardiac electrophysiology in health and disease, *Circ Res* 116(10) (2015) 1633-5.
- [29] J. Pinnell, S. Turner, S. Howell, Cardiac muscle physiology, *Continuing Education in Anaesthesia Critical Care & Pain* 7(3) (2007) 85-88.
- [30] M. Renganathan, H. Wei, Y. Zhao, Cardiac Action Potential Measurement in Human Embryonic Stem Cell Cardiomyocytes for Cardiac Safety Studies Using Manual Patch-Clamp Electrophysiology, in: M. Clements, L. Roquemoire (Eds.), *Stem Cell-Derived Models in Toxicology*, Springer New York, New York, NY, 2017, pp. 37-56.
- [31] D.M. Bers, Calcium Cycling and Signaling in Cardiac Myocytes, *Annual Review of Physiology* 70(1) (2008) 23-49.
- [32] A.O. Grant, Cardiac ion channels, *Circ Arrhythm Electrophysiol* 2(2) (2009) 185-94.
- [33] A.M. Katz, Cardiac ion channels, *N Engl J Med* 328(17) (1993) 1244-51.
- [34] H. Terlau, W. Stuhmer, Structure and function of voltage-gated ion channels, *Naturwissenschaften* 85(9) (1998) 437-44.
- [35] B. Roux, Ion channels and ion selectivity, *Essays Biochem* 61(2) (2017) 201-209.
- [36] M. Pusch, M. Noda, W. Stuhmer, S. Numa, F. Conti, Single point mutations of the sodium channel drastically reduce the pore permeability without preventing its gating, *Eur Biophys J* 20(3) (1991) 127-33.
- [37] M. Noda, H. Suzuki, S. Numa, W. Stuhmer, A single point mutation confers tetrodotoxin and saxitoxin insensitivity on the sodium channel II, *FEBS Lett* 259(1) (1989) 213-6.
- [38] C.L. Mummery, J. Zhang, E.S. Ng, D.A. Elliott, A.G. Elefanty, T.J. Kamp, Differentiation of human embryonic stem cells and induced pluripotent stem cells to cardiomyocytes: a methods overview, *Circ Res* 111(3) (2012) 344-58.
- [39] C.E. Friedman, Q. Nguyen, S.W. Lukowski, A. Helfer, H.S. Chiu, H.K. Voges, S. Suo Suo, J.-D. Jackie Han, P. Osteil, G. Peng, N. Jing, G.J. Ballie, A. Senabouth, A.N. Christ, T.J. Bruxner, C.E. Murry, E.S. Wong, J. Ding, Y. Wang, J. Hudson, Z. Bar-Joseph, P.P.L. Tam, J.E. Powell, N.J. Palpant, Cardiac directed differentiation using small molecule Wnt modulation at single-cell resolution, *bioRxiv* (2017) 229294.
- [40] M. Litviňuková, C. Talavera-López, H. Maatz, D. Reichart, C.L. Worth, E.L. Lindberg, M. Kanda, K. Polanski, E.S. Fasouli, S. Samari, K. Roberts, L. Tuck, M. Heinig, D.M. DeLaughter, B. McDonough, H. Wakimoto, J.M. Gorham, E.R. Nadelmann, K.T. Mahbubani, K. Saeb-Parsy, G. Patone, J.J. Boyle, H. Zhang, H. Zhang, A. Viveiros, G.Y. Oudit, O. Bayraktar, J.G. Seidman, C. Seidman, M. Nosedá, N. Hübner, S.A. Teichmann, Cells and gene expression programs in the adult human heart, *bioRxiv* (2020) 2020.04.03.024075.
- [41] J.D. Hocker, O.B. Poirion, F. Zhu, J. Buchanan, K. Zhang, J. Chiou, T.-M. Wang, Q. Zhang, X. Hou, Y.E. Li, Y. Zhang, E.N. Farah, A. Wang, A.D. McCulloch, K.J. Gaulton, B. Ren, N.C. Chi, S. Preissl, Cardiac cell type-specific gene regulatory programs and disease risk association, *Science Advances* 7(20) (2021) eabf1444.
- [42] X. Luo, J. Yin, D. Dwyer, T. Yamawaki, H. Zhou, H. Ge, C.-Y. Han, A. Shkumatov, K. Snyder, B. Ason, C.-M. Li, O. Homann, M. Stolina, Chamber-enriched gene expression profiles in failing human hearts with reduced ejection fraction, *Scientific Reports* 11(1) (2021) 11839.
- [43] J. Magyar, A. Jenes, K. Kistamás, F. Ruzsnavszky, P.P. Nánási, J. Satin, N. Szentandrassy, T. Bányász, Long term regulation of cardiac L-type calcium channel by small G proteins, *Curr Med Chem* 18(24) (2011) 3714-9.

- [44] L. Cribbs, T-type calcium channel expression and function in the diseased heart, *Channels* 4(6) (2010) 447-452.
- [45] N. Niwa, K. Yasui, T. Opthof, H. Takemura, A. Shimizu, M. Horiba, J.-K. Lee, H. Honjo, K. Kamiya, I. Kodama, Cav3.2 subunit underlies the functional T-type Ca²⁺ channel in murine hearts during the embryonic period, *American Journal of Physiology-Heart and Circulatory Physiology* 286(6) (2004) H2257-H2263.
- [46] D. Baroni, O. Moran, On the multiple roles of the voltage gated sodium channel beta1 subunit in genetic diseases, *Front Pharmacol* 6 (2015) 108.
- [47] C. Nau, E. Leipold, Voltage-gated sodium channels and pain, *e-Neuroforum* 23(3) (2017) 123-130.
- [48] M.B. Rook, M.M. Evers, M.A. Vos, M.F. Bierhuizen, Biology of cardiac sodium channel Nav1.5 expression, *Cardiovasc Res* 93(1) (2012) 12-23.
- [49] Q. Wang, Z. Li, J. Shen, M.T. Keating, Genomic Organization of the Human SCN5A Gene Encoding the Cardiac Sodium Channel, *Genomics* 34(1) (1996) 9-16.
- [50] F.H. Yu, W.A. Catterall, Overview of the voltage-gated sodium channel family, *Genome Biology* 4(3) (2003) 207.
- [51] F.H. Yu, W.A. Catterall, Overview of the voltage-gated sodium channel family, *Genome Biol* 4(3) (2003) 207.
- [52] S.K. Maier, R.E. Westenbroek, K.A. McCormick, R. Curtis, T. Scheuer, W.A. Catterall, Distinct subcellular localization of different sodium channel alpha and beta subunits in single ventricular myocytes from mouse heart, *Circulation* 109(11) (2004) 1421-7.
- [53] L.L. Isom, K.S. De Jongh, D.E. Patton, B.F. Reber, J. Offord, H. Charbonneau, K. Walsh, A.L. Goldin, W.A. Catterall, Primary structure and functional expression of the beta 1 subunit of the rat brain sodium channel, *Science* 256(5058) (1992) 839-42.
- [54] D.S. Krafte, A.L. Goldin, V.J. Auld, R.J. Dunn, N. Davidson, H.A. Lester, Inactivation of cloned Na channels expressed in *Xenopus* oocytes, *Journal of General Physiology* 96(4) (1990) 689-706.
- [55] M. de Lera Ruiz, R.L. Kraus, Voltage-Gated Sodium Channels: Structure, Function, Pharmacology, and Clinical Indications, *Journal of Medicinal Chemistry* 58(18) (2015) 7093-7118.
- [56] A.R. Pérez-Riera, R.D. Raimundo, R.A. Watanabe, J.L. Figueiredo, L.C.d. Abreu, Cardiac sodium channel, its mutations and their spectrum of arrhythmia phenotypes, *Journal of Human Growth and Development* 26 (2016) 281-296.
- [57] E. Zaklyazminskaya, S. Dzemeshevich, The role of mutations in the SCN5A gene in cardiomyopathies, *Biochimica et Biophysica Acta (BBA) - Molecular Cell Research* 1863(7, Part B) (2016) 1799-1805.
- [58] C.A. Remme, Cardiac sodium channelopathy associated with SCN5A mutations: electrophysiological, molecular and genetic aspects, *J Physiol* 591(17) (2013) 4099-116.
- [59] L. Luo, F. Ning, Y. Du, B. Song, D. Yang, S.C. Salvage, Y. Wang, J.A. Fraser, S. Zhang, A. Ma, T. Wang, Calcium-dependent Nedd4-2 upregulation mediates degradation of the cardiac sodium channel Nav1.5: implications for heart failure, *Acta Physiol (Oxf)* 221(1) (2017) 44-58.
- [60] F. Potet, T.M. Beckermann, J.D. Kunic, A.L. George, Intracellular Calcium Attenuates Late Current Conducted by Mutant Human Cardiac Sodium Channels, *Circulation: Arrhythmia and Electrophysiology* 8(4) (2015) 933-941.
- [61] M. Abdelsayed, A.-E. Baruteau, K. Gibbs, S. Sanatani, A.D. Krahn, V. Probst, P.C. Ruben, Differential calcium sensitivity in Na(V) 1.5 mixed syndrome mutants, *The Journal of physiology* 595(18) (2017) 6165-6186.
- [62] M.M. Monasky, E. Micaglio, G. Ciconte, S. Benedetti, C. Di Resta, G. Vicedomini, V. Borrelli, A. Ghiroldi, M. Piccoli, L. Anastasia, V. Santinelli, M. Ferrari, C. Pappone, Genotype/Phenotype Relationship in a Consanguineal Family With Brugada Syndrome Harboring the R1632C Missense Variant in the SCN5A Gene, *Frontiers in Physiology* 10 (2019).
- [63] L. Martínez-Campelo, R. Cruz, A. Blanco-Verea, I. Moscoso, E. Ramos-Luis, R. Lage, M. Álvarez-Barredo, M. Sabater-Molina, P. Peñafiel-Verdú, J. Jiménez-Jáimez, M. Rodríguez-Mañero, M. Brion,

Searching for genetic modulators of the phenotypic heterogeneity in Brugada syndrome, PLOS ONE 17(3) (2022) e0263469.

[64] J. Weirich, W. Wenzel, [Current classification of anti-arrhythmia agents], Z Kardiol 89 Suppl 3 (2000) 62-7.

[65] U. Ravens, [Principles for the classification of anti-arrhythmia agents in cardiac arrhythmias], Z Kardiol 81 Suppl 4 (1992) 119-25.

[66] V. Yarov-Yarovoy, J.C. McPhee, D. Idsvoog, C. Pate, T. Scheuer, W.A. Catterall, Role of amino acid residues in transmembrane segments IS6 and IIS6 of the Na⁺ channel alpha subunit in voltage-dependent gating and drug block, J Biol Chem 277(38) (2002) 35393-401.

[67] G.K. Wang, C. Quan, S. Wang, A common local anesthetic receptor for benzocaine and etidocaine in voltage-gated mu1 Na⁺ channels, Pflugers Arch 435(2) (1998) 293-302.

[68] V. Yarov-Yarovoy, J. Brown, E.M. Sharp, J.J. Clare, T. Scheuer, W.A. Catterall, Molecular determinants of voltage-dependent gating and binding of pore-blocking drugs in transmembrane segment IIS6 of the Na⁺ channel alpha subunit, J Biol Chem 276(1) (2001) 20-7.

[69] A. Mike, P. Lukacs, The enigmatic drug binding site for sodium channel inhibitors, Curr Mol Pharmacol 3(3) (2010) 129-44.

[70] H. Zhang, B. Zou, F. Du, K. Xu, M. Li, Reporting sodium channel activity using calcium flux: pharmacological promiscuity of cardiac Nav1.5, Mol Pharmacol 87(2) (2015) 207-17.

[71] T.M. Gamal El-Din, M.J. Linares, N. Zheng, W.A. Catterall, Fenestrations control resting-state block of a voltage-gated sodium channel, Proceedings of the National Academy of Sciences 115(51) (2018) 13111.

[72] S.A. Pless, J.D. Galpin, A. Frankel, C.A. Ahern, Molecular basis for class Ib anti-arrhythmic inhibition of cardiac sodium channels, Nature Communications 2(1) (2011) 351.

[73] J.P. Gollivan, D.A. Dougherty, Cation- π interactions in structural biology, Proc Natl Acad Sci U S A 96(17) (1999) 9459-64.

[74] A.S. Mahadevi, G.N. Sastry, Cation- π Interaction: Its Role and Relevance in Chemistry, Biology, and Material Science, Chemical Reviews 113(3) (2013) 2100-2138.

[75] K. Kumar, S.M. Woo, T. Siu, W.A. Cortopassi, F. Duarte, R.S. Paton, Cation- π interactions in protein-ligand binding: theory and data-mining reveal different roles for lysine and arginine, Chem Sci 9(10) (2018) 2655-2665.

[76] R.W. Kreeger, J.A. Raza, A. Movahed, Anti-Arrhythmic Drugs: Pharmacokinetics and Pharmacodynamics, in: A. Movahed, G. Gnanasegaran, J. Buscombe, M. Hall (Eds.), Integrating Cardiology for Nuclear Medicine Physicians: A Guide to Nuclear Medicine Physicians, Springer Berlin Heidelberg, Berlin, Heidelberg, 2009, pp. 453-461.

[77] K. Kuga, Y. Sugishita, [Class-I antiarrhythmic drugs], Nihon Rinsho 54(8) (1996) 2110-6.

[78] M. Lei, L. Wu, D.A. Terrar, C.L. Huang, Modernized Classification of Cardiac Antiarrhythmic Drugs, Circulation 138(17) (2018) 1879-1896.

[79] D.P. Zipes, J. Jalife, Cardiac Electrophysiology: From Cell to Bedside, Saunders/Elsevier 2009.

[80] M.F. Sheets, D.A. Hanck, Outward stabilization of the S4 segments in domains III and IV enhances lidocaine block of sodium channels, J Physiol 582(Pt 1) (2007) 317-34.

[81] T.R. Cummins, Setting up for the block: the mechanism underlying lidocaine's use-dependent inhibition of sodium channels, J Physiol 582(Pt 1) (2007) 11.

[82] A. Scholz, Mechanisms of (local) anaesthetics on voltage-gated sodium and other ion channels, BJA: British Journal of Anaesthesia 89(1) (2002) 52-61.

[83] J.C. Makielski, J. Limberis, Z. Fan, J.W. Kyle, Intrinsic lidocaine affinity for Na channels expressed in Xenopus oocytes depends on α (hH1 vs. rSkM1) and β 1 subunits, Cardiovascular Research 42(2) (1999) 503-509.

[84] G.K. Wang, G.R. Strichartz, State-Dependent Inhibition of Sodium Channels by Local Anesthetics: A 40-Year Evolution, Biochem (Mosc) Suppl Ser A Membr Cell Biol 6(2) (2012) 120-127.

[85] S. Dhein, Antiarrhythmic Drugs, in: S. Offermanns, W. Rosenthal (Eds.), Encyclopedia of Molecular Pharmacology, Springer Berlin Heidelberg, Berlin, Heidelberg, 2008, pp. 96-102.

- [86] D.B. Tikhonov, B.S. Zhorov, Mechanism of sodium channel block by local anesthetics, antiarrhythmics, and anticonvulsants, *Journal of General Physiology* 149(4) (2017) 465-481.
- [87] G.S. King, A. Goyal, Y. Grigorova, M.F. Hashmi, *Antiarrhythmic Medications*, StatPearls, Treasure Island (FL), 2022.
- [88] D.W.G. Harron, R.G. Shanks, Clinical Use of Class Ib Antiarrhythmic Drugs, in: E.M. Vaughan Williams (Ed.), *Antiarrhythmic Drugs*, Springer Berlin Heidelberg, Berlin, Heidelberg, 1989, pp. 201-233.
- [89] G. Giannakoulas, D. Ntiloudi, Acquired cardiovascular disease in adult patients with congenital heart disease, *Heart* 104(7) (2018) 546.
- [90] R. Sun, M. Liu, L. Lu, Y. Zheng, P. Zhang, Congenital Heart Disease: Causes, Diagnosis, Symptoms, and Treatments, *Cell Biochem Biophys* 72(3) (2015) 857-60.
- [91] J. Li, Y. Hua, S. Miyagawa, J. Zhang, L. Li, L. Liu, Y. Sawa, hiPSC-Derived Cardiac Tissue for Disease Modeling and Drug Discovery, *International Journal of Molecular Sciences* 21(23) (2020) 8893.
- [92] A. Deicher, T. Seeger, Human Induced Pluripotent Stem Cells as a Disease Model System for Heart Failure, *Current Heart Failure Reports* 18(1) (2021) 1-11.
- [93] A. Sharma, J.C. Wu, S.M. Wu, Induced pluripotent stem cell-derived cardiomyocytes for cardiovascular disease modeling and drug screening, *Stem Cell Research & Therapy* 4(6) (2013) 150.
- [94] H. Savoji, M.H. Mohammadi, N. Rafatian, M.K. Toroghi, E.Y. Wang, Y. Zhao, A. Korolj, S. Ahadian, M. Radisic, Cardiovascular disease models: A game changing paradigm in drug discovery and screening, *Biomaterials* 198 (2019) 3-26.
- [95] L. Polonchuk, M. Chabria, L. Badi, J.-C. Hoflack, G. Figtree, M.J. Davies, C. Gentile, Cardiac spheroids as promising in vitro models to study the human heart microenvironment, *Scientific Reports* 7(1) (2017) 7005.
- [96] K. Takahashi, S. Yamanaka, Induction of pluripotent stem cells from mouse embryonic and adult fibroblast cultures by defined factors, *Cell* 126(4) (2006) 663-76.
- [97] K. Takahashi, K. Tanabe, M. Ohnuki, M. Narita, T. Ichisaka, K. Tomoda, S. Yamanaka, Induction of pluripotent stem cells from adult human fibroblasts by defined factors, *Cell* 131(5) (2007) 861-72.
- [98] E.I. Parrotta, V. Lucchino, L. Scaramuzzino, S. Scalise, G. Cuda, Modeling Cardiac Disease Mechanisms Using Induced Pluripotent Stem Cell-Derived Cardiomyocytes: Progress, Promises and Challenges, *International Journal of Molecular Sciences* 21(12) (2020).
- [99] D. Huangfu, R. Maehr, W. Guo, A. Eijkelenboom, M. Snitow, A.E. Chen, D.A. Melton, Induction of pluripotent stem cells by defined factors is greatly improved by small-molecule compounds, *Nat Biotechnol* 26(7) (2008) 795-797.
- [100] J. Silva, O. Barrandon, J. Nichols, J. Kawaguchi, T.W. Theunissen, A. Smith, Promotion of reprogramming to ground state pluripotency by signal inhibition, *PLoS Biol* 6(10) (2008) e253.
- [101] M. Nakagawa, M. Koyanagi, K. Tanabe, K. Takahashi, T. Ichisaka, T. Aoi, K. Okita, Y. Mochiduki, N. Takizawa, S. Yamanaka, Generation of induced pluripotent stem cells without Myc from mouse and human fibroblasts, *Nat Biotechnol* 26(1) (2008) 101-106.
- [102] J.S. Kim, H.W. Choi, S. Choi, J.T. Do, Reprogrammed pluripotent stem cells from somatic cells, *Int J Stem Cells* 4(1) (2011) 1-8.
- [103] T. Ma, M. Xie, T. Laurent, S. Ding, Progress in the reprogramming of somatic cells, *Circ Res* 112(3) (2013) 562-74.
- [104] S. Hamad, D. Derichsweiler, S. Papadopoulos, F. Nguemo, T. Šarić, A. Sachinidis, K. Brockmeier, J. Hescheler, B.J. Boukens, K. Pfannkuche, Generation of human induced pluripotent stem cell-derived cardiomyocytes in 2D monolayer and scalable 3D suspension bioreactor cultures with reduced batch-to-batch variations, *Theranostics* 9(24) (2019) 7222-7238.
- [105] P.W. Burridge, E. Matsa, P. Shukla, Z.C. Lin, J.M. Churko, A.D. Ebert, F. Lan, S. Diecke, B. Huber, N.M. Mordwinkin, J.R. Plews, O.J. Abilez, B. Cui, J.D. Gold, J.C. Wu, Chemically defined generation of human cardiomyocytes, *Nat Methods* 11(8) (2014) 855-60.

- [106] M. Zhao, Y. Tang, Y. Zhou, J. Zhang, Deciphering Role of Wnt Signalling in Cardiac Mesoderm and Cardiomyocyte Differentiation from Human iPSCs: Four-dimensional control of Wnt pathway for hiPSC-CMs differentiation, *Scientific Reports* 9(1) (2019) 19389.
- [107] R.E. Ahmed, T. Anzai, N. Chanthra, H. Uosaki, A Brief Review of Current Maturation Methods for Human Induced Pluripotent Stem Cells-Derived Cardiomyocytes, *Frontiers in Cell and Developmental Biology* 8(178) (2020).
- [108] J. Lewandowski, N. Rozwadowska, T.J. Kolanowski, A. Malcher, A. Zimna, A. Rugowska, K. Fiedorowicz, W. Łabędź, Ł. Kubaszewski, K. Chojnacka, K. Bednarek-Rajewska, P. Majewski, M. Kurpisz, The impact of in vitro cell culture duration on the maturation of human cardiomyocytes derived from induced pluripotent stem cells of myogenic origin, *Cell Transplantation* 27(7) (2018) 1047-1067.
- [109] S.M. Biendarra-Tiegs, X. Li, D. Ye, E.B. Brandt, M.J. Ackerman, T.J. Nelson, Single-Cell RNA-Sequencing and Optical Electrophysiology of Human Induced Pluripotent Stem Cell-Derived Cardiomyocytes Reveal Discordance Between Cardiac Subtype-Associated Gene Expression Patterns and Electrophysiological Phenotypes, *Stem Cells Dev* 28(10) (2019) 659-673.
- [110] X. Gu, F. Zhou, J. Mu, Recent Advances in Maturation of Pluripotent Stem Cell-Derived Cardiomyocytes Promoted by Mechanical Stretch, *Med Sci Monit* 27 (2021) e931063.
- [111] S. Tohyama, J. Fujita, C. Fujita, M. Yamaguchi, S. Kanaami, R. Ohno, K. Sakamoto, M. Kodama, J. Kurokawa, H. Kanazawa, T. Seki, Y. Kishino, M. Okada, K. Nakajima, S. Tanosaki, S. Someya, A. Hirano, S. Kawaguchi, E. Kobayashi, K. Fukuda, Efficient Large-Scale 2D Culture System for Human Induced Pluripotent Stem Cells and Differentiated Cardiomyocytes, *Stem Cell Reports* 9(5) (2017) 1406-1414.
- [112] A. Au - Sharma, G. Au - Li, K. Au - Rajarajan, R. Au - Hamaguchi, P.W. Au - Burridge, S.M. Au - Wu, Derivation of Highly Purified Cardiomyocytes from Human Induced Pluripotent Stem Cells Using Small Molecule-modulated Differentiation and Subsequent Glucose Starvation, *JoVE* (97) (2015) e52628.
- [113] M.-T. Zhao, N.-Y. Shao, V. Garg, Subtype-specific cardiomyocytes for precision medicine: Where are we now?, *STEM CELLS* 38(7) (2020) 822-833.
- [114] G. Gintant, P. Burridge, L. Gepstein, S. Harding, T. Herron, C. Hong, J. Jalife, J.C. Wu, Use of Human Induced Pluripotent Stem Cell-Derived Cardiomyocytes in Preclinical Cancer Drug Cardiotoxicity Testing: A Scientific Statement From the American Heart Association, *Circ Res* 125(10) (2019) e75-e92.
- [115] Z. Zhao, H. Lan, I. El-Battrawy, X. Li, F. Buljubasic, K. Sattler, G. Yücel, S. Lang, M. Tiburcy, W.-H. Zimmermann, L. Cyganek, J. Utikal, T. Wieland, M. Borggrefe, X.-B. Zhou, I. Akin, Ion Channel Expression and Characterization in Human Induced Pluripotent Stem Cell-Derived Cardiomyocytes, *Stem Cells Int* 2018 (2018) 6067096-6067096.
- [116] J. Li, Y. Hua, S. Miyagawa, J. Zhang, L. Li, L. Liu, Y. Sawa, hiPSC-Derived Cardiac Tissue for Disease Modeling and Drug Discovery, *Int J Mol Sci* 21(23) (2020).
- [117] L. Wang, V. Serpooshan, J. Zhang, Engineering Human Cardiac Muscle Patch Constructs for Prevention of Post-infarction LV Remodeling, *Frontiers in Cardiovascular Medicine* 8 (2021).
- [118] C.I. Berul, Neonatal long QT syndrome and sudden cardiac death, *Prog Pediatr Cardiol* 11(1) (2000) 47-54.
- [119] B.J.M. Hermans, F.C. Bennis, A.S. Vink, T. Koopsen, A. Lyon, A.A.M. Wilde, D. Nuyens, T. Robyns, L. Pison, P.G. Postema, T. Delhaas, Improving long QT syndrome diagnosis by a polynomial-based T-wave morphology characterization, *Heart Rhythm* 17(5) (2020) 752-758.
- [120] A. Porta-Sánchez, D.R. Spillane, L. Harris, J. Xue, P. Dorsey, M. Care, V. Chauhan, M.H. Gollob, D.A. Spears, T-Wave Morphology Analysis in Congenital Long QT Syndrome Discriminates Patients From Healthy Individuals, *JACC: Clinical Electrophysiology* 3(4) (2017) 374-381.
- [121] P.J. Schwartz, M. Stramba-Badiale, L. Crotti, M. Pedrazzini, A. Besana, G. Bosi, F. Gabbarini, K. Goulene, R. Insolia, S. Mannarino, F. Mosca, L. Nespola, A. Rimini, E. Rosati, P. Salice, C. Spazzolini, Prevalence of the congenital long-QT syndrome, *Circulation* 120(18) (2009) 1761-1767.
- [122] K. Nademanee, Genotype-Phenotype Relationship in the Long QT Syndrome, *Journal of the American College of Cardiology* 54(22) (2009) 2063-2064.

- [123] A.R. Pérez-Riera, R. Barbosa-Barros, R. Daminello Raimundo, M.P. da Costa de Rezende Barbosa, I.C. Esposito Sorpreso, L.C. de Abreu, The congenital long QT syndrome Type 3: An update, *Indian Pacing Electrophysiol J* 18(1) (2018) 25-35.
- [124] R. Wilders, A.O. Verkerk, Long QT Syndrome and Sinus Bradycardia-A Mini Review, *Frontiers in cardiovascular medicine* 5 (2018) 106-106.
- [125] B. Horváth, T. Hézső, D. Kiss, K. Kistamás, J. Magyar, P.P. Nánási, T. Bányász, Late Sodium Current Inhibitors as Potential Antiarrhythmic Agents, *Frontiers in Pharmacology* 11 (2020).
- [126] Z.F. Issa, J.M. Miller, D.P. Zipes, 2 - Cardiac Ion Channels, in: Z.F. Issa, J.M. Miller, D.P. Zipes (Eds.), *Clinical Arrhythmology and Electrophysiology (Third Edition)*, Elsevier, Philadelphia, 2019, pp. 15-50.
- [127] D. Malan, M. Zhang, B. Stallmeyer, J. Muller, B.K. Fleischmann, E. Schulze-Bahr, P. Sasse, B. Greber, Human iPS cell model of type 3 long QT syndrome recapitulates drug-based phenotype correction, *Basic Res Cardiol* 111(2) (2016) 14.
- [128] B. Ye, C.R. Valdivia, M.J. Ackerman, J.C. Makielski, A common human SCN5A polymorphism modifies expression of an arrhythmia causing mutation, *Physiological Genomics* 12(3) (2003) 187-193.
- [129] C. Veltmann, H. Barajas-Martinez, C. Wolpert, M. Borggrefe, R. Schimpf, R. Pfeiffer, G. Cáceres, E. Burashnikov, C. Antzelevitch, D. Hu, Further Insights in the Most Common *SCN5A* Mutation Causing Overlapping Phenotype of Long QT Syndrome, Brugada Syndrome, and Conduction Defect, *Journal of the American Heart Association* 5(7) (2016) e003379.
- [130] P.J. Schwartz, S.G. Priori, E.H. Locati, C. Napolitano, F. Cantù, J.A. Towbin, M.T. Keating, H. Hammoude, A.M. Brown, L.-S.K. Chen, T.J. Colatsky, Long QT Syndrome Patients With Mutations of the *SCN5A* and *HERG* Genes Have Differential Responses to Na⁺ Channel Blockade and to Increases in Heart Rate, *Circulation* 92(12) (1995) 3381-3386.
- [131] A.A.M. Wilde, A.S. Amin, P.G. Postema, Diagnosis, management and therapeutic strategies for congenital long QT syndrome, *Heart* (2021) heartjnl-2020-318259.
- [132] C. Bezzina, M.W. Veldkamp, M.P.v.d. Berg, A.V. Postma, M.B. Rook, J.-W. Viersma, I.M.v. Langen, G. Tan-Sindhunata, M.T.E. Bink-Boelkens, A.H.v.d. Hout, M.M.A.M. Mannens, A.A.M. Wilde, A Single Na⁺ Channel Mutation Causing Both Long-QT and Brugada Syndromes, *Circulation Research* 85(12) (1999) 1206-1213.
- [133] K. Saadeh, K. Shivkumar, K. Jeevaratnam, Targeting the β -adrenergic receptor in the clinical management of congenital long QT syndrome, *Annals of the New York Academy of Sciences* 1474(1) (2020) 27-46.
- [134] W. Vutthikraivit, P. Rattanawong, P. Putthapiban, W. Sukhumthammarat, P. Vathesatogkit, A. Thakkinian, Worldwide Prevalence of Brugada Syndrome: A Systematic Review and Meta-Analysis, *Acta Cardiologica Sinica* 34 (2018) 267-277.
- [135] A. Milman, J.B. Gourraud, A. Andorin, P.G. Postema, F. Sacher, P. Mabo, G. Conte, C. Giustetto, G. Sarquella-Brugada, A. Hochstadt, S.H. Kim, J.J.M. Juang, S. Maeda, Y. Takahashi, T. Kamakura, T. Aiba, E. Leshem, Y. Michowitz, M. Rahkovich, Y. Mizusawa, E. Arbelo, Z. Huang, I. Denjoy, Y.D. Wijeyeratne, C. Napolitano, R. Brugada, R. Casado-Arroyo, J. Champagne, L. Calo, J. Tfelt-Hansen, S.G. Priori, M. Takagi, C. Veltmann, P. Delise, D. Corrado, E.R. Behr, F. Gaita, G.X. Yan, J. Brugada, A. Leenhardt, A.A.M. Wilde, P. Brugada, K.F. Kusano, K. Hirao, G.B. Nam, V. Probst, B. Belhassen, Gender differences in patients with Brugada syndrome and arrhythmic events: Data from a survey on arrhythmic events in 678 patients, *Heart Rhythm* 15(10) (2018) 1457-1465.
- [136] M. Yuan, C. Tian, X. Li, X. Yang, X. Wang, Y. Yang, N. Liu, K.F. Kusano, H. Barajas-Martinez, D. Hu, H. Shang, Y. Gao, Y. Xing, Gender Differences in Prognosis and Risk Stratification of Brugada Syndrome: A Pooled Analysis of 4,140 Patients From 24 Clinical Trials, *Front Physiol* 9 (2018) 1127.
- [137] M. Argenziano, C. Antzelevitch, Recent advances in the treatment of Brugada syndrome, *Expert Rev Cardiovasc Ther* 16(6) (2018) 387-404.
- [138] J. Sieira, P. Brugada, The definition of the Brugada syndrome, *European Heart Journal* 38(40) (2017) 3029-3034.
- [139] C.M. Beaufort-Krol Gertie, P. van den Berg Maarten, A.M. Wilde Arthur, J.P. van Tintelen, W. Viersma Jan, R. Bezzina Connie, E. Bink-Boelkens Margreet Th, Developmental Aspects of Long QT

Syndrome Type 3 and Brugada Syndrome on the Basis of a Single SCN5A Mutation in Childhood, *Journal of the American College of Cardiology* 46(2) (2005) 331-337.

[140] M.M. Monasky, E. Micaglio, E.T. Locati, C. Pappone, Evaluating the Use of Genetics in Brugada Syndrome Risk Stratification, *Frontiers in Cardiovascular Medicine* 8(307) (2021).

[141] G. Baroudi, V. Pouliot, I. Denjoy, P. Guicheney, A. Shrier, M. Chahine, Novel mechanism for Brugada syndrome: defective surface localization of an SCN5A mutant (R1432G), *Circ Res* 88(12) (2001) E78-83.

[142] C.R. Valdivia, D.J. Tester, B.A. Rok, C.B. Porter, T.M. Munger, A. Jahangir, J.C. Makielski, M.J. Ackerman, A trafficking defective, Brugada syndrome-causing SCN5A mutation rescued by drugs, *Cardiovasc Res* 62(1) (2004) 53-62.

[143] D.W. Wang, N. Makita, A. Kitabatake, J.R. Balser, A.L. George, Jr., Enhanced Na(+) channel intermediate inactivation in Brugada syndrome, *Circ Res* 87(8) (2000) E37-43.

[144] M.B. Rook, C. Bezzina Alshinawi, W.A. Groenewegen, I.C. van Gelder, A.C. van Ginneken, H.J. Jongsma, M.M. Mannens, A.A. Wilde, Human SCN5A gene mutations alter cardiac sodium channel kinetics and are associated with the Brugada syndrome, *Cardiovasc Res* 44(3) (1999) 507-17.

[145] G. Ciconte, M.M. Monasky, V. Santinelli, E. Micaglio, G. Vicedomini, L. Anastasia, G. Negro, V. Borrelli, L. Giannelli, F. Santini, C. de Innocentiis, R. Rondine, E.T. Locati, A. Bernardini, B.C. Mazza, V. Mecarocci, Ž. Čalović, A. Ghiroldi, S. D'Imperio, S. Benedetti, C. Di Resta, I. Rivolta, G. Casari, E. Petretto, C. Pappone, Brugada syndrome genetics is associated with phenotype severity, *European Heart Journal* 42(11) (2020) 1082-1090.

[146] V.N. Batchvarov, The Brugada Syndrome - Diagnosis, Clinical Implications and Risk Stratification, *Eur Cardiol* 9(2) (2014) 82-87.

[147] M.V. Elizari, R. Levi, R.S. Acunzo, P.A. Chiale, M.M. Civetta, M. Ferreira, S. Sicouri, Abnormal expression of cardiac neural crest cells in heart development: A different hypothesis for the etiopathogenesis of Brugada syndrome, *Heart Rhythm* 4(3) (2007) 359-365.

[148] G. Tse, T. Liu, K.H.C. Li, V. Laxton, Y.W.F. Chan, W. Keung, R.A. Li, B.P. Yan, Electrophysiological Mechanisms of Brugada Syndrome: Insights from Pre-clinical and Clinical Studies, *Frontiers in Physiology* 7 (2016).

[149] M. Argenziano, C. Antzelevitch, Recent advances in the treatment of Brugada syndrome, *Expert Rev Cardiovasc Ther* 16(6) (2018) 387-404.

[150] S. Duffett, J. Roberts, Brugada Syndrome: Evolving Insights and Emerging Treatment Strategies, *The Journal of innovations in cardiac rhythm management* 8 (2017) 2613-2622.

[151] M. Grillo, C. Napolitano, P.J. Schwartz, R. Bloise, E. Ronchetti, S. Priori, Beyond LQT3 and brugada syndrome: The search for the overlapping phenotypes, *Europace* 2 (2010) A24-A24.

[152] R.P. Davis, S. Casini, C.W. van den Berg, M. Hoekstra, C.A. Remme, C. Dambrot, D. Salvatori, D.W. Oostwaard, A.A. Wilde, C.R. Bezzina, A.O. Verkerk, C. Freund, C.L. Mummery, Cardiomyocytes derived from pluripotent stem cells recapitulate electrophysiological characteristics of an overlap syndrome of cardiac sodium channel disease, *Circulation* 125(25) (2012) 3079-91.

[153] C. Veltmann, H. Barajas-Martinez, C. Wolpert, M. Borggrefe, R. Schimpf, R. Pfeiffer, G. Caceres, E. Burashnikov, C. Antzelevitch, D. Hu, Further Insights in the Most Common SCN5A Mutation Causing Overlapping Phenotype of Long QT Syndrome, Brugada Syndrome, and Conduction Defect, *J Am Heart Assoc* 5(7) (2016).

[154] S.M. Badenes, T.G. Fernandes, C.S. Cordeiro, S. Boucher, D. Kuninger, M.C. Vemuri, M.M. Diogo, J.M. Cabral, Defined Essential 8™ Medium and Vitronectin Efficiently Support Scalable Xeno-Free Expansion of Human Induced Pluripotent Stem Cells in Stirred Microcarrier Culture Systems, *PLoS One* 11(3) (2016) e0151264.

[155] G. Chen, D.R. Gulbranson, Z. Hou, J.M. Bolin, V. Ruotti, M.D. Probasco, K. Smuga-Otto, S.E. Howden, N.R. Diol, N.E. Propson, R. Wagner, G.O. Lee, J. Antosiewicz-Bourget, J.M. Teng, J.A. Thomson, Chemically defined conditions for human iPSC derivation and culture, *Nat Methods* 8(5) (2011) 424-9.

- [156] P. Ghasemi-Dehkordi, M. Allahbakhshian-Farsani, N. Abdian, A. Mirzaeian, J. Saffari-Chaleshtori, F. Heybati, G. Mardani, A. Karimi-Taghanaki, A. Doosti, M.S. Jami, M. Abolhasani, M. Hashemzadeh-Chaleshtori, Comparison between the cultures of human induced pluripotent stem cells (hiPSCs) on feeder-and serum-free system (Matrigel matrix), MEF and HDF feeder cell lines, *J Cell Commun Signal* 9(3) (2015) 233-46.
- [157] P.W. Burridge, A. Holmström, J.C. Wu, Chemically Defined Culture and Cardiomyocyte Differentiation of Human Pluripotent Stem Cells, *Current Protocols in Human Genetics* 87(1) (2015) 21.3.1-21.3.15.
- [158] D. Abbey, P.B. Seshagiri, Ascorbic acid-mediated enhanced cardiomyocyte differentiation of mouse ES-cells involves interplay of DNA methylation and multiple-signals, *Differentiation* 96 (2017) 1-14.
- [159] N. Cao, Z. Liu, Z. Chen, J. Wang, T. Chen, X. Zhao, Y. Ma, L. Qin, J. Kang, B. Wei, L. Wang, Y. Jin, H.T. Yang, Ascorbic acid enhances the cardiac differentiation of induced pluripotent stem cells through promoting the proliferation of cardiac progenitor cells, *Cell Res* 22(1) (2012) 219-36.
- [160] M. Finlay, J. Bhar-Amato, K.E. Ng, D. Santos, M. Orini, V. Vyas, P. Taggart, A.A. Grace, C.L. Huang, P.D. Lambiase, A. Tinker, Autonomic modulation of the electrical substrate in mice haploinsufficient for cardiac sodium channels: a model of the Brugada syndrome, *Am J Physiol Cell Physiol* 317(3) (2019) C576-C583.
- [161] J. Kaindl, I. Meiser, J. Majer, A. Sommer, F. Krach, A. Katsen-Globa, J. Winkler, H. Zimmermann, J.C. Neubauer, B. Winner, Zooming in on Cryopreservation of hiPSCs and Neural Derivatives: A Dual-Center Study Using Adherent Vitrification, *Stem Cells Transl Med* 8(3) (2019) 247-259.
- [162] S. Mollamohammadi, A. Taei, M. Pakzad, M. Totonchi, A. Seifinejad, N. Masoudi, H. Baharvand, A simple and efficient cryopreservation method for feeder-free dissociated human induced pluripotent stem cells and human embryonic stem cells, *Human reproduction (Oxford, England)* 24 (2009) 2468-76.
- [163] A. Fatima, S. Kaifeng, S. Dittmann, G. Xu, M.K. Gupta, M. Linke, U. Zechner, F. Nguemo, H. Milting, M. Farr, J. Hescheler, T. Sarić, The disease-specific phenotype in cardiomyocytes derived from induced pluripotent stem cells of two long QT syndrome type 3 patients, *PloS one* 8(12) (2013) e83005-e83005.
- [164] J.K. Park, L.J. Martin, X. Zhang, A.G. Jegga, D.W. Benson, Genetic variants in SCN5A promoter are associated with arrhythmia phenotype severity in patients with heterozygous loss-of-function mutation, *Heart Rhythm* 9(7) (2012) 1090-6.
- [165] R. Lowe, N. Shirley, M. Bleackley, S. Dolan, T. Shafee, Transcriptomics technologies, *PLoS Comput Biol* 13(5) (2017) e1005457.
- [166] F. Stahl, B. Hitzmann, K. Mutz, D. Landgrebe, M. Lübbecke, C. Kasper, J. Walter, T. Scheper, Transcriptome analysis, *Adv Biochem Eng Biotechnol* 127 (2012) 1-25.
- [167] D. Groth, S. Hartmann, S. Klie, J. Selbig, Principal components analysis, *Methods Mol Biol* 930 (2013) 527-47.
- [168] I.T. Jolliffe, J. Cadima, Principal component analysis: a review and recent developments, *Philos Trans A Math Phys Eng Sci* 374(2065) (2016) 20150202.
- [169] B. Meunier, E. Dumas, I. Piec, D. Béchet, M. Hébraud, J.F. Hocquette, Assessment of hierarchical clustering methodologies for proteomic data mining, *J Proteome Res* 6(1) (2007) 358-66.
- [170] A. Pham, M. Melchior, Screening for fetal congenital heart disease, *CMAJ* 189(12) (2017) E468-E468.
- [171] M. Waern, M. Mellander, A. Berg, Y. Carlsson, Prenatal detection of congenital heart disease - results of a Swedish screening program 2013–2017, *BMC Pregnancy and Childbirth* 21(1) (2021) 579.
- [172] L. Sala, D. Ward-van Oostwaard, L.G.J. Tertoolen, C.L. Mummery, M. Bellin, Electrophysiological Analysis of human Pluripotent Stem Cell-derived Cardiomyocytes (hPSC-CMs) Using Multi-electrode Arrays (MEAs), *J Vis Exp* (123) (2017) 55587.
- [173] R. Owczuk, M.A. Wujtewicz, W. Sawicka, A. Piankowski, A. Polak-Krzeminska, E. Morzuch, The effect of intravenous lidocaine on QT changes during tracheal intubation, *Anaesthesia* 63 (2008) 924-31.

- [174] C. Paech, P. Suchowerskyj, R.A. Gebauer, Successful Treatment of a Newborn With Genetically Confirmed Long QT Syndrome 3 and Repetitive Torsades De Pointes Tachycardia, *Pediatric Cardiology* 32(7) (2011) 1060-1061.
- [175] A. Pérez-Riera, R. Barros, R. Raimundo, M. Barbosa, I. Sorpreso, L. Abreu, The congenital long QT syndrome Type 3: An update, *Indian Pacing Electrophysiol J* 18 (2017).
- [176] K. Mizumaki, A. Fujiki, K. Nishida, M. Sakabe, T. Tsuneda, M. Sugao, J. Iwamoto, H. Nagasawa, H. Inoue, Bradycardia-Dependent ECG Changes in Brugada Syndrome, *Circulation journal : official journal of the Japanese Circulation Society* 70 (2006) 896-901.
- [177] E. Laurila, A. Ahola, J. Hyttinen, K. Aalto-Setälä, Methods for in vitro functional analysis of iPSC derived cardiomyocytes — Special focus on analyzing the mechanical beating behavior, *Biochimica et Biophysica Acta (BBA) - Molecular Cell Research* 1863(7, Part B) (2016) 1864-1872.
- [178] M. Paci, E. Passini, S. Severi, J. Hyttinen, B. Rodriguez, Phenotypic variability in LQT3 human induced pluripotent stem cell-derived cardiomyocytes and their response to antiarrhythmic pharmacologic therapy: An in silico approach, *Heart Rhythm* 14(11) (2017) 1704-1712.
- [179] P. Liang, K. Sallam, H. Wu, Y. Li, I. Itzhaki, P. Garg, Y. Zhang, V. Vermglinchan, F. Lan, M. Gu, T. Gong, Y. Zhuge, C. He, A.D. Ebert, V. Sanchez-Freire, J. Churko, S. Hu, A. Sharma, C.K. Lam, M.M. Scheinman, D.M. Bers, J.C. Wu, Patient-Specific and Genome-Edited Induced Pluripotent Stem Cell-Derived Cardiomyocytes Elucidate Single-Cell Phenotype of Brugada Syndrome, *J Am Coll Cardiol* 68(19) (2016) 2086-2096.
- [180] G.A. Roth, G.A. Mensah, C.O. Johnson, G. Addolorato, E. Ammirati, L.M. Baddour, N.C. Barengo, A.Z. Beaton, E.J. Benjamin, C.P. Benziger, A. Bonny, M. Brauer, M. Brodmann, T.J. Cahill, J. Carapetis, A.L. Catapano, S.S. Chugh, L.T. Cooper, J. Coresh, M. Criqui, N. DeCleene, K.A. Eagle, S. Emmons-Bell, V.L. Feigin, J. Fernández-Solà, G. Fowkes, E. Gakidou, S.M. Grundy, F.J. He, G. Howard, F. Hu, L. Inker, G. Karthikeyan, N. Kassebaum, W. Koroshetz, C. Lavie, D. Lloyd-Jones, H.S. Lu, A. Mirijello, A.M. Temesgen, A. Mokdad, A.E. Moran, P. Muntner, J. Narula, B. Neal, M. Ntsekhe, G. Moraes de Oliveira, C. Otto, M. Owolabi, M. Pratt, S. Rajagopalan, M. Reitsma, A.L.P. Ribeiro, N. Rigotti, A. Rodgers, C. Sable, S. Shakil, K. Sliwa-Hahnle, B. Stark, J. Sundström, P. Timpel, I.M. Tleyjeh, M. Valgimigli, T. Vos, P.K. Whelton, M. Yacoub, L. Zuhlke, C. Murray, V. Fuster, G.A. Roth, G.A. Mensah, C.O. Johnson, G. Addolorato, E. Ammirati, L.M. Baddour, N.C. Barengo, A. Beaton, E.J. Benjamin, C.P. Benziger, A. Bonny, M. Brauer, M. Brodmann, T.J. Cahill, J.R. Carapetis, A.L. Catapano, S. Chugh, L.T. Cooper, J. Coresh, M.H. Criqui, N.K. DeCleene, K.A. Eagle, S. Emmons-Bell, V.L. Feigin, J. Fernández-Solà, F.G.R. Fowkes, E. Gakidou, S.M. Grundy, F.J. He, G. Howard, F. Hu, L. Inker, G. Karthikeyan, N.J. Kassebaum, W.J. Koroshetz, C. Lavie, D. Lloyd-Jones, H.S. Lu, A. Mirijello, A.T. Misganaw, A.H. Mokdad, A.E. Moran, P. Muntner, J. Narula, B. Neal, M. Ntsekhe, G.M.M. Oliveira, C.M. Otto, M.O. Owolabi, M. Pratt, S. Rajagopalan, M.B. Reitsma, A.L.P. Ribeiro, N.A. Rigotti, A. Rodgers, C.A. Sable, S.S. Shakil, K. Sliwa, B.A. Stark, J. Sundström, P. Timpel, I.I. Tleyjeh, M. Valgimigli, T. Vos, P.K. Whelton, M. Yacoub, L.J. Zuhlke, M. Abbasi-Kangevari, A. Abdi, A. Abedi, V. Aboyans, W.A. Abrha, E. Abu-Gharbieh, A.I. Abushouk, D. Acharya, T. Adair, O.M. Adebayo, Z. Ademi, S.M. Advani, K. Afshari, A. Afshin, G. Agarwal, P. Agasthi, S. Ahmad, S. Ahmadi, M.B. Ahmed, B. Aji, Y. Akalu, W. Akande-Sholabi, A. Aklilu, C.J. Akunna, F. Alahdab, A. Al-Eyadhy, K.F. Alhabib, S.M. Alif, V. Alipour, S.M. Aljunid, F. Alla, A. Almasi-Hashiani, S. Almustanyir, R.M. Al-Raddadi, A.K. Amegah, S. Amini, A. Aminorroaya, H. Amu, D.A. Amugsi, R. Ancuceanu, D. Anderlini, T. Andrei, C.L. Andrei, A. Ansari-Moghaddam, Z.A. Anteneh, I.C. Antonazzo, B. Antony, R. Anwer, L.T. Appiah, J. Arabloo, J. Ärnlöv, K.D. Artanti, Z. Ataro, M. Ausloos, L. Avila-Burgos, A.T. Awan, M.A. Awoke, H.T. Ayele, M.A. Ayza, S. Azari, D.B. B, N. Baheiraei, A.A. Baig, A. Bakhtiari, M. Banach, P.C. Banik, E.A. Baptista, M.A. Barboza, L. Barua, S. Basu, N. Bedi, Y. Béjot, D.A. Bennett, I.M. Bensenor, A.E. Berman, Y.M. Bezabih, A.S. Bhagavathula, S. Bhaskar, K. Bhattacharyya, A. Bijani, B. Bikbov, M.M. Birhanu, A. Boloor, L.C. Brant, H. Brenner, N.I. Briko, Z.A. Butt, F.L. Caetano dos Santos, L.E. Cahill, L. Cahuana-Hurtado, L.A. Cámara, I.R. Campos-Nonato, C. Cantu-Brito, J. Car, J.J. Carrero, F. Carvalho, C.A. Castañeda-Orjuela, F. Catalá-López, E. Cerin, J. Charan, V.K. Chattu, S. Chen, K.L. Chin, J.-Y.J. Choi, D.-T. Chu, S.-C. Chung, M. Cirillo, S. Coffey, S. Conti, V.M. Costa, D.K. Cundiff, O. Dadras, B. Dagnew, X. Dai, A.A.M. Damasceno, L. Dandona, R. Dandona, K. Davletov, V. De

la Cruz-Góngora, F.P. De la Hoz, J.-W. De Neve, E. Denova-Gutiérrez, M. Derbew Molla, B.T. Derseh, R. Desai, G. Deuschl, S.D. Dharmaratne, M. Dhimal, R.R. Dhungana, M. Dianatinasab, D. Diaz, S. Djalalinia, K. Dokova, A. Douiri, B.B. Duncan, A.R. Duraes, A.W. Eagan, S. Ebtehaj, A. Eftekhari, S. Eftekhazadeh, M. Ekholuenetale, N. El Nahas, I.Y. Elgendy, M. Elhadi, S.I. El-Jaafary, S. Esteghamati, A.E. Etisso, O. Eyawo, I. Fadhil, E.J.A. Faraon, P.S. Faris, M. Farwati, F. Farzadfar, E. Fernandes, C. Fernandez Prendes, P. Ferrara, I. Filip, F. Fischer, D. Flood, T. Fukumoto, M.M. Gad, S. Gaidhane, M. Ganji, J. Garg, A.K. Gebre, B.G. Gebregiorgis, K.Z. Gebregzabiher, G.G. Gebremeskel, L. Getacher, A.G. Obsa, A. Ghajar, A. Ghashghaee, N. Ghith, S. Giampaoli, S.A. Gilani, P.S. Gill, R.F. Gillum, E.V. Glushkova, E.V. Gnedovskaya, M. Golechha, K.B. Gonfa, A.H. Goudarzian, A.C. Goulart, J.S. Guadamuz, A. Guha, Y. Guo, R. Gupta, V. Hachinski, N. Hafezi-Nejad, T.G. Haile, R.R. Hamadeh, S. Hamidi, G.J. Hankey, A. Hargono, R.K. Hartono, M. Hashemian, A. Hashi, S. Hassan, H.Y. Hassen, R.J. Havmoeller, S.I. Hay, K. Hayat, G. Heidari, C. Herteliu, R. Holla, M. Hosseini, M. Hosseinzadeh, M. Hostiuc, S. Hostiuc, M. Househ, J. Huang, A. Humayun, I. Iavicoli, C.U. Ibeneme, S.E. Ibitoye, O.S. Ilesanmi, I.M. Ilic, M.D. Ilic, U. Iqbal, S.S.N. Irvani, S.M.S. Islam, R.M. Islam, H. Iso, M. Iwagami, V. Jain, T. Javaheri, S.K. Jayapal, S. Jayaram, R. Jayawardena, P. Jeemon, R.P. Jha, J.B. Jonas, J. Jonnagaddala, F. Joukar, J.J. Jozwiak, M. Jürisson, A. Kabir, T. Kahlon, R. Kalani, R. Kalhor, A. Kamath, I. Kamel, H. Kandel, A. Kandel, A. Karch, A.S. Kasa, P.D.M.C. Katoto, G.A. Kayode, Y.S. Khader, M. Khammarnia, M.S. Khan, M.N. Khan, M. Khan, E.A. Khan, K. Khatab, G.M.A. Kibria, Y.J. Kim, G.R. Kim, R.W. Kimokoti, S. Kisa, A. Kisa, M. Kivimäki, D. Kolte, A. Koolivand, V.A. Korshunov, S.L. Koulmane Laxminarayana, A. Koyanagi, K. Krishan, V. Krishnamoorthy, B. Kuate Defo, B. Kucuk Bicer, V. Kulkarni, G.A. Kumar, N. Kumar, O.P. Kurmi, D. Kusuma, G.F. Kwan, C. La Vecchia, B. Lacey, T. Lallukka, Q. Lan, S. Lasrado, Z.S. Lassi, P. Lauriola, W.R. Lawrence, A. Laxmaiah, K.E. LeGrand, M.-C. Li, B. Li, S. Li, S.S. Lim, L.-L. Lim, H. Lin, Z. Lin, R.-T. Lin, X. Liu, A.D. Lopez, S. Lorkowski, P.A. Lotufo, A. Lugo, N.K. M, F. Madotto, M. Mahmoudi, A. Majeed, R. Malekzadeh, A.A. Malik, A.A. Mamun, N. Manafi, M.A. Mansournia, L.G. Mantovani, S. Martini, M.R. Mathur, G. Mazzaglia, S. Mehata, M.M. Mehndiratta, T. Meier, R.G. Menezes, A. Meretoja, T. Mestrovic, B. Miazgowski, T. Miazgowski, I.M. Michalek, T.R. Miller, E.M. Mirrakhimov, H. Mirzaei, B. Moazen, M. Moghadaszadeh, Y. Mohammad, D.K. Mohammad, S. Mohammed, M.A. Mohammed, Y. Mokhayeri, M. Molokhia, A.A. Montasir, G. Moradi, R. Moradzadeh, P. Moraga, L. Morawska, I. Moreno Velásquez, J. Morze, S. Mubarik, W. Muruet, K.I. Musa, A.J. Nagarajan, M. Nalini, V. Nangia, A.A. Naqvi, S. Narasimha Swamy, B.R. Nascimento, V.C. Nayak, J. Nazari, M. Nazarzadeh, R.I. Negoj, S. Neupane Kandel, H.L.T. Nguyen, M.R. Nixon, B. Norrving, J.J. Noubiap, B.E. Nouthe, C. Nowak, O.O. Odukoya, F.A. Ogbo, A.T. Olagunju, H. Orru, A. Ortiz, S.M. Ostroff, J.R. Padubidri, R. Palladino, A. Pana, S. Panda-Jonas, U. Parekh, E.-C. Park, M. Parvizi, F. Pashazadeh Kan, U.K. Patel, M. Pathak, R. Paudel, V.C.F. Pepito, A. Perianayagam, N. Perico, H.Q. Pham, T. Pilgrim, M.A. Piradov, F. Pishgar, V. Podder, R.V. Polibin, A. Pourshams, D.R.A. Pribadi, N. Rabiee, M. Rabiee, A. Radfar, A. Rafiei, F. Rahim, V. Rahimi-Movaghar, M.H. Ur Rahman, M.A. Rahman, A.M. Rahmani, I. Rakovac, P. Ram, S. Ramalingam, J. Rana, P. Ranasinghe, S.J. Rao, P. Rathi, L. Rawal, W.F. Rawasia, R. Rawassizadeh, G. Remuzzi, A.M.N. Renzaho, A. Rezapour, S.M. Riahi, R.L. Roberts-Thomson, L. Roeber, P. Rohloff, M. Romoli, G. Roshandel, G.M. Rwegerera, S. Saadatagah, M.M. Saber-Ayad, S. Sabour, S. Sacco, M. Sadeghi, S. Saeedi Moghaddam, S. Safari, A. Sahebkar, S. Salehi, H. Salimzadeh, M. Samaei, A.M. Samy, I.S. Santos, M.M. Santric-Milicevic, N. Sarrafzadegan, A. Sarveazad, T. Sathish, M. Sawhney, M. Saylan, M.I. Schmidt, A.E. Schutte, S. Senthilkumaran, S.G. Sepanlou, F. Sha, S. Shahabi, I. Shahid, M.A. Shaikh, M. Shamali, M. Shamsizadeh, M.S.R. Shawon, A. Sheikh, M. Shigematsu, M.-J. Shin, J.I. Shin, R. Shiri, I. Shiue, K. Shuval, S. Siabani, T.J. Siddiqi, D.A.S. Silva, J.A. Singh, A.S. Mtech, V.Y. Skryabin, A.A. Skryabina, A. Soheili, E.E. Spurlock, L. Stockfelt, S. Stortecky, S. Stranges, R. Suliankatchi Abdulkader, H. Tadbiri, E.G. Tadesse, D.B. Tadesse, M. Tajdini, M. Tariqujjaman, B.F. Teklehaimanot, M.-H. Temsah, A.K. Tesema, B. Thakur, K.R. Thankappan, R. Thapar, A.G. Thrift, B. Timalcina, M. Tonelli, M. Touvier, M.R. Tovani-Palone, A. Tripathi, J.P. Tripathy, T.C. Truelsen, G.M. Tsegay, G.W. Tsegaye, N. Tsilimparis, B.S. Tusa, S. Tyrovolas, K.K. Umapathi, B. Unim, B. Unnikrishnan, M.S. Usman, M. Vaduganathan, P.R. Valdez, T.J. Vasankari, D.Z. Velazquez, N. Venketasubramanian, G.T. Vu, I.S. Vujcic, Y. Waheed, Y. Wang, F. Wang, J. Wei, R.G. Weintraub, A.H. Weldemariam, R. Westerman, A.S. Winkler, C.S. Wiysonge, C.D.A. Wolfe, B.L.

- Wubishet, G. Xu, A. Yadollahpour, K. Yamagishi, L.L. Yan, S. Yandrapalli, Y. Yano, H. Yatsuya, T.Y. Yeheyis, Y. Yeshaw, C.S. Yilgwan, N. Yonemoto, C. Yu, H. Yusefzadeh, G. Zachariah, S.B. Zaman, M.S. Zaman, M. Zamanian, R. Zand, A. Zandifar, A. Zarghi, M.S. Zastrozhin, A. Zastrozhina, Z.-J. Zhang, Y. Zhang, W. Zhang, C. Zhong, Z. Zou, Y.M.H. Zuniga, C.J.L. Murray, V. Fuster, Global Burden of Cardiovascular Diseases and Risk Factors, 1990–2019: Update From the GBD 2019 Study, *Journal of the American College of Cardiology* 76(25) (2020) 2982-3021.
- [181] G.A. Roth, C. Johnson, A. Abajobir, F. Abd-Allah, S.F. Abera, G. Abyu, M. Ahmed, B. Aksut, T. Alam, K. Alam, F. Alla, N. Alvis-Guzman, S. Amrock, H. Ansari, J. Ärnlöv, H. Asayesh, T.M. Atey, L. Avila-Burgos, A. Awasthi, A. Banerjee, A. Barac, T. Bärnighausen, L. Barregard, N. Bedi, E. Belay Ketema, D. Bennett, G. Berhe, Z. Bhutta, S. Bitew, J. Carapetis, J.J. Carrero, D.C. Malta, C.A. Castañeda-Orjuela, J. Castillo-Rivas, F. Catalá-López, J.Y. Choi, H. Christensen, M. Cirillo, L. Cooper, Jr., M. Criqui, D. Cundiff, A. Damasceno, L. Dandona, R. Dandona, K. Davletov, S. Dharmaratne, P. Dorairaj, M. Dubey, R. Ehrenkranz, M. El Sayed Zaki, E.J.A. Faraon, A. Esteghamati, T. Farid, M. Farvid, V. Feigin, E.L. Ding, G. Fowkes, T. Gebrehiwot, R. Gillum, A. Gold, P. Gona, R. Gupta, T.D. Habtewold, N. Hafezi-Nejad, T. Hailu, G.B. Hailu, G. Hankey, H.Y. Hassen, K.H. Abate, R. Havmoeller, S.I. Hay, M. Horino, P.J. Hotez, K. Jacobsen, S. James, M. Javanbakht, P. Jeemon, D. John, J. Jonas, Y. Kalkonde, C. Karimkhani, A. Kasaieian, Y. Khader, A. Khan, Y.H. Khang, S. Khera, A.T. Khoja, J. Khubchandani, D. Kim, D. Kolte, S. Kosen, K.J. Krohn, G.A. Kumar, G.F. Kwan, D.K. Lal, A. Larsson, S. Linn, A. Lopez, P.A. Lotufo, H.M.A. El Razek, R. Malekzadeh, M. Mazidi, T. Meier, K.G. Meles, G. Mensah, A. Meretoja, H. Mezgebe, T. Miller, E. Mirrakhimov, S. Mohammed, A.E. Moran, K.I. Musa, J. Narula, B. Neal, F. Ngalesoni, G. Nguyen, C.M. Obermeyer, M. Owolabi, G. Patton, J. Pedro, D. Qato, M. Qorbani, K. Rahimi, R.K. Rai, S. Rawaf, A. Ribeiro, S. Safiri, J.A. Salomon, I. Santos, M. Santric Milicevic, B. Sartorius, A. Schutte, S. Sepanlou, M.A. Shaikh, M.J. Shin, M. Shishehbor, H. Shore, D.A.S. Silva, E. Sobngwi, S. Stranges, S. Swaminathan, R. Tabarés-Seisdedos, N. Tadele Atnafu, F. Tesfay, J.S. Thakur, A. Thrift, R. Topor-Madry, T. Truelsen, S. Tyrovolas, K.N. Ukwaja, O. Uthman, T. Vasankari, V. Vlassov, S.E. Vollset, T. Wakayo, D. Watkins, R. Weintraub, A. Werdecker, R. Westerman, C.S. Wiysonge, C. Wolfe, A. Workicho, G. Xu, Y. Yano, P. Yip, N. Yonemoto, M. Younis, C. Yu, T. Vos, M. Naghavi, C. Murray, Global, Regional, and National Burden of Cardiovascular Diseases for 10 Causes, 1990 to 2015, *J Am Coll Cardiol* 70(1) (2017) 1-25.
- [182] B. Ortiz-Bonnin, S. Rinné, R. Moss, A.K. Streit, M. Scharf, K. Richter, A. Stöber, A. Pfeufer, G. Seemann, S. Käb, B.M. Beckmann, N. Decher, Electrophysiological characterization of a large set of novel variants in the SCN5A-gene: identification of novel LQTS3 and BrS mutations, *Pflugers Arch* 468(8) (2016) 1375-87.
- [183] Q. Wang, X. Mou, H. Cao, Q. Meng, Y. Ma, P. Han, J. Jiang, H. Zhang, Y. Ma, A novel xeno-free and feeder-cell-free system for human pluripotent stem cell culture, *Protein Cell* 3(1) (2012) 51-59.
- [184] H.F. Lu, C. Chai, T.C. Lim, M.F. Leong, J.K. Lim, S. Gao, K.L. Lim, A.C. Wan, A defined xeno-free and feeder-free culture system for the derivation, expansion and direct differentiation of transgene-free patient-specific induced pluripotent stem cells, *Biomaterials* 35(9) (2014) 2816-26.
- [185] Y. Hua, K. Yoshimochi, J. Li, K. Takekita, M. Shimotsuma, L. Li, X. Qu, J. Zhang, Y. Sawa, L. Liu, S. Miyagawa, Development and evaluation of a novel xeno-free culture medium for human-induced pluripotent stem cells, *Stem cell research & therapy* 13(1) (2022) 223-223.
- [186] P. Ghasemi-Dehkordi, M. Allahbakhshian-Farsani, N. Abdian, A. Mirzaeian, J. Saffari-Chaleshtori, F. Heybati, G. Mardani, A. Karimi-Taghanaki, A. Doosti, M.-S. Jami, M. Abolhasani, M. Hashemzadeh-Chaleshtori, Comparison between the cultures of human induced pluripotent stem cells (hiPSCs) on feeder-and serum-free system (Matrigel matrix), MEF and HDF feeder cell lines, *Journal of cell communication and signaling* 9(3) (2015) 233-246.
- [187] H. Hongisto, T. Ilmarinen, M. Vattulainen, A. Mikhailova, H. Skottman, Xeno- and feeder-free differentiation of human pluripotent stem cells to two distinct ocular epithelial cell types using simple modifications of one method, *Stem Cell Research & Therapy* 8(1) (2017) 291.
- [188] L.-H. Chen, T.-C. Sung, H.H.-C. Lee, A. Higuchi, H.-C. Su, K.-J. Lin, Y.-R. Huang, Q.-D. Ling, S.S. Kumar, A.A. Alarfaj, M.A. Munusamy, M. Nasu, D.-C. Chen, S.-T. Hsu, Y. Chang, K.-F. Lee, H.-C. Wang,

A. Umezawa, Xeno-free and feeder-free culture and differentiation of human embryonic stem cells on recombinant vitronectin-grafted hydrogels, *Biomaterials Science* 7(10) (2019) 4345-4362.

[189] P.W. Burridge, E. Matsa, P. Shukla, Z.C. Lin, J.M. Churko, A.D. Ebert, F. Lan, S. Diecke, B. Huber, N.M. Mordwinkin, J.R. Plews, O.J. Abilez, B. Cui, J.D. Gold, J.C. Wu, Chemically defined generation of human cardiomyocytes, *Nature Methods* 11(8) (2014) 855-860.

[190] I. Karakikes, G.D. Senyei, J. Hansen, C.W. Kong, E.U. Azeloglu, F. Stillitano, D.K. Lieu, J. Wang, L. Ren, J.S. Hulot, R. Iyengar, R.A. Li, R.J. Hajjar, Small molecule-mediated directed differentiation of human embryonic stem cells toward ventricular cardiomyocytes, *Stem Cells Transl Med* 3(1) (2014) 18-31.

[191] X. Lian, C. Hsiao, G. Wilson, K. Zhu, L.B. Hazeltine, S.M. Azarin, K.K. Raval, J. Zhang, T.J. Kamp, S.P. Palecek, Robust cardiomyocyte differentiation from human pluripotent stem cells via temporal modulation of canonical Wnt signaling, *Proceedings of the National Academy of Sciences* 109(27) (2012) E1848-E1857.

[192] N. Cao, Z. Liu, Z. Chen, J. Wang, T. Chen, X. Zhao, Y. Ma, L. Qin, J. Kang, B. Wei, L. Wang, Y. Jin, H.-T. Yang, Ascorbic acid enhances the cardiac differentiation of induced pluripotent stem cells through promoting the proliferation of cardiac progenitor cells, *Cell research* 22(1) (2012) 219-236.

[193] D. Ivanyuk, G. Budash, Y. Zheng, J.A. Gaspar, U. Chaudhari, A. Fatima, S. Bahmanpour, V.K. Grin, A.G. Popandopulo, A. Sachinidis, J. Hescheler, T. Šarić, Ascorbic Acid-Induced Cardiac Differentiation of Murine Pluripotent Stem Cells: Transcriptional Profiling and Effect of a Small Molecule Synergist of Wnt/ β -Catenin Signaling Pathway, *Cellular Physiology and Biochemistry* 36(2) (2015) 810-830.

[194] K. Prill, J.F. Dawson, Assembly and Maintenance of Sarcomere Thin Filaments and Associated Diseases, *Int J Mol Sci* 21(2) (2020).

[195] J.M. Pioner, A.W. Racca, J.M. Klaiman, K.-C. Yang, X. Guan, L. Pabon, V. Muskheli, R. Zaunbrecher, J. Macadangdang, M.Y. Jeong, D.L. Mack, M.K. Childers, D.-H. Kim, C. Tesi, C. Poggesi, C.E. Murry, M. Regnier, Isolation and Mechanical Measurements of Myofibrils from Human Induced Pluripotent Stem Cell-Derived Cardiomyocytes, *Stem cell reports* 6(6) (2016) 885-896.

[196] M.S. Fontes, T.A. van Veen, J.M. de Bakker, H.V. van Rijen, Functional consequences of abnormal Cx43 expression in the heart, *Biochim Biophys Acta* 1818(8) (2012) 2020-9.

[197] T. Martins-Marques, T. Ribeiro-Rodrigues, S.C. de Jager, M. Zuzarte, C. Ferreira, P. Cruz, L. Reis, R. Baptista, L. Gonçalves, J.P. Sluiter, H. Girao, Myocardial infarction affects Cx43 content of extracellular vesicles secreted by cardiomyocytes, *Life Science Alliance* 3(12) (2020) e202000821.

[198] P.D. Lampe, C.D. Cooper, T.J. King, J.M. Burt, Analysis of Connexin43 phosphorylated at S325, S328 and S330 in normoxic and ischemic heart, *J Cell Sci* 119(Pt 16) (2006) 3435-42.

[199] W. Roell, A.M. Klein, M. Breitbach, T.S. Becker, A. Parikh, J. Lee, K. Zimmermann, S. Reining, B. Gabris, A. Ottersbach, R. Doran, B. Engelbrecht, M. Schiffer, K. Kimura, P. Freitag, E. Carls, C. Geisen, G.D. Duerr, P. Sasse, A. Welz, A. Pfeifer, G. Salama, M. Kotlikoff, B.K. Fleischmann, Overexpression of Cx43 in cells of the myocardial scar: Correction of post-infarct arrhythmias through heterotypic cell-cell coupling, *Scientific Reports* 8(1) (2018) 7145.

[200] W. Li, M. Stauske, X. Luo, S. Wagner, M. Vollrath, C.S. Mehnert, M. Schubert, L. Cyganek, S. Chen, S.-M. Hasheminasab, G. Wulf, A. El-Armouche, L.S. Maier, G. Hasenfuss, K. Guan, Disease Phenotypes and Mechanisms of iPSC-Derived Cardiomyocytes From Brugada Syndrome Patients With a Loss-of-Function SCN5A Mutation, *Frontiers in cell and developmental biology* 8 (2020) 592893-592893.

[201] K. Nademanee, H. Raju, S.V. de Noronha, M. Papadakis, L. Robinson, S. Rothery, N. Makita, S. Kowase, N. Boonmee, V. Vitayakritsirikul, S. Ratanarapee, S. Sharma, A.C. van der Wal, M. Christiansen, H.L. Tan, A.A. Wilde, A. Nogami, M.N. Sheppard, G. Veerakul, E.R. Behr, Fibrosis, Connexin-43, and Conduction Abnormalities in the Brugada Syndrome, *Journal of the American College of Cardiology* 66(18) (2015) 1976-1986.

[202] M. Stein, T.A.B. van Veen, C.A. Remme, M. Boulaksil, M. Noorman, L. van Stuijvenberg, R. van der Nagel, C.R. Bezzina, R.N.W. Hauer, J.M.T. de Bakker, H.V.M. van Rijen, Combined reduction of intercellular coupling and membrane excitability differentially affects transverse and longitudinal cardiac conduction, *Cardiovascular Research* 83(1) (2009) 52-60.

- [203] A. Rodríguez-Sinovas, J.A. Sánchez, L. Valls-Lacalle, M. Consegal, I. Ferreira-González, Connexins in the Heart: Regulation, Function and Involvement in Cardiac Disease, *International Journal of Molecular Sciences* 22(9) (2021) 4413.
- [204] A.A.M. Wilde, A.S. Amin, Clinical Spectrum of SCN5A Mutations: Long QT Syndrome, Brugada Syndrome, and Cardiomyopathy, *JACC: Clinical Electrophysiology* 4(5) (2018) 569-579.
- [205] P.P. de Tombe, Altered contractile function in heart failure, *Cardiovascular Research* 37(2) (1998) 367-380.
- [206] D.I. Keller, F.Z. Barrane, L. Gouas, J. Martin, S. Pilote, V. Suarez, S. Osswald, M. Brink, P. Guicheney, N. Schwick, M. Chahine, A novel nonsense mutation in the SCN5A gene leads to Brugada syndrome and a silent gene mutation carrier state, *Can J Cardiol* 21(11) (2005) 925-31.
- [207] S. Okata, S. Yuasa, T. Suzuki, S. Ito, N. Makita, T. Yoshida, M. Li, J. Kurokawa, T. Seki, T. Egashira, Y. Aizawa, M. Kodaira, C. Motoda, G. Yozu, M. Shimojima, N. Hayashiji, H. Hashimoto, Y. Kuroda, A. Tanaka, K. Fukuda, Embryonic type Na⁺ channel β -subunit, SCN3B masks the disease phenotype of Brugada syndrome, *Scientific Reports* 6 (2016).
- [208] R.M. Shaw, H.M. Colecraft, L-type calcium channel targeting and local signalling in cardiac myocytes, *Cardiovasc Res* 98(2) (2013) 177-86.
- [209] S.A. Goonasekera, K. Hammer, M. Auger-Messier, I. Bodi, X. Chen, H. Zhang, S. Reiken, J.W. Elrod, R.N. Correll, A.J. York, M.A. Sargent, F. Hofmann, S. Moosmang, A.R. Marks, S.R. Houser, D.M. Bers, J.D. Molkentin, Decreased cardiac L-type Ca²⁺ channel activity induces hypertrophy and heart failure in mice, *The Journal of Clinical Investigation* 122(1) (2012) 280-290.
- [210] F. Schröder, R. Handrock, D.J. Beuckelmann, S. Hirt, R. Hullin, L. Priebe, R.H. Schwinger, J. Weil, S. Herzig, Increased availability and open probability of single L-type calcium channels from failing compared with nonfailing human ventricle, *Circulation* 98(10) (1998) 969-76.
- [211] R.G. Gregg, A. Messing, C. Strube, M. Beurg, R. Moss, M. Behan, M. Sukhareva, S. Haynes, J.A. Powell, R. Coronado, P.A. Powers, Absence of the beta subunit (cchb1) of the skeletal muscle dihydropyridine receptor alters expression of the alpha 1 subunit and eliminates excitation-contraction coupling, *Proceedings of the National Academy of Sciences of the United States of America* 93(24) (1996) 13961-13966.
- [212] H.M. Viola, P.G. Arthur, L.C. Hool, Evidence for regulation of mitochondrial function by the L-type Ca²⁺ channel in ventricular myocytes, *Journal of Molecular and Cellular Cardiology* 46(6) (2009) 1016-1026.
- [213] M. Biel, P. Ruth, E. Bosse, R. Hullin, W. Stühmer, V. Flockerzi, F. Hofmann, Primary structure and functional expression of a high voltage activated calcium channel from rabbit lung, *FEBS Lett* 269(2) (1990) 409-12.
- [214] A. Welling, E. Bosse, A. Cavalié, R. Bottlender, A. Ludwig, W. Nastainczyk, V. Flockerzi, F. Hofmann, Stable co-expression of calcium channel alpha 1, beta and alpha 2/delta subunits in a somatic cell line, *The Journal of physiology* 471 (1993) 749-765.
- [215] F. Hofmann, V. Flockerzi, S. Kahl, J.W. Wegener, L-Type CaV1.2 Calcium Channels: From In Vitro Findings to In Vivo Function, *Physiological Reviews* 94(1) (2014) 303-326.
- [216] I. Bodi, G. Mikala, S.E. Koch, S.A. Akhter, A. Schwartz, The L-type calcium channel in the heart: the beat goes on, *The Journal of clinical investigation* 115(12) (2005) 3306-3317.
- [217] B.S. Finlin, S.M. Crump, J. Satin, D.A. Andres, Regulation of voltage-gated calcium channel activity by the Rem and Rad GTPases, *Proceedings of the National Academy of Sciences* 100(24) (2003) 14469-14474.
- [218] L. Yang, A. Katchman, J. Kushner, A. Kushnir, S. Zakharov, B.-x. Chen, Z. Shuja, P. Subramanyam, G. Liu, A. Papa, D. Roybal, G. Pitt, H. Colecraft, S. Marx, Cardiac CaV1.2 channels require β subunits for β -adrenergic-mediated modulation but not trafficking, *Journal of Clinical Investigation* 129 (2018).
- [219] E. Perez-Reyes, Molecular Physiology of Low-Voltage-Activated T-type Calcium Channels, *Physiological Reviews* 83(1) (2003) 117-161.
- [220] M.F. Rossier, T-Type Calcium Channel: A Privileged Gate for Calcium Entry and Control of Adrenal Steroidogenesis, *Frontiers in Endocrinology* 7 (2016).

- [221] L. Sen, T.W. Smith, T-type Ca^{2+} channels are abnormal in genetically determined cardiomyopathic hamster hearts, *Circulation Research* 75(1) (1994) 149-155.
- [222] G. Bkaily, A. Sculptoreanu, D. Jacques, G. Jasmin, Increases of T-type Ca^{2+} current in heart cells of the cardiomyopathic hamster, *Molecular and Cellular Biochemistry* 176(1) (1997) 199-204.
- [223] B. Huang, D. Qin, L. Deng, M. Boutjdir, E.-S. N, Reexpression of T-type Ca^{2+} channel gene and current in post-infarction remodeled rat left ventricle, *Cardiovasc Res* 46(3) (2000) 442-9.
- [224] L. Cribbs, T-type calcium channel expression and function in the diseased heart, *Channels (Austin)* 4(6) (2010) 447-52.
- [225] E. Dirx, P.A. da Costa Martins, L.J. De Windt, Regulation of fetal gene expression in heart failure, *Biochimica et Biophysica Acta (BBA) - Molecular Basis of Disease* 1832(12) (2013) 2414-2424.
- [226] K. Ono, T. Iijima, Cardiac T-type Ca^{2+} channels in the heart, *Journal of Molecular and Cellular Cardiology* 48(1) (2010) 65-70.
- [227] H. Nakayama, I. Bodi, R.N. Correll, X. Chen, J. Lorenz, S.R. Houser, J. Robbins, A. Schwartz, J.D. Molkentin, $\alpha_1\text{G}$ -dependent T-type Ca^{2+} current antagonizes cardiac hypertrophy through a NOS3-dependent mechanism in mice, *The Journal of clinical investigation* 119(12) (2009) 3787-3796.
- [228] J. Wei, X. Ni, Y. Dai, X. Chen, S. Ding, J. Bao, L. Xing, Identification of genes associated with sudden cardiac death: a network- and pathway-based approach, *J Thorac Dis* 13(6) (2021) 3610-3627.
- [229] G.M. De Ferrari, P.J. Schwartz, Long QT syndrome, a purely electrical disease? Not anymore, *European Heart Journal* 30(3) (2009) 253-255.
- [230] I.S. Leren, N.E. Hasselberg, J. Saberniak, T.F. Håland, E. Kongsgård, O.A. Smiseth, T. Edvardsen, K.H. Haugaa, Cardiac Mechanical Alterations and Genotype Specific Differences in Subjects With Long QT Syndrome, *JACC: Cardiovascular Imaging* 8(5) (2015) 501-510.
- [231] F. van Hoorn, M.E. Campian, A. Spijkerboer, M.T. Blom, R.N. Planken, A.C. van Rossum, J.M.T. de Bakker, A.A.M. Wilde, M. Groenink, H.L. Tan, SCN5A Mutations in Brugada Syndrome Are Associated with Increased Cardiac Dimensions and Reduced Contractility, *PLOS ONE* 7(8) (2012) e42037.
- [232] E.M. Snyder, B.D. Johnson, M.J. Joyner, Genetics of β_2 -Adrenergic Receptors and the Cardiopulmonary Response to Exercise, *Exercise and Sport Sciences Reviews* 36(2) (2008).
- [233] G. Jung, G. Fajardo, A.J. Ribeiro, K.B. Kooiker, M. Coronado, M. Zhao, D.Q. Hu, S. Reddy, K. Kodo, K. Sriram, P.A. Insel, J.C. Wu, B.L. Pruitt, D. Bernstein, Time-dependent evolution of functional vs. remodeling signaling in induced pluripotent stem cell-derived cardiomyocytes and induced maturation with biomechanical stimulation, *Faseb j* 30(4) (2016) 1464-79.
- [234] P. Yampolsky, M. Koenen, M. Mosqueira, P. Geschwill, S. Nauck, M. Witzemberger, C. Seyler, T. Fink, M. Kruska, C. Bruehl, A.P. Schwoerer, H. Ehmke, R.H.A. Fink, A. Draguhn, D. Thomas, H.A. Katus, P.A. Schweizer, Augmentation of myocardial I(f) dysregulates calcium homeostasis and causes adverse cardiac remodeling, *Nat Commun* 10(1) (2019) 3295.
- [235] G. d'Amati, A. Bagattin, B. Bauce, A. Rampazzo, C. Autore, C. Basso, K. King, M.D. Romeo, P. Gallo, G. Thiene, G.A. Danieli, A. Nava, Juvenile sudden death in a family with polymorphic ventricular arrhythmias caused by a novel RyR2 gene mutation: evidence of specific morphological substrates, *Human Pathology* 36(7) (2005) 761-767.
- [236] G. Tse, K.H.C. Li, G. Li, T. Liu, G. Bazoukis, W.T. Wong, M.T.V. Chan, M.C.S. Wong, Y. Xia, K.P. Letsas, G.C.P. Chan, Y.S. Chan, W.K.K. Wu, Higher Dispersion Measures of Conduction and Repolarization in Type 1 Compared to Non-type 1 Brugada Syndrome Patients: An Electrocardiographic Study From a Single Center, *Frontiers in Cardiovascular Medicine* 5 (2018).
- [237] M. Finlay, J. Bhar-Amato, K.-E. Ng, D. Santos, M. Orini, V. Vyas, P. Taggart, A.A. Grace, C.L.-H. Huang, P.D. Lambiase, A. Tinker, Autonomic modulation of the electrical substrate in mice haploinsufficient for cardiac sodium channels: a model of the Brugada syndrome, *American Journal of Physiology-Cell Physiology* 317(3) (2019) C576-C583.
- [238] Y. Zhou, B. Zhou, L. Pache, M. Chang, A.H. Khodabakhshi, O. Tanaseichuk, C. Benner, S.K. Chanda, Metascape provides a biologist-oriented resource for the analysis of systems-level datasets, *Nat Commun* 10(1) (2019) 1523.

- [239] G. Sarquella-Brugada, O. Campuzano, E. Arbelo, J. Brugada, R. Brugada, Brugada syndrome: clinical and genetic findings, *Genetics in Medicine* 18(1) (2016) 3-12.
- [240] E.D. Engelstein, Long QT syndrome: a preventable cause of sudden death in women, *Curr Womens Health Rep* 3(2) (2003) 126-34.
- [241] R. Schimpf, C. Veltmann, C. Wolpert, M. Borggrefe, Arrhythmogenic hereditary syndromes: Brugada Syndrome, long QT syndrome, short QT syndrome and CPVT, *Minerva Cardioangiol* 58(6) (2010) 623-36.
- [242] M. Wang, X. Tu, The Genetics and Epigenetics of Ventricular Arrhythmias in Patients Without Structural Heart Disease, *Frontiers in Cardiovascular Medicine* 9 (2022).
- [243] S. Roth, S. Zhang, J. Chiu, E.K. Wirth, U. Schweizer, Development of a serum-free supplement for primary neuron culture reveals the interplay of selenium and vitamin E in neuronal survival, *J Trace Elem Med Biol* 24(2) (2010) 130-7.
- [244] Y. Chen, B. Stevens, J. Chang, J. Milbrandt, B.A. Barres, J.W. Hell, NS21: re-defined and modified supplement B27 for neuronal cultures, *J Neurosci Methods* 171(2) (2008) 239-47.
- [245] A. Ebert, A.U. Joshi, S. Andorf, Y. Dai, S. Sampathkumar, H. Chen, Y. Li, P. Garg, K. Toischer, G. Hasenfuss, D. Mochly-Rosen, J.C. Wu, Proteasome-Dependent Regulation of Distinct Metabolic States During Long-Term Culture of Human iPSC-Derived Cardiomyocytes, *Circulation Research* 125(1) (2019) 90-103.
- [246] E. Karbassi, A. Fenix, S. Marchiano, N. Muraoka, K. Nakamura, X. Yang, C.E. Murry, Cardiomyocyte maturation: advances in knowledge and implications for regenerative medicine, *Nat Rev Cardiol* 17(6) (2020) 341-359.
- [247] T. Grancharova, K.A. Gerbin, A.B. Rosenberg, C.M. Roco, J.E. Arakaki, C.M. DeLizo, S.Q. Dinh, R.M. Donovan-Maiye, M. Hirano, A.M. Nelson, J. Tang, J.A. Theriot, C. Yan, V. Menon, S.P. Palecek, G. Seelig, R.N. Gunawardane, A comprehensive analysis of gene expression changes in a high replicate and open-source dataset of differentiating hiPSC-derived cardiomyocytes, *Scientific Reports* 11(1) (2021) 15845.
- [248] Y. Guo, W.T. Pu, Cardiomyocyte Maturation, *Circulation Research* 126(8) (2020) 1086-1106.
- [249] W.E. Knight, Y. Cao, Y.-H. Lin, C. Chi, B. Bai, G.C. Sparagna, Y. Zhao, Y. Du, P. Londono, J.A. Reisz, B.C. Brown, M.R.G. Taylor, A.V. Ambardekar, J.C. Cleveland, T.A. McKinsey, M.Y. Jeong, L.A. Walker, K.C. Woulfe, A. D'Alessandro, K.C. Chatfield, H. Xu, M.R. Bristow, P.M. Buttrick, K. Song, Maturation of Pluripotent Stem Cell-Derived Cardiomyocytes Enables Modeling of Human Hypertrophic Cardiomyopathy, *Stem Cell Reports* 16(3) (2021) 519-533.
- [250] E. Chorin, O. Havakuk, A. Adler, A. Steinvil, U. Rozovski, C. van der Werf, P.G. Postema, G. Topaz, A.A.M. Wilde, S. Viskin, R. Rosso, Diagnostic value of T-wave morphology changes during "QT stretching" in patients with long QT syndrome, *Heart Rhythm* 12(11) (2015) 2263-2271.
- [251] H. Horigome, Y. Ishikawa, K. Takahashi, M. Yoshinaga, N. Sumitomo, Analysis of the shape of the T-wave in congenital long-QT syndrome type 3 by geometric morphometrics, *Scientific Reports* 11(1) (2021) 11909.
- [252] M. Clements, Multielectrode Array (MEA) Assay for Profiling Electrophysiological Drug Effects in Human Stem Cell-Derived Cardiomyocytes, *Curr Protoc Toxicol* 68 (2016) 22.4.1-22.4.32.
- [253] D.A. Saint, The cardiac persistent sodium current: an appealing therapeutic target?, *Br J Pharmacol* 153(6) (2008) 1133-42.
- [254] C.R. Bezzina, M.B. Rook, A.A.M. Wilde, Cardiac sodium channel and inherited arrhythmia syndromes, *Cardiovascular Research* 49(2) (2001) 257-271.
- [255] A. Burashnikov, J.M. Di Diego, A.C. Zygmunt, L. Belardinelli, C. Antzelevitch, Atrium-selective sodium channel block as a strategy for suppression of atrial fibrillation: differences in sodium channel inactivation between atria and ventricles and the role of ranolazine, *Circulation* 116(13) (2007) 1449-57.
- [256] S. Abramovich-Sivan, Y. Bitton, J. Karin, D. David, S. Akselrod, The effects of lidocaine on cardiac parasympathetic control in normal subjects and in subjects after myocardial infarction, *Clin Auton Res* 6(6) (1996) 313-9.

- [257] B. Müller-Edenborn, G. Kania, E. Osto, P. Jakob, N. Krasniqi, B. Beck-Schimmer, P. Blyszczuk, U. Eriksson, Lidocaine Enhances Contractile Function of Ischemic Myocardial Regions in Mouse Model of Sustained Myocardial Ischemia, *PloS one* 11(5) (2016) e0154699-e0154699.
- [258] I.A. Khan, C.K. Nair, Brugada and long QT-3 syndromes: two phenotypes of the sodium channel disease, *Ann Noninvasive Electrocardiol* 9(3) (2004) 280-9.
- [259] D.M. Bers, S. Despa, Na⁺ transport in cardiac myocytes; Implications for excitation-contraction coupling, *IUBMB Life* 61(3) (2009) 215-221.
- [260] Z. Kubalova, I. Györke, R. Terentyeva, S. Viatchenko-Karpinski, D. Terentyev, S.C. Williams, S. Györke, Modulation of cytosolic and intra-sarcoplasmic reticulum calcium waves by calsequestrin in rat cardiac myocytes, *J Physiol* 561(Pt 2) (2004) 515-24.
- [261] M.V.K. Kanga, M. Reppel, J. Hescheler, F. Nguemo, Modeling genetic cardiac channelopathies using induced pluripotent stem cells – Status quo from an electrophysiological perspective, *Biochemical Pharmacology* 192 (2021) 114746.
- [262] M. Bébarová, Advances in patch clamp technique: towards higher quality and quantity, *Gen Physiol Biophys* 31(2) (2012) 131-40.
- [263] J.K. Park, L.J. Martin, X. Zhang, A.G. Jegga, D.W. Benson, Genetic variants in SCN5A promoter are associated with arrhythmia phenotype severity in patients with heterozygous loss-of-function mutation, *Heart Rhythm* 9(7) (2012) 1090-1096.
- [264] L. Núñez, A. Barana, I. Amorós, M.G. de la Fuente, P. Dolz-Gaitón, R. Gómez, I. Rodríguez-García, I. Mosquera, L. Monserrat, E. Delpón, R. Caballero, A. Castro-Beiras, J. Tamargo, p.D1690N Nav1.5 rescues p.G1748D mutation gating defects in a compound heterozygous Brugada syndrome patient, *Heart Rhythm* 10(2) (2013) 264-72.
- [265] S. Okata, S. Yuasa, T. Suzuki, S. Ito, N. Makita, T. Yoshida, M. Li, J. Kurokawa, T. Seki, T. Egashira, Y. Aizawa, M. Kodaira, C. Motoda, G. Yozu, M. Shimojima, N. Hayashiji, H. Hashimoto, Y. Kuroda, A. Tanaka, M. Murata, T. Aiba, W. Shimizu, M. Horie, K. Kamiya, T. Furukawa, K. Fukuda, Embryonic type Na(+) channel β -subunit, SCN3B masks the disease phenotype of Brugada syndrome, *Scientific reports* 6 (2016) 34198-34198.
- [266] B. Ortiz-Bonnin, S. Rinné, R. Moss, A. Streit, M. Scharf, K. Richter, A. Stöber, A. Pfeufer, G. Seemann, S. Käb, B.M. Beckmann, N. Decher, Electrophysiological characterization of a large set of novel variants in the SCN5A-gene: identification of novel LQTS3 and BrS mutations, *Pflügers Archiv - European Journal of Physiology* 468 (2016).
- [267] R.-M. Hu, D.J. Tester, R. Li, T. Sun, B.Z. Peterson, M.J. Ackerman, J.C. Makielski, B.-H. Tan, Mexiletine rescues a mixed biophysical phenotype of the cardiac sodium channel arising from the SCN5A mutation, N406K, found in LQT3 patients, *Channels* 12(1) (2018) 176-186.
- [268] P. Schwartz, S. Priori, C. Spazzolini, A. Moss, G. Vincent, C. Napolitano, I. Denjoy, P. Guicheney, G. Breithardt, M. Keating, J. Towbin, A. Beggs, P. Brink, A. Wilde, L. Toivonen, W. Zareba, J. Robinson, K. Timothy, V. Corfield, R. Bloise, Genotype-Phenotype Correlation in the Long-QT Syndrome : Gene-Specific Triggers for Life-Threatening Arrhythmias, *Circulation* 103 (2001) 89-95.
- [269] Y.-K. Lee, K.-M. Ng, W.-H. Lai, Y.-C. Chan, Y.-M. Lau, Q. Lian, H.-F. Tse, C.-W. Siu, Calcium Homeostasis in Human Induced Pluripotent Stem Cell-Derived Cardiomyocytes, *Stem Cell Reviews and Reports* 7(4) (2011) 976-986.
- [270] A. Ahola, R.P. Pölönen, K. Aalto-Setälä, J. Hyttinen, Simultaneous Measurement of Contraction and Calcium Transients in Stem Cell Derived Cardiomyocytes, *Ann Biomed Eng* 46(1) (2018) 148-158.
- [271] A. Walter, T. Šarić, J. Hescheler, S. Papadopoulos, Calcium Imaging in Pluripotent Stem Cell-Derived Cardiac Myocytes, *Methods Mol Biol* 1353 (2016) 131-46.
- [272] P.P. Kanade, N.-E. Oyunbaatar, D.-W. Lee, Effects of low temperature on electrophysiology and mechanophysiology of human induced pluripotent stem cell-derived cardiomyocytes (hiPSC-CMs), *Micro and Nano Systems Letters* 9(1) (2021) 9.
- [273] P. Liang, K. Sallam, H. Wu, Y. Li, I. Itzhaki, P. Garg, Y. Zhang, V. Vermglinchan, F. Lan, M. Gu, T. Gong, Y. Zhuge, C. He, A.D. Ebert, V. Sanchez-Freire, J. Churko, S. Hu, A. Sharma, C.K. Lam, M.M. Scheinman, D.M. Bers, J.C. Wu, Patient-Specific and Genome-Edited Induced Pluripotent Stem Cell-

- Derived Cardiomyocytes Elucidate Single-Cell Phenotype of Brugada Syndrome, *Journal of the American College of Cardiology* 68(19) (2016) 2086-2096.
- [274] T.D. Tsai, M.E. Barish, Imaging of caffeine-inducible release of intracellular calcium in cultured embryonic mouse telencephalic neurons, *J Neurobiol* 27(2) (1995) 252-65.
- [275] T. Lv, H.-Q. Gong, P.-J. Liang, Caffeine-Induced Ca²⁺ Oscillations in Type I Horizontal Cells of the Carp Retina and the Contribution of the Store-Operated Ca²⁺ Entry Pathway, *PLOS ONE* 9(6) (2014) e100095.
- [276] C. Szegedi, S. Sárközi, A. Herzog, I. Jóna, M. Varsányi, Calsequestrin: more than 'only' a luminal Ca²⁺ buffer inside the sarcoplasmic reticulum, *Biochem J* 337 (Pt 1)(Pt 1) (1999) 19-22.
- [277] G. Tse, Mechanisms of cardiac arrhythmias, *J Arrhythm* 32(2) (2016) 75-81.
- [278] V.N. Batchvarov, The Brugada Syndrome - Diagnosis, Clinical Implications and Risk Stratification, *Eur Cardiol* 9(2) (2014) 82-87.
- [279] B. Belhassen, Management of Brugada Syndrome 2016: Should All High Risk Patients Receive an ICD?, *Circulation: Arrhythmia and Electrophysiology* 9(11) (2016) e004185.
- [280] C.A. Remme, A.O. Verkerk, D. Nuyens, A.C.G.v. Ginneken, S.v. Brunschot, C.N.W. Belterman, R. Wilders, M.A.v. Roon, H.L. Tan, A.A.M. Wilde, P. Carmeliet, J.M.T.d. Bakker, M.W. Veldkamp, C.R. Bezzina, Overlap Syndrome of Cardiac Sodium Channel Disease in Mice Carrying the Equivalent Mutation of Human *SCN5A*-1795insD, *Circulation* 114(24) (2006) 2584-2594.
- [281] W. Schillinger, J.W. Fiolet, K. Schlotthauer, G. Hasenfuss, Relevance of Na⁺-Ca²⁺ exchange in heart failure, *Cardiovascular Research* 57(4) (2003) 921-933.
- [282] V. Piacentino, 3rd, C.R. Weber, X. Chen, J. Weisser-Thomas, K.B. Margulies, D.M. Bers, S.R. Houser, Cellular basis of abnormal calcium transients of failing human ventricular myocytes, *Circ Res* 92(6) (2003) 651-8.
- [283] M. Lindner, E. Erdmann, D.J. Beuckelmann, Calcium content of the sarcoplasmic reticulum in isolated ventricular myocytes from patients with terminal heart failure, *J Mol Cell Cardiol* 30(4) (1998) 743-9.
- [284] M.A. Høydal, I. Kirkeby-Garstad, A. Karevold, R. Wiseth, R. Haaverstad, A. Wahba, T.L. Stølen, R. Contu, G. Condorelli, Ø. Ellingsen, G.L. Smith, O.J. Kemi, U. Wisløff, Human cardiomyocyte calcium handling and transverse tubules in mid-stage of post-myocardial-infarction heart failure, *ESC Heart Fail* 5(3) (2018) 332-342.

7 Publications

Michelle Vanessa Kapchoup Kamga¹, Michael Reppel, Jürgen Hescheler, Filomain Nguemo¹ (2021). Modeling genetic cardiac channelopathies using induced pluripotent stem cells – Status quo from an electrophysiological perspective. *Biochemical Pharmacology*

<https://doi.org/10.1016/j.bcp.2021.114746>

Filomain Nguemo¹, Erastus Nembu Nembo¹, **Michelle Vanessa Kamga Kapchoup**, Franz Enzmann, Jürgen Hescheler (2021). QuinoMit Q10-Fluid attenuates hydrogen peroxide-induced irregular beating in mouse pluripotent stem cell-derived cardiomyocytes. *Biomedicine and Pharmacotherapy*

<https://doi.org/10.1016/j.biopha.2021.112089>

Helfenrath, Kathrin, Sauer, Markus, **Kamga, Michelle**, Wisniewsky, Michelle, Burmester, Thorsten, Fabrizio, Andrej (2021). The more, the merrier? Multiple myoglobin genes in fish species, especially in gray bichir (*Polypterus senegalus*) and reedfish (*Erpetoichthys calabaricus*). *Genome Biology and Evolution*.

<https://doi.org/10.1093/gbe/evab078>

8 Curriculum Vitae

Michelle Vanessa Kamga Kapchoup

Tel.: +49 221 478 6996

Email: kamga.mv@gmail.com

Link: www.linkedin.com/in/michelle-vanessa-kamga-kapchoup-28b680163

Personal details

Date of birth	Mai 14 1990
Place of birth	Douala/Cameroon
Nationality	Cameroonian
Gender	Female

Education

University

Since April 2018

Ph.D. Student at the University Hospital of Cologne

October 2015 – January 2018

University of Hamburg: Biology

Thesis title: Analysis and function of dendritic cells during *Plasmodium falciparum* malaria

Thesis Lab: Bernhard-Nocht-Institute for tropical medicine, PD Dr. Thomas Jacobs

Degree: Master of Science

October 2011 – December 2013

University of Yaoundé/Cameroon: Biology of animal organisms

Master's program not completed

October 2008 – July 2011

University of Yaoundé/Cameroon: Biology of animal organisms

Degree: Bachelor of Science

Secondary school

September 2000 – June 2008

Bilingual high school application

Degree: Higher education entrance qualification

Erklärung

Hiermit versichere ich an Eides statt, dass ich die vorliegende Dissertationsschrift selbstständig und ohne die Benutzung anderer als der angegebenen Hilfsmittel angefertigt habe. Alle Stellen - einschließlich Tabellen, Karten und Abbildungen -, die wörtlich oder sinngemäß aus veröffentlichten und nicht veröffentlichten anderen Werken im Wortlaut oder dem Sinn nach entnommen sind, sind in jedem Einzelfall als Entlehnung kenntlich gemacht. Ich versichere an Eides statt, dass diese Dissertationsschrift noch keiner anderen Fakultät oder Universität zur Prüfung vorgelegen hat; dass sie - abgesehen von unten angegebenen Teilpublikationen - noch nicht veröffentlicht worden ist sowie, dass ich eine solche Veröffentlichung vor Abschluss der Promotion nicht ohne Genehmigung der / des Vorsitzenden des IPHS-Promotionsausschusses vornehmen werde. Die Bestimmungen dieser Ordnung sind mir bekannt. Die von mir vorgelegte Dissertation ist von PD Dr. Filomain Nguemo betreut worden.

Darüber hinaus erkläre ich hiermit, dass ich die Ordnung zur Sicherung guter wissenschaftlicher Praxis und zum Umgang mit wissenschaftlichem Fehlverhalten der Universität zu Köln gelesen und sie bei der Durchführung der Dissertation beachtet habe und verpflichte mich hiermit, die dort genannten Vorgaben bei allen wissenschaftlichen Tätigkeiten zu beachten und umzusetzen.

Übersicht der Publikation

Michelle Vanessa Kapchoup Kamga¹, Michael Reppel, Jürgen Hescheler, Filomain Nguemo¹ (2021).
Modelling genetic cardiac channelopathies using induced pluripotent stem cells – Status quo from an electrophysiological perspective. Biochemical Pharmacology
<https://doi.org/10.1016/j.bcp.2021.114746>

Ich versichere, dass ich alle Angaben wahrheitsgemäß nach bestem Wissen und Gewissen gemacht habe und verpflichte mich, jedmögliche, die obigen Angaben betreffenden Veränderungen, dem IPHS-Promotionsausschuss unverzüglich mitzuteilen.

Köln, den 22.12.2022

Datum

Michelle Kamga

Unterschrift